DOKUZ EYLÜL UNIVERSITY
GRADUATE SCHOOL OF NATURAL AND APPLIED SCIENCES

EARTHQUAKE INDUCED LANDSLIDES

by
Dyson Nelson MOSES

January, 2017
İZMİR

EARTHQUAKE INDUCED LANDSLIDES

A Thesis Submitted to the
Graduate School of Natural and Applied Sciences of Dokuz Eylül University in
Partial Fulfilment of the Requirements for the Masters of Science Degree in
Geological Engineering, Applied Geology Program

by

Dyson Nelson MOSES

January, 2017
İZMİR

THESIS EXAMINATION RESULT FORM

We have read the thesis entitled **"EARTHQUAKE INDUCED LANDSLIDES"** completed by **DYSON NELSON MOSES** under supervision of **PROF. DR. NECDET TÜRK** and we certify that in our opinion it is fully adequate, in scope and in quality, as a thesis for the degree of Master of Science.

....

Prof. Dr.Necdet TÜRK

Supervisor

Doç.Dr. Sener Ceryan

(Jury Member)

Prof.Dr Talip Güngör

(Jury Member)

Prof. Dr. Emine İlknur CÖCEN
Director
Graduate School of Natural and Applied Sciences

ACKNOWLEDGEMENTS

I would like to thank my supervisor Prof. Dr. Necdet TÜRK for his mentorship, critics, advices and overall guidance in production of the thesis. His patience and accommodative attributes granted me the opportunity to ask questions with liberty and earn priority during the entire duration of writing my thesis even when he could be busy. I also want to thank Dr. Cem KINCAL, Prof. Dr. Mehmet Yalçin KOCA and Prof. Dr. Talip GÜNGÖR for their comments, contribution and generosity in sharing information.

Special thanks go to Dr. David KEEFER, Dr. Scot MILES, and Prof. Dr. Reşat ULUSAY, Dr. Okan FISTIKOĞLU and Dr. Randall JIBSON for sharing information. Dr D. Keefer and Dr S. Miles did not only share information, they permitted me to apply their program called Comprehensive Areal Model for Earthquake induced Landslides (CAMEL) which operates in ArcGIS for analysis.

I would not forget to acknowledge the role played by my colleagues; Takudzwa MUSHAMBA, Moalosi LEBEKWE, Suleiman Kweyu SIGORO and Ibrahim MAMBO. It is true that a*n iron sharpens an iron*; my partnership with these colleagues redefined my approach to life. I also thank Hilal AKIN for helping me in various ways during my study period. My special thanks go to my beloved partners; Jennifer and Aviyah and my mother (Fainess Champiti) and all family members for moral support in the course of my studies.

Many thanks go to the Government of Turkey for the scholarship that enabled me to complete this program. Above all I thank GOD ALMIGHTY for making all things possible. I did all things through HIM who strengthens me.

Dyson Nelson MOSES

EARTHQUAKE INDUCED LANDSLIDES

ABSTRACT

Earthquake is among the principal triggering factors of landslides. Triggering of landslides revolves around two principal domains: seismology and landslides mechanics. In this study, earthquakes that induced landslides between 1998 and 2015 in the world were investigated and the factors that contributed to the landsliding activities were evaluated. This was accomplished through a comprehensive and meticulous review of data on landslides that were caused by the earthquakes. Secondly, the 1949 Karaburun and the 2009 Karonga earthquakes were investigated as case studies to assess the possibility of occurrence of landslides in the absence of data by applying CAMEL and GIS programs.

It emerged that the triggering of landslides by earthquakes is greatly governed by two main classes of parameters: (i) the earthquake parameters (magnitude, peak ground acceleration or Arias intensity, epicentral and rupture dynamics), (ii) the site parameters (geology, tectonic setting and topography). The results indicate that there is no proportional correlation between magnitude and Peak Ground Acceleration against seismically induced landslides. However, a fairly positive correlation between peak ground acceleration and landslides is obtained when earthquake duration component is integrated. Landslides concentration tends to decrease as focal depth increases and as fault length and distance from the epicentre increases.

Geology also show a strong control of landslides occurrence; most earthquake induced landslides occur in sedimentary rocks more than any other lithological unit and the occurrence of landslides is concentrated on thrust faults in hanging walls. Regarding topography, the landslides concentration generally increases with increasing slope angle until the maximum is reached in the 30 - 40 degrees category, and then drops as slope gradient augment.

In a case where landslides data is not available, the study attempted to assess a possibility of occurrence of landslides by applying CAMEL and GIS program. It emerged that the possibility of occurrence of earthquake induced landslides was relatively high for the Karaburun earthquake, Turkey and below par in case of Karonga earthquake, Malawi.

Keywords: Earthquake induced landslides, peak ground acceleration, fuzzy logic, degree of support, slope susceptibility, controlling factors and landslides concentration.

DEPREMİN OLUŞTURDUĞU HEYELANLAR

ÖZ

Deprem heyelanların ana tetikleyici faktörlerinden biridir. Heyelanların oluş nedeni iki başlıca alanı kapsar: Sismoloji ve yer kayması mekaniği. Bu çalışmada, dünyada 1998 ve 2015 yılları arasında heyelanlara yol an depremler incelenmiştir ve depremi tetikleyen faktörler değerlendirilmiştir. Bu depremlerin neden olduğu heyelan verileri kapsamlı ve titiz bir incelemeyle gerçekleştirilmiştir. İkinci olarak, heyelan oluşma olasılığını değerlendirmek için veri eksikliğinde 1949 Karaburun 2009 Karonga depremleri DKAMK ve CBS programları uygulanarak incelenmiştir

Bu çalışmada, depremin neden olduğu heyelanlar büyük ölçüde iki ana parametre sınıfı tarafından kontrol edilir. i) deprem özellikleri (büyüklük, pik yer ivmesi veya Arias şiddeti, dış merkez(episentır merkezüssü ve çatlak dinamikleri), (ii) yer özellikleri (jeoloji, tektonik ve topografya). Sonuçlar, deprem büyüklüğü ve pik yer ivmesinin heyelanları sismik olarak harekete geçirmiş olmasına karşın aralarındaki ilişkinin orantılı olmadığını göstermiştir. Ancak, deprem süresi ogesiyle birleştirildiğinde pik yer ivmesi ve heyelanlar arasında oldukça pozitif bir korelasyon elde edilmiştir. Negatif bir korelasyon heyelanlara karşı odak derinliği ve toprak kaymalarına karşı depremin merkezi ve arıza rüptürü mesafe için elde edilmiştir.

Jeoloji heyelan oluşumunun güçlü bir kontrolü olduğunu gösterir ; çoğu heyelanlar diğer litolojik birimlerden daha çok sedimanter kayaçlarda meydana gelir ve heyelanların oluşumu asılı duvarlarda bindirme fayları üzerinde yoğunlaşmıştır. Topoğrafik olarak, toprak kaymaları genellikle eğim 30 dereceden 40 dereceye ulaşıncaya kadar artan eğim açısı ile artmaktadır ve daha sonra artan şev eğimiyle birlikte azalmaktadır.

Heyelanlar veriler olmayan bir durumda, çalışma DKAMK ve CBS programı uygula~~y~~narak heyelan oluşma olasılığını değerlendirmek için çalışılmıştır.

Bu çalışmada, depremin tetiklediği heyelan oluşma olasılığının Karaburun depremi ve aşağısında bulunan Karonga depremi-için nispeten yüksek olduğu ortaya çıkmıştır.

Anahtar kelimeler: Heyelanları tetikleyen depremler, pik yer ivmesi, Bulanık mantık, destek derecesi, yamaç duyarlılığı, kontrol faktörleri, heyelanlar konsantrasyonu.

CONTENTS

Page

THESIS EXAMINATION RESULT FORM ii

ACKNOWLEDGEMENTS iii

ABSTRACT iv

ÖZ vi

LIST OF FIGURES xii

LIST OF TABLES xvi

CHAPTER ONE-INTRODUCTION 1

1.1 Problem Statement 3

1.2 Research Significance 3

CHAPTER TWO-RESEARCH QUESTIONS AND OBJECTIVES 5

2.1 Principal Research Questions 5

2.3 Objectives 5

CHAPTER THREE-LITERATURE REVIEW 7

3.1 Landsliding and Earthquakes 7

3.2 Characteristics of Earthquake Induced Landslides 8

3.3 Relative Abundance of Earthquake Induced Landslides 13

CHAPTER FOUR-HISTORICAL LANDSLIDES INDUCING EARTHQUAKES IN THE WORLD (1998-2015) 15

4.1 Types of Earthquake Induced Landslides 30

4.2 Methodology for the Analytical Study 33

4.3 Earthquake Induced Landslides Controlling Factors 35

4.3.1 Seismic Parameters 35

4.3.2 Geological Environments 56

4.3.3 Topography 64

4.4 Discussion 72

CHAPTER FIVE-CASE STUDY OF İZMİR; KARABURUN 76

5.1 Background Information 76

5.2 General Geology of İzmir 77

5.3 Tectonic Setting 78

5.6 Study Area 82

5.6.1 Location and Geological Setting of the Study Area 82

5.6.2 Structural Geology 84

5.6.3 Seismicity of Karaburun 85

5.7 Methodology 85

5.7.1 Review Data 86

5.7.2 Data Collection 86

5.7.3 Approach 86

5.8 Results……… 103

5.8.1 Structure of CAMEL for Analysis 103

5.8.2 Slope Height 105

5.8.3 Slope Angle 107

5.8.4 Slope Aspect 109

5.8.5 Terrain Roughness 111

5.8.6 Material Type 114

5.8.7 Soil Depth 115

5.8.8 Moisture 115

5.8.9 Shake Intensity 115

5.9 Evaluation of Membership Function 118

CHAPTER SIX-CASE STUDY OF KARONGA; MALAWI 120

6.1 Location of Study Area 120
6.2 Geology of the Study Area 121
6.3 Seismotectonic Setting 123
6.4 Earthquake Damage 125
6.5 Assessment of Possible Landslides Occurrence 126
6.5.1 Slope Height 127
6.5.2 Slope Angle 130
6.5.3 Slope Aspect 132
6.5.4 Terrain Roughness 134
6.5.5 Material Type 136
6.5.6 Soil Depth 137
6.5.7 Moisture 137
6.5.8 Shake Intensity 137
6.6 Evaluation of Membership Function 138

CHAPTER SEVEN-DISCUSSION AND CONCLUSION 140

7.1 Limitations 141

REFERENCES 142

APPENDICES 157

Appendix A Hazard module of CAMEL 157
Appendix B CAMEL input variables – variables and modifiers for hazard module 158

Appendix C Membership functions of disturbance distance for CAMEL hazard module 159
Appendix D Membership functions of ground class for CAMEL hazard module 159
Appendix E Knowledge describing increasing likelihood of landslides with respect to quality of rock cementation or induration 160
Appendix F Membership functions of moisture variable for CAMEL hazard module 161
Appendix G Membership functions of shake intensity for CAMEL hazard module 161
Appendix H Seismic variables rule block for disrupted rock slides and falls..... 162
Appendix I Membership functions of slope angle for CAMEL hazard module 162
Appendix J Membership functions of Vegetation variable for CAMEL hazard module 163
Appendix K Abbreviations and Acronyms 164

LIST OF FIGURES

Page

Figure 3.1 Schematic illustrations of the characteristics of earthquake induced landslides……………………………………………………………….13
Figure 4.1 The Nepal landslides and the blocked road after the Mw 7.8, 2015 Nepal earthquake ………………………………………………………………15
Figure 4.2 Earthquake induced landslides during the Christchurch earthquake in New Zealand…………………………………………………………………..17
Figure 4.3 An eye into the Wenchuan 2013 and 2008 earthquake induced landslides respectively ……………………………………………………………...18
Figure 4.4 Earthquake induced landslides during the West Sumatra 2009 earthquake and rescue efforts after the event ………………………………………..20
Figure 4.5 Part of the damage by the 2007, Mw 6.6 Niigata Chuetsu–Oki earthquake earthquake induced landslides during the Mw 9.0 Tohoku earthquake ...20
Figure 4.6 Extensive shallow rockslides after the Kashmir Mw 7.6 earthquake……21
Figure 4.7 Destroyed houses as seen on a hillside due to earthquake induced landslides after the 2010 Mw 7.0 Haiti earthquake ……………………..22
Figure 4.8 Part of the earthquake induced landslides during the Aysén Fjord 2007 earthquake ………………………………………………………………23
Figure 4.9 Earthquake induced landslides during the 2002 Denali, the 2001 Elsavado, the 1994 Northridge and the 1989 Loma Prieta earthquakes……………25
Figure 4.10 Earthquake induced landslides during the 2003 Bingöl earthquake…....27
Figure 4.11 Relative frequency of each type of landslides during earthquakes …….31
Figure 4.12 Relative frequency of each type of landslides during earthquakes …….32
Figure 4.13 Relative frequency of each type of landslides during earthquakes …….32
Figure 4.14 Flow-chart of the methodology used for assessing the earthquake induced landslides ……………………………………………………34
Figure 4.15 Relationship between earthquake magnitude and number of reported landslides………………………………………………………………...36
Figure 4.16 Relationship between earthquake magnitude and the area affected by landslides after…………………………………………………………37

Figure 4.17 Relationship between earthquake magnitude and square root of area affected by earthquake induced landslides……………………………38
Figure 4.18 Relationship between earthquake magnitude and the estimated volume of landslides…………………………………………………………….39
Figure 4.19 Relationship of PGA and number of landslides occurrence.....………...41
Figure 4.20 Relationship of PGA*t and number of landslides occurrence….………42
Figure 4.21 Relationship between PGA and area affected by landslides ..…………42
Figure 4.22 Relationship between PGA*t and area affected by earthquake induced landslides…………………………………………………………….42
Figure 4.23 Relationship between PGA and estimated volume of landslides ………43
Figure 4.24 Relationship between PGA*t and estimated volume of landslides …….44
Figure 4.25 Relationship between Arias intensity and area affected by landslides ………………………………………………………………………46
Figure 4.26 Relationship between arias intensity and volume ……………………..46
Figure 4.27 Relationship between focal depth and earthquake induced landslides…47
Figure 4.28 Relationship between focal depth and area affected by landslides …....48
Figure 4.29 Relationship between focal depth and estimated volume of earthquake induced landslides ……………………………………………………..49
Figure 4.30 The 3D plot of magnitude and focal depth with landslide-affected area.49
Figure 4.31 Relationship between fault length and landslides occurrence………….50
Figure 4.32 Relationship between fault length and area affected by landslides …….51
Figure 4.33 Relationship between fault length and estimated volume of landslides..52
Figure 4.34 Distribution of landslide with respect to distance from the epicentre ….53
Figure 4.35 Distribution of landslide with respect to distance from the epicentre ….54
Figure 4.36 Distribution of landslide with respect to distance from the fault plane after…………………………………………………………………55
Figure 4.37 Distribution of landslide with respect to distance from the fault plane...56
Figure 4.38 Distribution of earthquake induced landslides with respect to lithology after the 2013 Lushan earthquake ……………………………………..58
Figure 4.39 Distribution of earthquake induced landslides with respect to lithology after the 2011 Tohoku Japan earthquake………………………………58

Figure 4.40 Distribution of earthquake induced landslides with respect to lithology after the 2008 Wenchuan Earthquake …………………………………99
Figure 4.41 Distribution of earthquake induced landslides with respect to lithology after the 2007 Niigata earthquake ………..……………………………59
Figure 4.42 Distribution of earthquake induced landslides with respect to lithology after the 1999 Chi Chi earthquake……………………..……………60
Figure 4.43 Distribution of earthquake induced landslides with respect to lithology after the 1994 Northridge Earthquake…………………………………60
Figure 4.44 Distribution of earthquake induced landslides with respect to lithology after the 1989 Loma Prieta Earthquake………………………………..70
Figure 4.45 Locations of main shocks between 1977 and 2012 in the GCMT catalogue…………………………………………………………………62
Figure 4.46 Relationship between fault type and landslides ………………………..64
Figure 4.47 Distribution of landslides with respect to slope angles ………………...66
Figure 4.48 Distribution of orientation of the slopes………………………………..69
Figure 4.49 Distribution of landslides with respect to orientation of slopes …..……70
Figure 4.50 Distribution of landslides with respect to elevation ……………………71
Figure 4.51 Distribution of landslides with respect to slope curvature ……………..72
Figure 5.1 Earthquake distribution across Turkey…………………………………..77
Figure 5.2 The general geology of the region for the study area……………………81
Figure 5.3 Landslide and rock fall areas of İzmir metropolitan area………………..83
Figure 5.4 Geological map of the Karaburun peninsula…………………………….84
Figure 5.5 Structural setting of the study area ……………………………………..89
Figure 5.6 The two module framework of CAMEL ………………………………..90
Figure 5.7 Design of the possibility module of CAMEL……………………………93
Figure 5.8 Membership functions for *pTerrainRough*………………………………95
Figure 5.9 Membership functions for *pShakeIntensity* ……………………………..96
Figure 5.10 Membership function for *pSoilDepth* ………………………………….97
Figure 5.11 Membership functions for *pSlopeHeight* ………………………………99
Figure 5.12 Membership functions of *pMoisture* …………………………………101
Figure 5.13 Membership functions for *pSlopeAngle* ……………………………...103
Figure 5.14 The structure of CAMEL in ArcGIS …………………………………104

Figure 5.15 Digital elevation model for Karaburun ……………………………105
Figure 5.16 Slope height map derived from the Karaburun DEM ………………...106
Figure 5.17 Fuzzy membership map of slope height ……………………………107
Figure 5.18 Slope angle map derived from the Karaburun DEM …………………108
Figure 5.19 Fuzzy membership map of slope angle ……………………………….109
Figure 5.20 Aspect map for Karaburun ……………………………………………110
Figure 5.21 Fuzzy membership map of slope aspect ……………………………111
Figure 5.22 Terrain curvature or roughness map for Karaburun …………………..112
Figure 5.23 Fuzzy membership map of terrain roughness or curvature …………...113
Figure 5.24 Relationship between landslides and the seismic intensity …………...116
Figure 6.1 Location of study area …………………………………………………121
Figure 6.2 Geological map of the study area ……………………………………122
Figure 6.3 The damage experienced during the 2009 Karonga earthquakes ………125
Figure 6.4 The tectonic setting of Karonga.………………………………………..124
Figure 6.5 Digital elevation model for Karonga.…………………………………..127
Figure 6.6 Slope height map derived from the Karonga DEM ……………………128
Figure 6.7 Fuzzy slope hieght map derived from the Karonga DEM ……………129
Figure 6.8 Slope angle map derived from the Karonga DEM ……………………..130
Figure 6.9 Fuzzy slope angle map derived from the Karonga DEM ………………130
Figure 6.10 Slope aspect map of Karonga.………………………………………...132
Figure 6.11 Fuzzy slope aspect map of Karonga…………………………………..133
Figure 6.12 Terrain roughness calculated from the Karonga DEM ……………….134
Figure 6.13 Fuzzy membership of terrain roughness……………………………135
Figure 6.14 Membership function of the material type. …………………………...135

LIST OF TABLES

Page

Table 3.1 Characteristics of earthquake induced landslides ……………………….....12

Table 3.2 Relative abundance of earthquake induced landslides……………………14

Table 4.1 Summary of historic earthquakes that induced landslides……………….….28

Table 4.2 Data sources referenced ………………………………………………..30

Table 4.3 Distribution of landslides with respect to fault type ……………………...63

Table 4.4 Relationship between slope angle and geology in inducing landslides …..67

Table 5.1 Summary of some major earthquakes in İzmir city………………………80

Table 5.2 Major landslides and rock fall areas in İzmir city.………………………..82

Table 5.3 CAMEL possibility module input variables ……………………………..91

Table 5.4 Possibility rule block expressing knowledge about *pTerrainRough* …….94

Table 5.5 Possibility rule block expressing knowledge about *pSoilDepth* …………96

Table 5.6 Possibility rule block expressing knowledge about *pSlopeHieght* ……....97

Table 5.7 Possibility rule block expressing knowledge about *pMaterialType* ……..98

Table 5.8 Possibility rule block expressing knowledge about *pMoisture* …………100

Table 5.9 Knowledge about minimum slope angles required for a particular type of landslides ……………………………………………………………..101

Table 5.10 Possibility rule block expressing knowledge about *pSlopeAngle.*……..102

Table 5.11 Typical relationship between earthquake magnitude and typical modified mercali intensity.…………………………………………………….115

Table 5.12 Representative shake map ……………………………………………..117

Table 5.13 Summary of fuzzy membership to assess degree of support in relation to susceptibility to EI landslides at Karaburun …………………………...118

Table 6.1 List of the earthquakes that occurred in Karonga 2009. ………………..123

Table 6.2 Representative shake map ………………………………………………137

Table 6.3 Summary of fuzzy membership to assess degree of support. ………….138

CHAPTER ONE
INTRODUCTION

Earthquakes are inarguably annihilating geological events on Earth. Adding to the destruction of structures and properties worthy billions of money, earthquakes can induce different forms of ground rupture and instability in the ground which include: ground displacement with tectonic uplifting or subsidence of vast areas and lateral movements, the formation of devastating seismic sea waves culminating from the sudden vertical movement of the sea bed, liquefaction of unconsolidated water saturated deposits and mass movement (Anderson & Richards, 1989).

Earthquakes can cause slopes to become less stable due to force exerted on it or by making the materials to lose strength thereby inducing failure. Landslides characterised with catastrophic fast motions are among the worst annihilating events accompanied by failure of slopes when earthquakes occur. Keefer (1984) and Jibson (1993) established that earthquakes with moment magnitude (Mw) equal or greater than 4.0 are capable of triggering landslides on very susceptible slopes and those earthquakes having magnitude ≥ 6.0 are capable of generating widespread landslides. Landslides have been defined as phenomena that encompass lateral and downslope motion of geological matters due to gravity, and in most cases water (Keefer, 1984; Walker & Fell, 1987).

According to Korup (2010), the horizontal and vertical ground acceleration ensuing from seismic shaking put extra transient shear stress and augments to ambient pore water pressure through cyclic gravitational loading, hence negatively affecting slope stability. Furthermore, Korup (2010) contends that earthquakes can serve as preparatory factors of landslides giving an instance of repeated seismic hanging-wall shattering in reverse faults which can play a role in weakening rock-mass strength through fragmentation.

Trandafir et al. (2012) add that slopes characterised by extremely small gradients close to horizontal ground state may be exposed to large landslides as a result of earthquake induced (EI) liquefaction which is due to ground liquefaction

It is inarguable fact that there is a strong connection between earthquakes and landslides with the former being a triggering aspect to the later. Generally, it is not perplexing that seismically induced landslides happen in young active tectonic mountain ranges and along active faults particularly along mobile marginal zones of continental blocks. The geographical location of the case study areas; Karaburun, Turkey and Karonga, Malawi render them vulnerable to natural disasters like earthquakes, landslides and floods. These study areas, despite being located in seismically active regions, just as Korup (2010) noted with most parts of the world, the overall research on earthquake triggered landslides has little documentation. Instead much of the studies have focused on rainfall induced landslides (REL). However, it is evident that fatalities and damage attributed earthquakes are to a significant fraction incurred by ‘secondary’ earthquake effects like tsunami, landslides, liquefaction and fire other than the ground motion itself.

Korup (2010) reasons that the use of the term “secondary hazards” to describe the accompanying landslides during earthquakes is potentially misleading, given that any proceeding cascades may eventually incur the highest fraction of total damage. The preceding discussion tress the significance of analysing the factors that contribute to EI landslides. The understanding of the parameters that play a role in causing landslides is crucial for studying the mechanism of landslides generation, locating zones of landslides exposure and modelling or forecasting their risk in landslides-prone areas. Therefore, based on the landslides inventory and historical information, the study endeavours to evaluate the feasibility of occurrence of landslides in the absence of data on EI landslides in the selected study areas.

1.1 Problem Statement

Lei (2012) discusses that the investigation of landslides triggered by earthquakes dates back to the 18th century. However, in Turkey as well as Malawi, just as other parts of the world, overall research on earthquake-triggered landslides has not been given a considerable treat. Korup (2010) ascribes the trend to a minimal understanding of the role of seismic shaking to weaken slope stability and the general limitations of predicting the magnitude, location and timing of large landslides-triggering earthquakes.

Cotecchia in Anderson et al. (1989) admits that the complexity of the analysis of ground stability due to earthquake comes about because it involves numerous fields such as geology, geophysics, seismology and geotechnics. However, the difficulties in the analysis do not deter us from researching and comprehending such destructive phenomena. Therefore, this necessitates a strong retrospective and empirical approach to research on seismic slope instability by analysis of the destructive past landslide events and application of Remote Sensing (RS) to find the likelihood of occurrence of EI landslides.

1.2 Research Significance

Earthquakes really pose a precarious and costly threat to people around the world. Hashimoto, Fukushima, Takada, & Group (2012) subscribe to this assertion by citing tragedy caused by the devastating March 11, 2011 earthquake ($Mw = 9.0$) in Japan. EI hazards such as landslides often have a greater danger to life and property than the ground shaking that occurs during an earthquake (Korup, 2010). EI landslides are seismic hazards that can damage and destroy life and property, disrupt service provision, block roads and hamper relief efforts.

Therefore, to be resilient to the effects of EI landslides requires momentous hazard planning on the part of the communities and local governments. The hazard planning efforts can only be supported by thorough research on the mechanism of seismic slope failure and how to predict them in future.

To realise this, the application of Geographic Information System (GIS) to create seismic landslides hazard maps has turned out to be widespread and effective because it has the capabilities to collect, store, manipulate, display and analyse large volume of spatially-referenced data as applied by Lin & Tung (2003), Yalcin (2008), Nandi & Shakoor (2009), Xu, Xu, Yao, & Wang (2013), Chalkias, Ferentinou, & Polykretis (2014), Shahabi & Hashim (2015) and Kamp & Owen (2016) among many authors. The significance of this study is that it will demonstrate the approach to assess the likelihood of occurence of landslides in the absence of data on EI landslides that could have been induced during and/or after an earthquake by using Comprehensive Areal Model of Earthquake (CAMEL) built on fuzzy logic. The qualitative approach to draw conclusions in this case is based on the extensive understanding of the landslides inducing earthquakes and the governing parameters for the occurence of EI landslides.

CHAPTER TWO
RESEARCH QUESTIONS AND OBJECTIVES

2.1 Principal Research Questions

1. What are the main controlling factors that render slopes susceptible to landslides during and/or after an earthquake?

To address this research question the study applies a holistic approach to examine all practical aspects related to landslides induced by earthquakes. In this regard, the study is guided by the following questions:

a. Which factors genuinely render slopes vulnerable to landslides during and/or after a ground shaking by earthquakes?
b. Can one factor be singled out as a sole controlling factor of the seismically induced landslides? If not, how do the controlling factors interrelate to induce landslides when an earthquake occurs?

2. Can CAMEL and GIS effectively assist us to assess the possibility of occurence of landslides in the absence of EI landslides data?

2.3 Objectives

The principal objectives of the study are split into two:

1. To document earthquakes that induced between 1998 and 2015 in the world with Mw ≥ 5.0 and evaluate the factors that contributed to the landsliding activities. In this regard attempts are made to establish relationship between earthquake parameters, geology and topographic parameters and EI landslides.

2. To assess the feasibility of occurence of landslides after the 1949 (Mw 7.0) İzmir-Karaburun and the 2009 Karonga, Malawi (Mw 6.0) earthquakes using the possibility module of CAMEL and GIS. In this regard, a quasi-quantitative approach is used to draw conclusion on the possibility of occurence of landslides by applying the knowledged gained from the documented worldwide landslides inducing earthquakes.

CHAPTER THREE
LITERATURE REVIEW

3.1 Landsliding and Earthquakes

Clague & Stead (2012) established that earthquake ground shaking culminates in short and continuous changes of normal and shear stress on slopes during earthquakes. And these strong ground motions can lead to instantaneous failure as result of peak ground motion or as a result the progressive substratum attenuation due to rock mass fracturing. Thus, the greater the amplitude of the incoming seismic waves and the duration of shaking the greater the likelihood of failure of unstable slopes

Global compilations of earthquakes and landslides data have been useful in exploring the effect of earthquake magnitude on the size of an area affected by landslides. Keefer (1984) tentatively defined maximum affected areas for earthquakes of different magnitudes. The analyses, which involved 40 cases, took into account the depth and focal mechanism of earthquakes, the frequencies at which seismic waves carry most energy, and the local geology and topography. Though it is difficult to pinpoint the magnitude at which landslides can be induced by earthquakes, Keefer (1984) managed to analyse various earthquakes that induced landslides to come up with a specific value. In the analysis it was noted that earthquakes with moment magnitude (M_w) of < 5.5 were not presented in the intensity data. However, earthquakes having Mw ≥ 4.0 were noted to be able to induce landslides on very susceptible slopes and earthquakes having Mw ≥ 6.0 have by far generated widespread landsliding (Jibson, 1993). Bommer, Chandler, & Rodriguez (1999) in their study of EI landslides between 1958 and 1997 came across smaller magnitude earthquakes (Mw ≥ 4.0) that caused landslides. With regards to intensity it has been found out by Keefer (1984) that the common lowest intensity for disrupted landslides and rock falls was VI on Modified Mercali Intensity (MMI) scale and the minimum intensity of earthquake given by Keefer (1984) MMI IV.

On the other hand, the common lowest intensity for coherent slides, lateral spreads, and flows was found to be MMI VII and the minimum documented intensity MMI V.

3.2 Characteristics of Earthquake Induced Landslides

EI landslides account for the great damage than all other seismic hazards amalgamated (Lei, 2012). Keefer (1984) discussed that landslides take various forms and are categorised as falls, topples, slides and flows (Table 3.1 and Figure 3.1) and are broadly characterised as active or inactive. Duman et al. (2005) adds that landslides can as well be put in categories depending on the deepths, as shallow (depth < 5m) and deep-seated (depth >5 m). It can be observed that characterisation of landslides vary with respect to the kind of movement and material conditions. However, EI landslides are unanimously agreed to fall in three principal classes: (1) disrupted slides and falls, (2) coherent slides and (3) lateral spreads and flows (Keefer, 1984; Jibson, 2013)

Category I

Category I landslides include slides, falls and avalanches of snow, soil and rocks since such landslides are typically disaggregated to a large extent during movement. Landslides in this category occur on steep slopes and move with high speed, and may carry the geological materials for long distance. Free fall may occur if the slope is in excess of 76^0 with the falling mass striking a slope with less inclination (Keefer, 1984). Furthermore, Keefer (1984) noted that, on longer slopes with angles at or below 45^0, the materails' movement is characterised by bouncing or free falling. However, changes in slope angles in the path of the landslides could restart the sequence of falling, jumping and rolling.

Disrupted rock slides and rock falls: disrupted rock slides move by translational sliding disrupted during movement into masses of rock fragments and blocks that slide on planar or gently curved surfaces where joints, bedding planes, or other surfaces of discontinuity dip down out of the slope. Disrupted slides activate under any moisture conditions, from dry to completely saturated and usually on slopes with 35^0.

Rock falls and Disrupted rock slides: Rock falls are the most abundant of EI landslides. Falls start with the extrication of soil and/or rock from a steep slope, along with little or no shear displacement occurs. Rock falls comprise of discrete boulders that move rapidly, typically through the air by falling, bouncing or rolling. The EI rock falls typically occur in closely jointed or weak cemented materials like pumice, tuff, shale, siltstone, sandstone and conglomerate (Keefer,1984). Rock falls originate on slopes $\geq 40^0$, usually on ridge cuts and man-made cuts.

Soil falls, disrupted soil slides and soil avalanches: Soil falls are similar to rock falls in most aspects. Soil falls consist of blocks or disrupted masses of soil that bound, roll and/or free fall down slopes. Normally, soil falls happen along bluffs, canyon walls, stream banks, terrace faces and cut slopes. Most soil falls involve weakly cemented gravel and sand but a few may occur in unconsolidated or weakly cemented clay (Keefer, 1984). Disrupted soil slides comprise of sheets of soil up to a few meters thick that disaggregate during movement into assortment of small blocks and individual grains. Usually, soil slides move along a basal shear surface formed at the soil-bedrock interface or at boundaries between different soil layers though some move on basal zones of weakened sensitive clays. Sensitive clays become cohesionless when the bonds between clay particles and adsorbed films of water are broken during earthquake vibrations.

The materials most commonly involved in disrupted soil slides are loose, unsaturated, and residual or colluvial sand with little or no clay fraction and occur at a minimum slope inclination of 15^0.

Rock avalanches: Rock avalanches are landslides that disintegrate into streams of rock fragments. They are extremely fast moving flows of dry debris created by large falls and slides with velocities that exceed 50m/sec and the source-slope inclination and height, based on 50 observed rock avalanches, indicate that the minimum inclination and height are 25 and 150 m respectively (Keefer, 1984)

Category II

Keefer (1999) defined coherent landslides as block slides, slumps, and slow earth slides because they remain relatively intact during movement, generally consisting of one to several large blocks separated by fissure and graben. Category II landslides move in the following mechanisms: (a) block slides by translational sliding on relatively planar basal shear surfaces, (b) slumps along basal shear surfaces curving concave upward so as a head ward rotation of the landslides occur and (c) slow earth slides by a combination of translational sliding and internal flow. Typical velocities for category II landslides are low (<0.005m/s) with relatively low displacements (<100m)

Rock block slides and rock slumps: Rock block slides consist of one or a few blocks sliding on planar basal shear surface involving little or no rotation. The shear planes are along discontinuities or bedding planes dipping out of the slope. Therefore, the blocks move relatively coherent. Rock block slides typically originate on slopes steeper than 150 in materials such as tuff, andesite, weakly cemented pumice, weakly cemented or closely jointed shale, mudstone, siltstone and sandstone.

Rock slumps on the other hand consist of one or a few coherent blocks sliding on a basal shear surface curving upward causing a head ward rotation.

Generally, rock slumps develop on 15^0 in basalt with interbedded ash and breccia, pumice, andesite, granite, greenstone, slate, schist, amphibole, siltstone, shale and sandstone typically due to weak cementation, weathering and/or shearing

Soil block slides and soil slumps: Soil block slides, just like rock block slides, move transitionally on planar or gently curved shear surfaces. The movement creates grabens at the landslide head with internal fissures and pressure ridges at the toe.
Most soil block slides are produced by fill, alluvial materials, till, volcanic ash, colluvium, clayey sediment, sandy Aeolian sediment, sandy alluvial-fan sediment and periglacial sediment (Keefer, 1984). Most soil block slides involve flat topped slopes and near horizontal basal shear surface on slope inclination as low as 5^0. Soil slumps are very similar to rock slumps in most respects. Soil slumps slides with similar mechanism of movement; curved, basal shear surface with head ward rotation of the slump just as with rock slump. The landslides are characterised by crescent shaped scarps, blocks with surfaces tilted back toward the crests of slopes and bulging toes. Slumps occur in a wide variety of materials, and are most commonly in uncompact and poorly compacted fills with a minimum inclination of 10^0.

Category III

Category III landslides include rapid soil flows, soil lateral spreads and subaqueous landslides. The mechanisms causing the lateral spreads are significantly different from the other types of landslides.

Rapid soil flows: Rapid soil flows, move as a stream of soil grains that flow viscously at high velocities and typically partially or completely saturated. Rapid soil flows can be initiated on inclinations as low as few degrees, travelling several kilometres and transporting large boulders (Keefer, 1984).

Table 3.1 Characteristics of earthquake induced landslides (Keefer, 1984)

SUMMARY OF CHARACTERISTICS OF EI LANDSLIDES					
Name	**Type of movement**	**Velocity†**	**Depth††**	**Internal disruption†††**	**Water content‡**
Landslides in rocks					D U PS S
Rock falls*	Bounding, rolling, free fall	Extremely rapid	Shallow	High or very high	X X X X
Rockslides*	Translational sliding on basal shear surface	Rapid to extremely rapid	Shallow	High	X X X X
Rock avalanches*	Complex involving sliding and/or as stream of rock fragments	Extremely rapid	Deep	Very high	X X X X
Rock block slides**	Translational sliding on basal shear surface	Slow to rapid	Deep	Slight or moderate	? X X X
Rock slumps**	sliding on basal shear surface with component of headward rotation	Slow to rapid	Deep	Slight or moderate	? X X X
Landslides in soils					
Soil falls*	Bounding, rolling, free fall	Extremely rapid	Shallow	High or very high	X X X X
Disrupted soil slides*	Translational sliding on basal shear surface or zones of weakened, sensitive clay	Rapid to extremely rapid	Shallow	High	X X X X
soil avalanches*	Complex involving sliding and/or as stream of rock fragments	Extremely rapid	Deep	Very high	X X X X
Soil block slides**	Translational sliding on basal shear surface	Slow to rapid	Deep	Slight to moderate	? ? X X
Soil slumps**	sliding on basal shear surface with component of head ward rotation	Slow to rapid	Deep	Slight to moderate	? X X X
Slow earth flows**	Translational sliding on basal shear surface with minor flow	Very low to moderate with very rapid surge	Generally shallow and occasionally deep	Slight	- - X X
Soil lateral spreads***	Translation on basal zone of liquefied gravel, sand or silt, or weakened, sensitive clay	Very rapid	Variable	Generally moderate, occasionally slight and high	- - X X
Rapid soil flows***	Flow	Very rapid to extremely rapid	Shallow	Very high	? ? ? X
Subaqueous landslides ***	Complex, generally involving lateral spreading and/or flow, occasionally involving slumping and/or block sliding	Generally rapid to extremely rapid, occasionally slow moderate	Variable	Generally high or very high; occasionally moderate or slight	- - X X

Notes: †**Velocity;** "***extremely slow***" = ≤ 0.6m/yr., "***very slow***" = 0.6m/yr. - 1.5 m/yr., "***slow"*** = 1.5 m/yr. – 1.5 m/Mo, "***moderate***" = 1.5 m/Mo – 1.5 m/day, "r***apid***" = 1.5 m/day – 0.3 m/min, "***very rapid***" = 0.3 m/min – 3 m/sec and "***extremely rapid***" = ≥ 3 m/sec. * Disrupted slides and falls, ** Coherent slides, *** Lateral spreads and flow. ††**Depth;** "**swallow**" thickness < 3m, "**deep**" depth > 3m.‡**Water content; D** = dry, **U** = moist and unsaturated, **PS** = partly saturated, **S** = saturated.

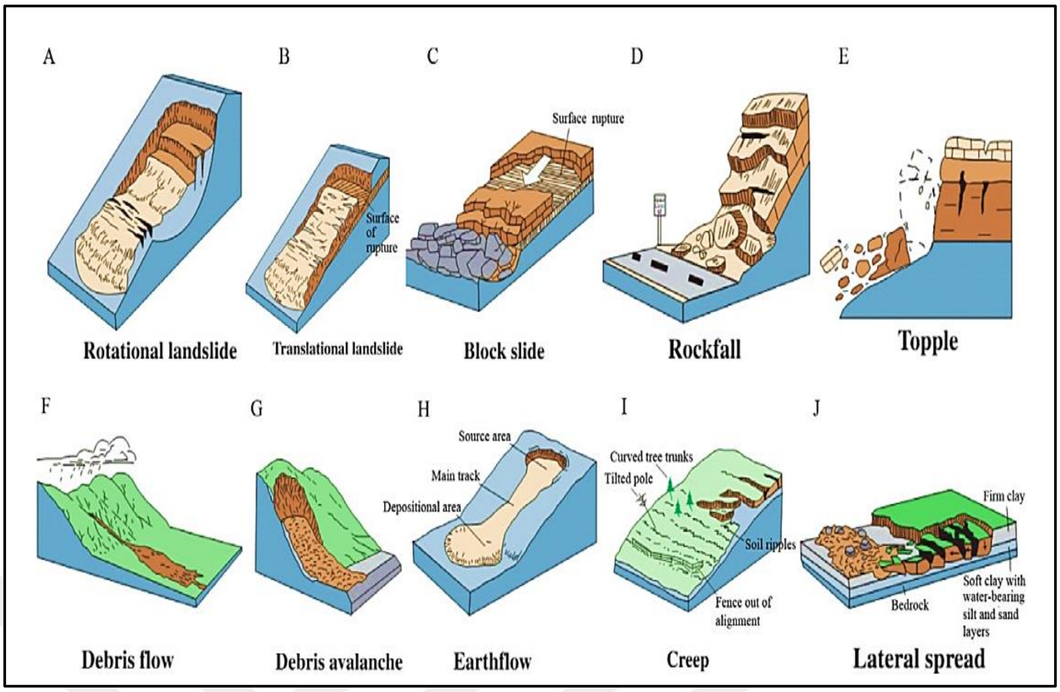

Figure 3.1 Schematic illustrations of the characteristics of EI landslides (Varnes, 1978)[1]

3.3 Relative Abundance of Earthquake Induced Landslides

Keefer (1984) observed that various kinds of EI landslides happen at variant frequency. Rock falls, disrupted soil slides, and rock slides seem to be the common types of landslides observed in historic earthquakes. Subaqueous landslides, slow earth flows, rock block slides, and rock avalanches are the least common, although the problems associated with observing subaqueous slides may contribute to their evident scarcity (Table 3.2).

[1] http://pubs.usgs.gov/fs/2004/3072

Table 3.2 Relative abundance of EI Landslides (Keefer, 1984)[2]

Abundance	**Description**
Very abundant (> 100,000 in the 40 earthquakes)	Rock falls, disrupted soil slides, rock slides
Abundant (10,000 to 100,000 in the 40 earthquakes)	Soil lateral spreads, soil slumps, soil block slides, soil avalanches
Moderately common (1000 to 10,000 in the 40 earthquakes)	Soil falls, rapid soil flows, rock slump
Uncommon	Subaqueous landslides, slow earth flows, rock block slides, rock avalanches

[2] The relative abundance is based on a study of 40 historic earthquakes ranging from Mw = 5.2 to Mw = 9.5 by Keefer 1984.

CHAPTER FOUR

HISTORICAL LANDSLIDES INDUCING EARTHQUAKES IN THE WORLD (1998-2015)

Asian Continent

Seismic shakings are the cause of large landslides often with devastating consequences for the people and property concerned (Anderson & Richards, 1989). Based on the 2015 United States Geological Survey's (USGS) report on Nepal earthquake, the 25/05/2015 Nepal earthquake (Mw = 7.8) affected the central Nepal and resulted into causing many landslides. Approximately 8,900 died, most of whom died due to direct impacts of landslides. In agreement, Ulusay and Aydna (2015) reported that the earthquake produced a major avalanche on the south slopes of Mt. Everest, situated nearly 160 km east-east-northeast of the epicentre which over 17 people and injured 61 others. Further, the landslides blocked vital roads, rivers and resulted in creation of temporary dams as shown in Figure 4.1.

Figure 4.1 The Nepal landslides and the blocked road after the Mw 7.8, 2015 Nepal earthquake (Tasnimnews, 2013)

In New Zealand, on 4th May 2015 a magnitude Mw 5.8 earthquake occurred in Matukutuki region. The earthquake's epicentre was situated at 44.5366S and 168.8369E and had a focal depth of 5km.

The reconnaissance survey, according to Cox et al. (2015) identified 37 landslides 27 of which were reactivations of existing landslides. The Matukutuki landslides covered nearly 800km^2 and had an estimated volume of 30,000m^3. The earthquake also led to fatalities and destruction of structures. The 2015 phenomenon was preceded by the 22nd February 2011, Mw 6.2-6.3 earthquake which took place below the city of Christchurch bringing about incomparable degree of damage in the country's history, and the biggest number of affected people since the 1931 Napier earthquake (Dellow et al., 2011). In comparison to the earthquake before the 4th September 2010 Darfield earthquake, which happened nearly 30 km to the west of Christchurch, in the shortest period to the 22nd February event (focal depth 5km) led to ground shaking of considerably higher amplitude and lead to numerous landslides in the Port Hills (Dellow et al., 2011).

It is believed that the 22nd February 2011 earthquake was the second strong earthquake to affect Christchurch in a period of less than six months, and closely succeeded by two other notable strong earthquakes on 13thJune 2011. Rock falls, block failures, and other forms of landslides were widespread in the near-fault region around the Port (Figure 4.2). These slope failures, according to Kaiser et al. (2012) culminated into five fatalities and destruction of many roads, tracks, and structures. The landslides that occurred were approximated to be ≥ 200.

The 1993 Finesterre earthquake, which in this study has been included for reference purposes, is reported to have induced >4,700 landslides with a total surface area of 55 km^2. The two earthquakes occurred at the southern boundary of the Finisterre Mountains, Papua New Guinea (PNG), along the Ramu-Markham thrust fault on 13rd October (M_w = 6.9) and 25th October (M_w = 6.7), 1993 (Meunier, Hovius, & Haines, 2007).

Figure 4.2 EI landslides during the Christchurch earthquake in New Zealand (Kaiser et al., 2012)

China is one of the most vulnerable countries to earthquakes. The 20 April 2013 Lushan earthquake with a magnitude of Mw = 6.6 which happened within five years after the 2008 Wenchuan Mw 7.9 triggered widespread landslides along the southern segment of the Longmen Shan fault zone (Figure 4.3). According to Tang et al. (2015), 3810 discrete landslide points were recorded through a carefully executed and field investigation and from digital aerial photographs taken after the Lushan earthquake. However, another rigorous field investigation by the Department of Land and Resources (DLR) revealed 15,000 landslides. The event in Lushan is reported to have led to 217 fatalities and destruction of roughly 193,000 houses. As for the 12th May 2008 Wenchuan Earthquake, which according to Chinese Earthquake Administration (CEA) measured Mw 8.3 (USGS Mw 7.9), caused deaths of more than 69,225 people and left 374,640 injured and about 17,393 unaccounted for (Xu, Xu,Yao & Dai, 2014) . The phenomenon took place after a crust movement along the Yingxiu–Beichuan Fault. An investigation by Qi, Xu, Lan, Zhang, & Liu (2010) revealed that more than 15,000 landslides were triggered by the earthquake resulting in instant deaths of about 20,000 and the most of affected city of Beichuan was ruined by two of the landslides induced by earthquake and caused fatalities of around 3000.

Still in China, another event occurred on April 14, 2010 Yushu, China. The Yushu earthquake had a reported magnitude of Mw 6.9. According to Xu & Xu (2014) the earthquake triggered over 2,036 landslides, having a total coverage area of 1.194 km^2 and 2,698 people were confirmed dead, 270 missing, and 12,135 injured due to the phenomena.

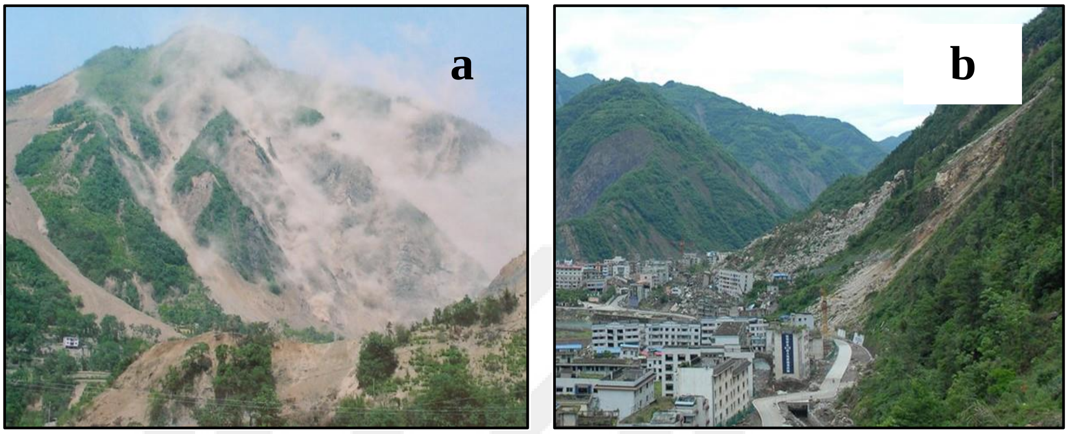

Figure 4.3 An eye into the; (a) 2008 Wenchuan and (b) 2013 Lushan EI landslides respectively (American Geophysical Union, 2016).

In india, Dangol, Yagi , & Higaki (2013) and Chakraborty, Saibal , Bhattacharya , & Bora (2011) discussed the Bhedetar landslide as one of the numerous landslides in India and Eastern Nepal that were triggered by the 30th September 2011 Sikkim earthquake (Mw 6.9). The landslide was a rock avalanche type which inflicted severe damage to the chain ages of the Koshi Highway: big boulders dropped off from the hill slope and rolled down smashing, sweeping and damaging the road surface. A latest field observation by Chakraborty et al. (2011) revealed that lithology and relief contributed a significantly in causing EI landslides.

Just before the 2011 Sikkim earthquake, India had experienced another fatal landslide after the March 28, 1999, Garhwali earthquake during which 338 active landslides, including 56 EI landslides, were Mapped in a 226-km^2 -study area in the Garhwali Himalaya, northern India (Barnard, Owen, Sharma, & Finkel, 2001).

The Sikkim earthquake had focal depth of 15 km. Thus these landslides principaly consisted of shallow failures in regolith and highly weathered bedrock involving avalanches, slides, and flows

In Indonesia, an 8 magnitude earthquake hit West Sumatra on Wednesday, 30 September 2009. The epicentre of this earthquake was situated at latitude 0° 84′ South, and longitude 99° 65′ East, 57 miles South-West of the city of Pariaman, ata depth of 71 km. A total of 89 landslides were identified after the earthquake Figure 4.4 (Umar, Pradhan, Ahmad, Neamah, & Shafapour, 2014) .

In the neighbouring Japan, The Mw 9.0 Tohoku earthquake struck Japan on 11 March 2011. The earthquake triggered 3477 coseismic landslides which affected 28;380 km^2 area of northeast Japan (Wartman, Dunham, Tiwari, & Pradel, 2013). According to Wartman et al. (2013) the Tohoku earthquake triggered landslides were directly attributed to be the cause of at least 14 fatalities, damaged buildings, temporarily obstructed transportation networks, and impeded surface-water flow within fluvial networks. Just 3 years before the Tohoku earthquake, Japan was hit by the Iwate–Miyagi Nairiku Earthquake (Mw 7.2) which happened on 14th June 2008 with the focus located at N 39.02°, E 140.88° and 8 km in depth. According to Yagi, Sato, Higaki & Yam (2009) losses after the earthquake were mostly induced by innumerable landslides throughout the region. The earthquake generated 4161 landslides most of which were concentrated in a hanging wall side of the seismic fault (Yagi et al., 2009).

The July 16, 2007, M_w 6.6 Niigata Chuetsu–Oki earthquake in Japan triggered yet another 70 landslides (Figure 4.5). The earthquake and accompanying geo-hazards caused 11 fatalities, about 1100 damaged residences and was accounted for approximately two year closure of the Kashiwazaki–Kariwa power plant (Collins, Kayen, & Tanaka, 2012a). The 2007 earthquake happened just after the 2004 M_w 6.9 Niigata Ken Chuetsu earthquake which was reported by Kieffer et al (2006) to have triggered a vast number of landslides estimated at 1,353 in the epicentral region.

Figure 4.4 EI landslides during the West Sumatra 2009 earthquake and rescue efforts after the event (American Geophysical Union, 2016)

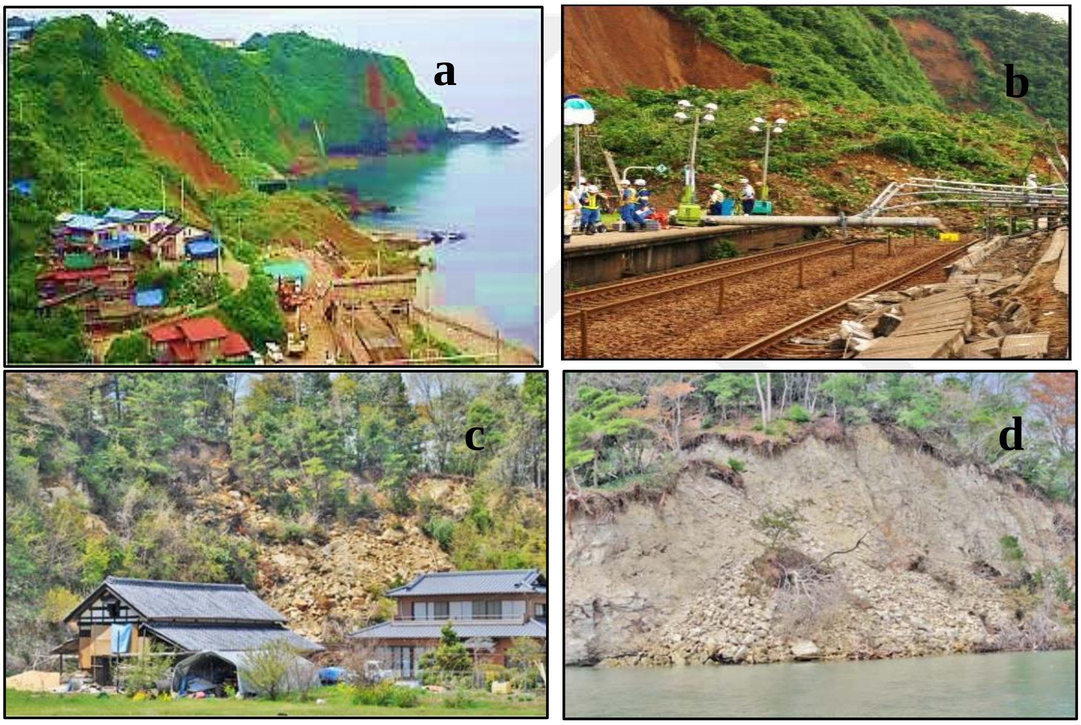

Figure 4.5 Picture (a) and (b) show part of the damage by the 2007, Mw 6.6 Niigata Chuetsu–Oki earthquake (Collins et al., 2012) and (c) and (d) show EI landslides during the Mw 9.0 Tohoku earthquake (Wartman et al., 2013).

The Kashmir earthquake (M 7.6) in Pakistan, which occurred in October 8, 2005, caused many landslides primarily rock falls and rock slides (Figure 4.6) around the cities of Muzaffarabad and Balakot, Pakistan (Harp & Crone, 2006). The avalanche deposit induced by the 2005 Khashmir earthquake reportedly travelled for about 1.5 kilometres downslope and 300 meters or more up the opposite slope in the lcosest Karli stream drainage and also went beyond into the Tang stream drainage. It was reported by Harp & Crone (2006) that the avalanche covered in material the village of Dandbeh and culminated into roughly 1,000 fatalities.

Figure 4.6 Extensive shallow rockslides after the Kashmir Mw 7.6 earthquake (American Geophysical Union, 2016)

In Iran, the Avaj earthquake of June 22, 2002 took place about 250 km west of Tehran. The earthquake which had Mw = 6.5 triggered 550 landslides over an area of about 3600 km^2 (Mahdavifar, Solaymani, & Jafari, 2006). However, Mahdavifar et al. (2006) further highlight that the landslide data base of Iran developed in 1996 by the Iranian government has, at the time of producing their paper, recorded over 14,000 seismic and non-seismic landslides throughout Iran.

American Continent

Moving to American continent, In the Caribbean region the 12 January 2010 M_w 7.0 Haiti earthquake triggered > 4490 landslides, mainly shallow, disrupted rock falls, debris-soil falls and slides, and a few lateral spreads (Figure 4.7) over an area of ~ 2150 km^2 (Gorum et al., 2013). The death toll estimates ranged from 100,000 to about 160,000. Gorum et al. (2013) attributed the occurrence of the 2010 Haiti earthquake landslides to a an amalgamated impact of intricate rupture dynamics and topography as principal controls.

In addition to the Haiti earthquake landslides, the Tecomán Mw 7.6 earthquake which took place close to the western coast of the Mexican state of Colima on 22 January 2003 induced a reported 103 landslides and had a volume of 32,265 km^3 (Keefer, Wartman, Navarro, Rodriguez-marek & Wieczorek, 2006). Keefer et al. (2006) further explain that the Government of Mexico reported 30 fatalities and 500 injuries directly linked to the seismically induced landslides.

Figure 4.7 Destroyed houses as seen on a hillside due to EI landslides after the 2010 Mw 7.0 Haiti earthquake (Xu, Shyu & Xu, 2014)

In South American continent, In Chile, On January 22, 2007, an unusual seismic swarm of shallow earthquakes (focal depths < 10 km) began in the Aysén Fjord (45.3° S, 73.0° W).

The Aysén Fjord earthquake shaking triggered a number of landslides along the fjord coast in and near the epicentral area and total area affected by landsliding was 59km^2 (Figure 4.8) (Sepúlveda, Serey, Lara, Pavez, & Rebolledo, 2010). The most common type of landslide reported were soil–rock slides, with 282 Mapped events, followed by soil slides with 135. Furthermore, Sepúlveda et al. (2010) indicate that most of landslides induced by the earthquake and majority of failures occurred between 5 and 15 km from the epicentre.

In the same South American continent, the Mw 8.0 Pisco earthquake occurred along the seismically active western coast of Peru. Overall, 520 fatalities were recorded and over 1000 persons were injured in the earthquake (Wartman, Cox, Meneses, Moreno & Olcese, 2008). The Piasco event was recorded by several strong motion seismographs in the region with horizontal peak ground acceleration values as high as 0.50g. Lacroix, Zavala, Berthier & Audin (2013) reported a total of 866 large landslides that covered an area of 1.29 km^2.

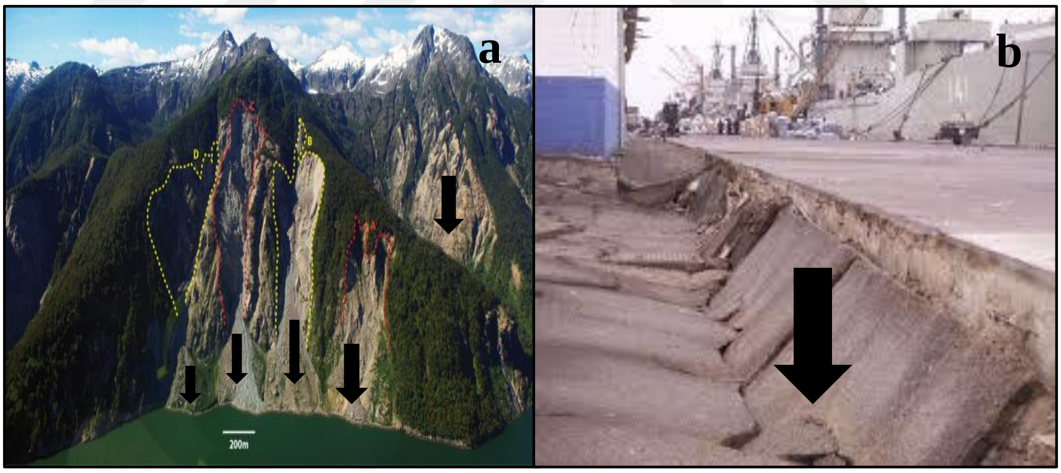

Figure 4.8 (a) A section of the EI landslides during the Aysén Fjord 2007 earthquake (Sepúlveda et al., 2010) and (b) road sliding after the Mw 8.0 Pisco earthquake in Peru (Natural hazards, n.d)

In Central America, the 2002 Denali earthquake in Alaska caused mass landslides. The earthquake that measured Mw 7.9 on Richter scale occurred close to Denali fault triggering an estimated 10,000 landslides, primarily rock falls and rock slides (Figure 4.9a) (Jibson et al., 2004).

The 2002 Denali earthquake landslides ranged in volume from rock falls of a few cubic meters to rock avalanches having volumes as great as $15x10^6$ m^3.

The 13th January 2001 Elsavado earthquake (Mw 7.7) reportedly generated more than 600 landslides (Figure 4.9b). The earthquake's epicentre located off the western coast of El Salvador in the subduction zone between the Cocos and Caribbean plates (Garc-Rodr´ıguez, 2010). On 17th January, 1994 Northridge, California earthquake (*Mw*=6.7) instigated widespread damage and economic losses, But one of the most momentous geologic impact of the earthquake was the triggering of thousands of landslides. It was reported that the Northridge earthquake triggered more than 11,000 landslides over an area of about 10,000 km^2 in a pattern that is roughly concentric about the epicentre and they caused severe damage (Figure 4.9c) (Parise & Jibson, 2000). The figure of the landslides for the Northridge earthquake is almost similar to the landslides caused by the September 21, 1999, Chi-Chi Earthquake in which over 10,000 landslides were triggered (Khazai & Sitar, 2003).

In the same region, the 1989 Loma Prieta, California earthquake M_w 6.9 caused 4,000 landslides throughout an area of about 15,000 km^2 in central California (Figure 4.9d) (Keefer, 2000). Despite the fact that the earthquake hypocentre was under a relatively sparsely populated, Keefer (2000) reported that 62 people lost their lives. Additionally, the landslides triggered by the earthquake killed one person, blocked numerous roads, and damaged or destroyed more than 100 residences and other structures.

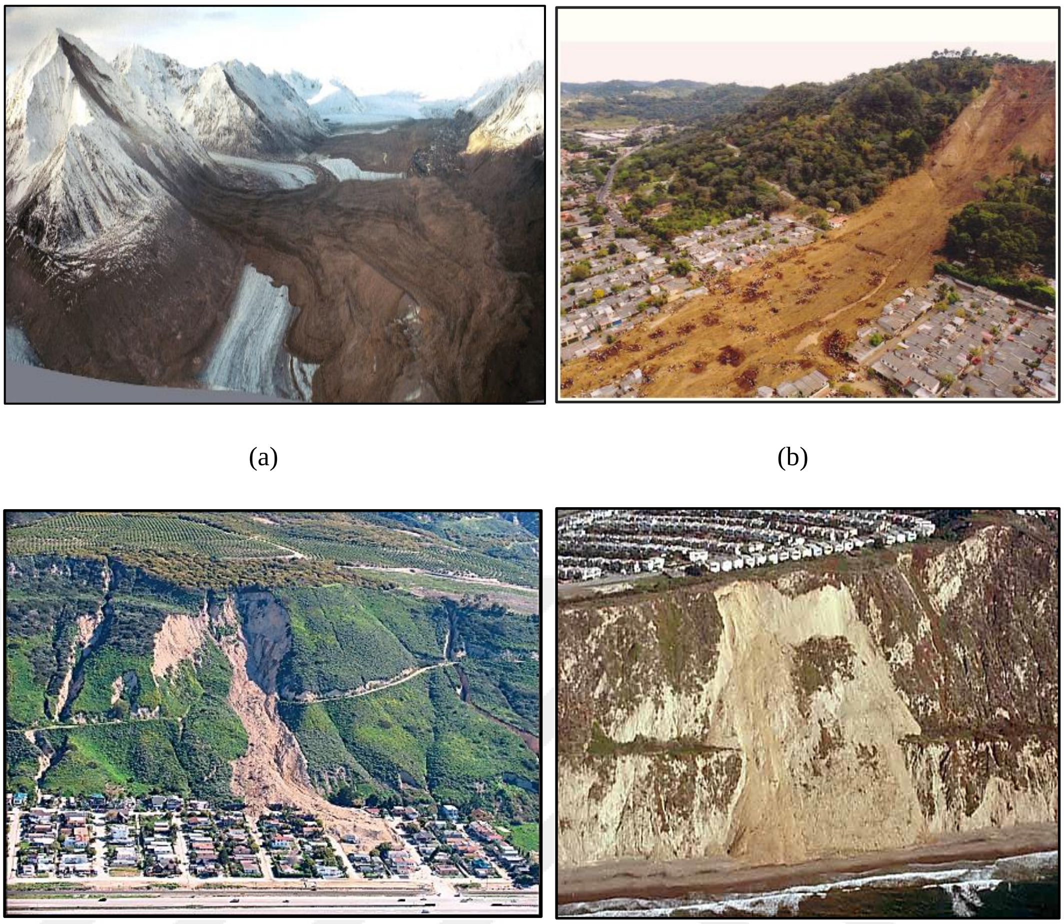

(a) (b)

(c) (d)

Figure 4.9 EI landslides during: (a) the 2002 Denali (Jibson et al., 2004), (b) the 2001 Elsavado (Garc-Rodr´ıguez, 2010), (c) the 1994 Northridge (Parise & Jibson, 2000) and (d) the 1989 Loma Prieta (Keefer, 2000) earthquakes respectively.

European Continent

European content, in comparison with the Asian and of course American continent, is not known for EI landslides, but it is not spared of landslides. Delgado et al. (2015) highlights that most EI landslide inventories have been reported for earthquakes of magnitudes > 6.0, and that the study of EI landslides for earthquakes of lower magnitude is still uncommon. However, on 11 May 2011, an earthquake Mw 5.1 occurred in the city of Lorca in Spain at a focal depth of 3 km.

Field inspection of the area affected by Alfaro et al. (2012) culminated into location and characterization of more than 250 induced landslides, mainly of disrupted type (rock/soil falls, disrupted soil slides and rock avalanches). The landslides after the Lorca earthquake reportedly covered an area of approximately 1000 km^2 and led to 9 fatalities (Alfaro et al., 2012).

In Italy, the Umbrian-Marche, 1997-1998 earthquakes (Mw 5.8) with a focal depth of 7 km caused 1700 landslides. It is reported that the landslides affected an area as large as 2000km^2 (Esposito, Porfido, Simonelli, Mastrolorenzo, & Iaccarino, 2000). The earthquake took place on a fault plane causing a rupture of up to 25 km along the fault plane. Esposito et al. (2000) identified the landslides as comprised of 60% rock fall, 35% rotational and translation slides.

Turkey, located in the seismically active Eurasian zone, has also been affected by the several earthquake but not much EI landslides has been reported. On 01st May 2003, a major earthquake (Mw = 6.4) hit Bingöl, eastern Turkey. Lozıos, Lekkas & Danamos (2004) descibe the earthquake as having the epicentre located at 38.991N, 40.462E and the focal depth was 25 Km. The earthquake caused considerable damage; approximately 174 deaths, 520 injuries 2000 buildings collapse occurred including surface raptures and geotechnical effects -mainly landslides (Lozıos et al., 2004). Seismically triggered landslides were reported by Aydan, Ulusay, & Miyajima (2003) to have occurred in the form of rotational or shallow-seated planar failures, rock falls and 45 mudflows (Figure 4.10). According to Aydan et al. (2003) the landslides were generally widespread close to the epicentre of the earthquake and the depth and type of the landslides were primarily controlled by the degree of weathering.

On 17th August and 12th November, 1999 an earthquake of magnitude 7.4 and 7.2 struck Turkey in İzmit (Kocaeli) and Duzce respectively (Tang, 2000). The earthquake, which caused 15,000 fatalities and left 27,000 people injured and 200,000 homeless, occurred along the Duzce fault, south of Duzce city east of Istanbul.

Occurrence of landslides following the 1999 earthquake have been reported in; the eastern part of Avcilar peninsula, Istanbul where the Büyükçekmece landslide was located (Bourdeau, Lenti, Martino, Ozel, & Yalcinkaya, 2015), Bakacak, Bolu region where landslides removed two lanes of the four-lane highway (Tang, 2000 ; Aydan & Ulusay, 2002) and in Degirmendere nose along the southern coast of İzmit Bay, Kocaeli (Cetin, Isik, & Unutmaz, 2004). However, absolute Figures of the landslides have not been precisely documented by the authors.

Figure 4.10 EI landslides during the 2003 Bingöl earthquake (Aydan et al., 2003)

African Continent

It is very uncommon for earthquakes to occur in Africa given its seismically non active location on the globe. But even in the slightest of the probability, geo-hazards take place. On 21st May 2003, a damaging earthquake of Mw: 6.8 struck the region of Boumerdès 40 km east of Algiers in northern Algeria. The 10 seconds lasting earthquake which took place at a focal depth of 12km is reported by Bouhadad (2010) to have caused over 24 landslides and led to approximately 2,266 deaths and 10,261 injuries. The Boumerdes earthquake was followed by the 20th, 2006 a moderate-sized earthquake (Mw=5.2) which affected the Laalam (NE- Algeria) region, however, there was no precise quantification of the landslides.

Table 4.1 Summary of historic earthquakes that induced landslides between 1998 and 2015

No	Date	Name	Magnitude (Mw)	PGA (g)	Focal depth (km)	Duration (sec)	Fault Type*	Fault Length(km)	Reported No of Landslide	Landslide area (km^2)	Source†
1	04/05/2015	Matukutuki NZ	5.8	0.11	5	120	SSF	-	37	800	C
2	25/05/2015	Gorkha, Nepal	7.8	0.35	15	50	TF	160	25,000	1,000	A
3	20/05/2013	Lushan	6.6	1.00	13	20	TF	35	3810	2200	T
4	18/09/2011	Sikkim, India	6.9	0.55	10	10	TF	68-119	210	22.2	C_2
5	11/03/2011	Tohoku, Japan	9.0	0.80	24	360	TF	500	3477	28380	H, F & T
6	11/05/2011	Lorca, Spain	5.1	0.39	3	8	SSF	85	250	1000	A
7	22/02/1998	Christchurch, NZ	6.0	0.80	5	20	SSF	-	>200	-	D & K
8	14/05/2010	Yushu, China	6.9	0.38	17	15	SSF	30-51	2,036	1194	X&X
9	12/01/2010	Haiti	7.0	0.55	13	30	SSF	65	> 4490	2150	G
10	27/02/2010	Maule, Chile	8.8	0.65	35	180	TF	500	410	74131	D
11	30/11/2009	Sumatra, Indonesia	8.0	0.60	71	15	TF	60	89	-	U
12	12/05/2008	Wenchuan, China	7.9	0.62	19	60	TF	200	>15,000	1,160	Q
13	14/06/2008	Iwate-Miyagi , Japan	6.9	1.00	8	10	TF	20	4161	600	Y
14	21/04/2007	Aysen Fjord, Chile	6.2	0.50	10	-	SSF	12	538	17000	S
15	16/07/2007	Niigata Chuetsu–Oki	6.6	1.01	10	10	TF	38.5	70	250	C, K & T
16	15/09/2007	Pisco, Peru	8.0	0.50	39	48	TF	103	866	-	W
17	08/10/2005	Kashmir, Pakistan	7.6	0.56	10	25	TF	75	2,424	61	H & C
18	23/10/2004	Mid-Niigata, Japan	6.6	0.48	14	30	TF	22	>1,353	250	K
19	21/01/2003	Tecoman, Mexico	7.6	0.38	24	30	TF	50	103	-	Kc
20	01/05/2003	Bingöl, Turkey	6.4	0.55	15	-	SSF	360	>45	-	L & A
21	21/05/2003	Boumerdes, Algeria	6.8	0.58	12	10	TF	36	24	39	B
22	22/06/2002	Avaj, Iran	6.5	0.50	7.5	7	TF	13	14000	3600	M,S & J
23	03/11/2002	Denali fault, Alaska	7.9	0.36	5	140	TF	336.35	10,000	90,000	J

Table 4.1 Summary of historic earthquakes that induced landslides between 1998 and 2015

No	**Date**	**Name**	**Magnitude** (Mw)	**PGA** (g)	**Focal depth (km)**	**Duration** (sec)	**Fault Type***	**Fault Length(km)**	**Reported No of Landslide**	**Landslide area (km^2)**	**Source[†]**
24	13/02/2001	Elsavado	7.7	0.60	60	43	NF	65	600	-	G-R
24	28/03/1999	Garhwali	6.8	0.35	15	-	TF	16	394	226	B_a
26	21/09/1999	Chi-Chi, China	7.5	0.75	33	40	TF	125	>10,000	127.8	Ka & S
27	26/09/1998	Umbria-Marche, Italy	5.8	0.56	7	-	NF	25	>1700	2000	E
28	17/01/1994	Northridge, California	6.7	0.64	19	20	TF	15	>11,000	10,000	P & Ja
29	13/10/1993	Finisterre Papua New Guinea	6.9	0.35	19	20	TF	75	>4700	55	M, H & H
30	17/10/1989	Loma Prieta USA	6.9	0.65	19	15	OF	35	4,000	15,000	Kb

*TF = Thrust Fault, OF = Oblique-slip Fault, SSF = Strike Slip Fault, NF = Normal Fault

− = Data unavailable

†Table 4.2 Data sources referenced in Table 4.1

C	Cox et al (2015),	H & C	Harp & Crone,
A & U	Aydan and Ulusay (2015)	K	Kieffer et al (2006)
T	Tang et al. (2015	Kc	Keefer et al. (2006)
C_2	Chakraborty et al. (2011	L & A_2	Lozıos et al. (2004) & Aydan et al. (2003),
A	Alfaro et al. (2012)	B	Bouhadad (2010)
D & K	Dellow et al. (2011) and Kaiser et al. (2012)	M, S & J	Mahdavifar et al. (2006)
X & X	Xu & Xu (2014),	J	Jibson et al., 2004
G	Gorum et al. (2013),	G-R	Garc-Rodr´ıguez (2010)
H, F &T	Hashimoto et al. (2012)	B_a	Barnard et al. (2001)
D	Delgado et al. (2011)	Ka & S	Khazai & Sitar (2003)
U	Umar et al, 2014),	E	Esposito et al. (2000)
Q	Qi et al. (2010)	P & Ja	Parise & Jibson (2000)
Y	Yagi et al. (2009	M, H & H	Meunier et al. (2007)
S	Sepúlveda et al. (2010)	Kb	Keefer (2000)
C,K &T	Collins et al. (2012a)	W	Wartman et al. (2013)

4.1 Types of Earthquake Induced Landslides

Keefer (1984) and Rodriguez, Bommer & Chandler (1999) observed that various types of EI landslides happen with distinct rates. Rock falls, disrupted soil slides, soil slumps and rock slides appear to be the most common types of landslides observed while subaqueous landslides, slow earth flows, rock block slides, and rock avalanches tend to be least common (Figure 4.11). Keefer (1984) argued that the challenges in observing subaqueous slides may contribute to their apparent rarity.

Additionally, the EI landslides types by some recent major earthquakes were evaluated and results are presented in Figure 4.12 and 4.13. The trend on frequency of the occurrence of landslides by type indicate that rock falls, disrupted soil slides, soil slumps and rock slides appear to be the most common types of landslides whereas earth flows and lateral spreads are the least common (Figures 4.12 & 4.13). Although the outcome is in concordance with the cases reported by Rodriguez et al. (1999) in Figure 4.11 there is a need to standardise the EI landslides type classification for uniformity of presentation.

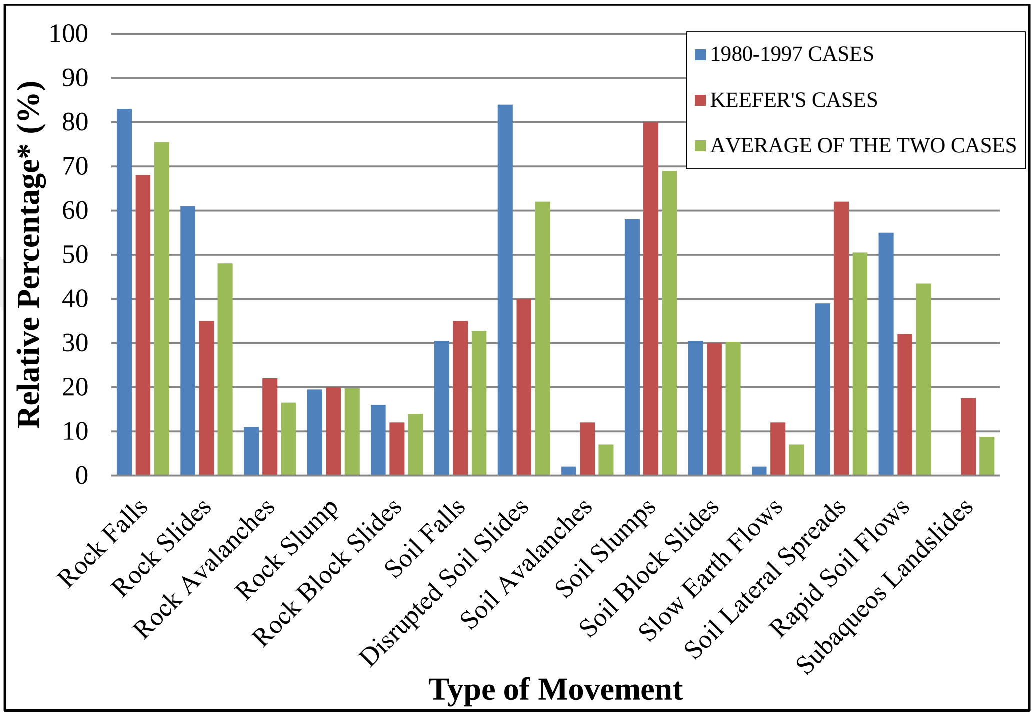

Figure 4.11 Relative frequency of types of landslides during earthquakes[3] (Rodriguez et al., 1999)

[3] In Figure 4.13 *Relative percentage is defined as the ratio between the number of earthquakes in each type occurred and the total number of earthquakes studied in each database.

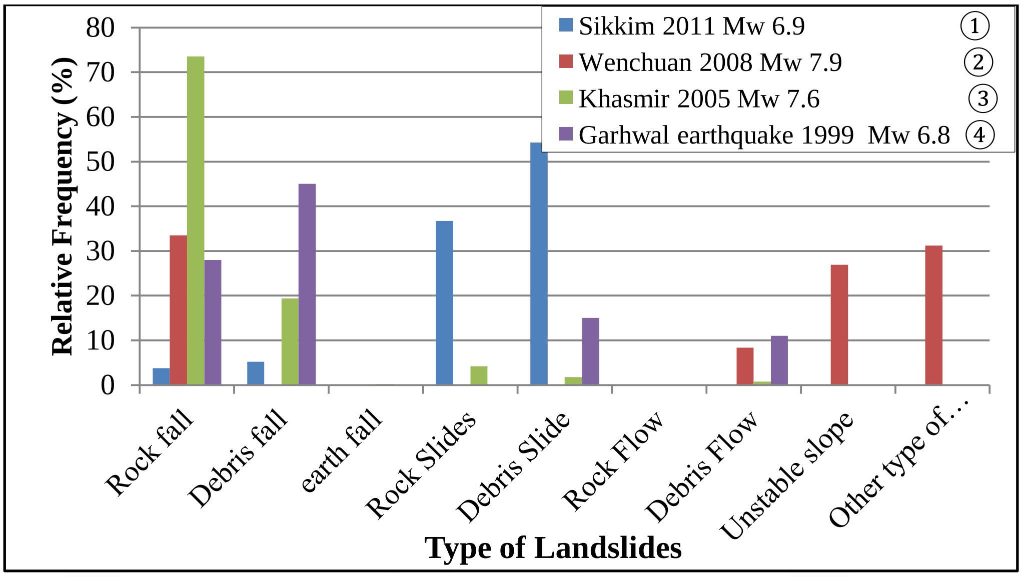

Figure 4.12 Relative frequency of types of landslides during earthquakes (data from ①Chakraborty et al., 2011, ②Qi et al., 2010 and ③Khazai & Sitar, 2004)

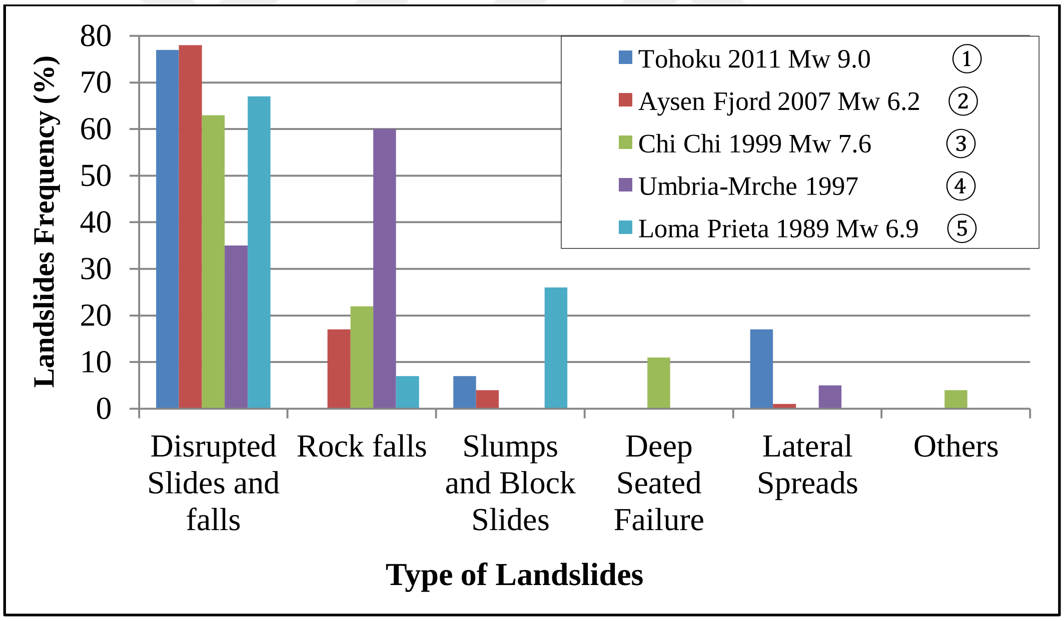

Figure 4.13 Relative frequency of each type of landslides during earthquakes (data from ①Hashimoto et al., 2012, ②Sepulveda et al, 2010, ③Khazai & Sitar, 2004, ④Esposito et al., 2000 and ⑤Keefer, 2000)

4.2 Methodology for the Analytical Study

In order to accomplish the first principal objective of this study, which is to document earthquakes that triggered landslides occurring between 1998 and 2015 in the world and evaluate the factors that contributed to the landsliding activities, a comprehensive and rigorous review of data on landslides induced by earthquakes that occurred between 1998 – 2015 and studies of some well documented historical EI landslides was performed. Data review entailed collecting all relevant information on EI landslides instigated by historical major earthquakes in the world presented in Table 4.1. In the analysis, some major well documented cases: the Northridge, California 1994, the Finisterre Papua New Guinea 1993 and the Loma Prieta USA 1989 were included for representativeness and validation of the study. Reviewed information sources include; scientific and technical papers, technical reports, seismological and landslides data from USGS. Valuable data was also gotten from internet sites and relevant books on EI landslides.

In this analytical review aspect of the study, I investigated the published EI landslides information from across the globe which occurred between 1998 -2015. In the analysis, a quantitative technique of data analysis was applied to correlate variables so as to understand their relationship. To perform the quantitative analysis Microsoft Excel and CorelDraw programs were applied to produce; frequency diagrams, tables and correlation diagram to appreciate the controlling factor's relationship. In assessing the susceptibility to EI landslides, the following parameters: earthquake parameters (magnitude, PGA, Arias intensity, focal depth and epicentral distance), geological parameters (lithology and fault type) and topographic parameters (slope angle, elevation, slope aspect and slope curvature) were taken into consideration (Figure 4.14).

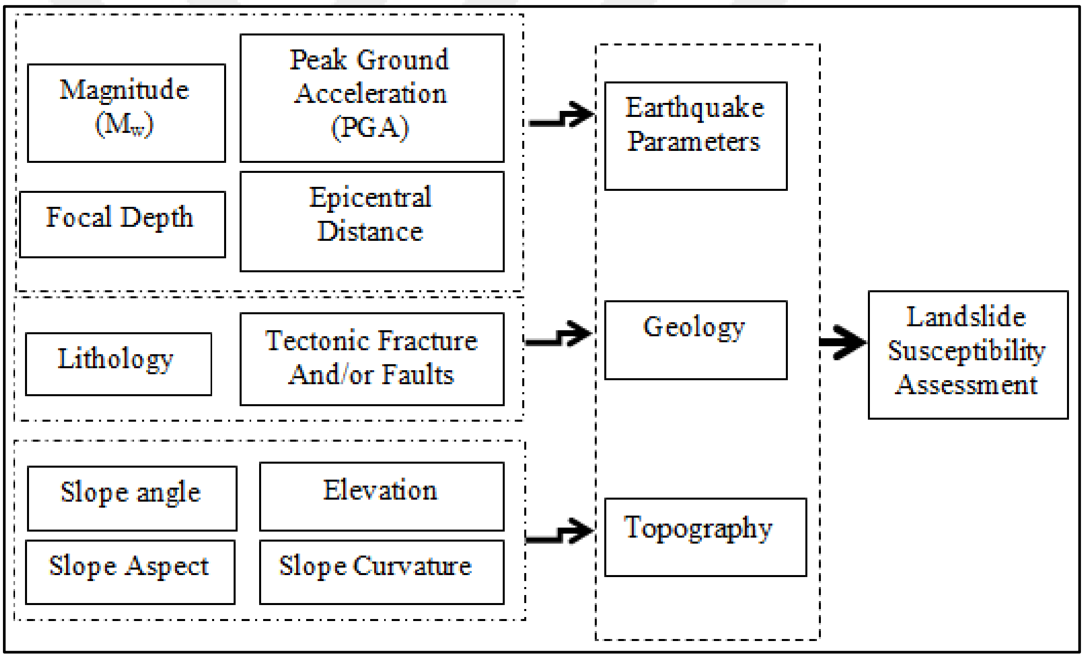

Figure 4.14 Flow-chart of the methodology used for assessing the EI Landslides

4.3 Earthquake Induced Landslides Controlling Factors

The susceptibility to sliding due to earthquakes has been extensively studied by Keefer (1984), Khazai & Sitar (2003), Qi et al. (2010), Xu & Xu (2014), Tang et al. (2015), Kamp & Owen (2016) among many authors. Most of these studies attempted to understand the role of: geological structure of the slope, seismic parameters, lithology and weathering condition of the rocks, hydrological and the state of morphological development of the area in inducing landslides.

Zaruba and Mencl (1982) stress that it is critical to realise and understand the conditions that cause slopes to become unstable. A great variety of slope movements reflect the miscellany and complexity of factors that may perturb slope stability. However, it is crucial to draw a clear distinction between causative and triggering factors. According to keefer (1984) and Zaruba & Mencl (1982) trigger events are the external or internal processes that make the slope to collapse at a particular point, in most cases include heavy rainfall or in this case earthquakes. On the other hand causative factors are those processes that have made the slope susceptible or vulnerable to failure, which include; weathering of rocks, deforestation etc. Realising that only accurate investigation would make it feasible to appreciate the extent of the danger of landslides and assist in proposing effective remedial measures, this study makes a deliberate effort to understand the interplay of the causative factors that act as catalysts to the triggering factor (s).

4.3.1 Seismic Parameters

4.3.1.1 Earthquake Magnitude

According to Keefer (1984), the strength of the earthquake shaking is a major parameter that determines the occurrence of landslides. Based on this statement, in the scope of this study, efforts were made to establish a relationship between earthquake magnitude and number of landslides during and/or after an earthquake. Figure 4.17 presents the relationship of earthquake magnitude and number of reported landslides.

The trend in Figure 4.15 suggests the significance of the role played by other factors such as geology and topography in influencing the occurrence of EI landslides.

To assess the likely impact of the EI landslides in an area, a relationship between earthquake magnitude and area affected by the landslides was carried out. The relationship of earthquake magnitude and the area affected by landslides for the major earthquakes (1998-2015) is presented in Figure 4.18. In this Figure 4.16 the upper bound curves presented by Rodriguez et al. (1999), Keefer and Wilson (1989) and Keefer (1984) are shown. Plotted values of the investigated EI Landslides areas with respect to the magnitude of earthquakes are apparently clustered just below the upper bounds with a few outliers above the curves (Figure 4.16).The curves are also observed to approach an area of A = 0 at M_w 4.0.

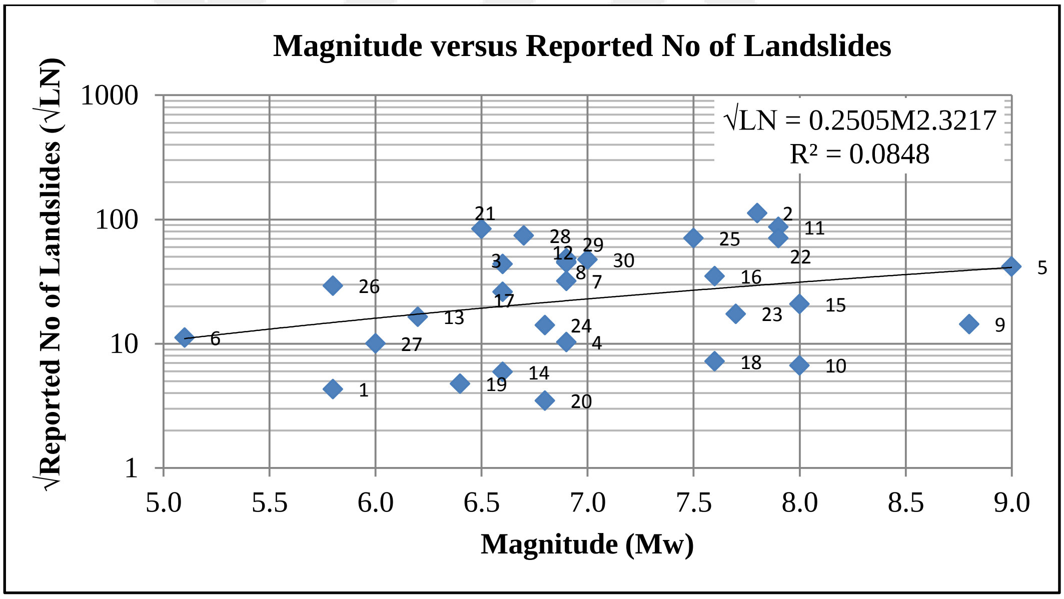

Figure 4.15 Relationship between earthquake magnitude and number of reported landslides (Numbers represent cases presented in Table 4.1)

In order to find a fitting model to better explain the relationship between magnitude and area affected by landslides, a statistical approach was adopted.

The statistical equation applied to evaluate the correlation between magnitude and area affected by EI landslides involved taking the square root of the area affected by EI landslides. It can be observed that there is a fairly weak correlation between the earthquake magnitude and the square root of area affected by the landslides (Figure 4.17). The coefficient of determination of R^2 = 0.28 supports the assertion that magnitude has somewhat an influence on the area affected by EI landslides.

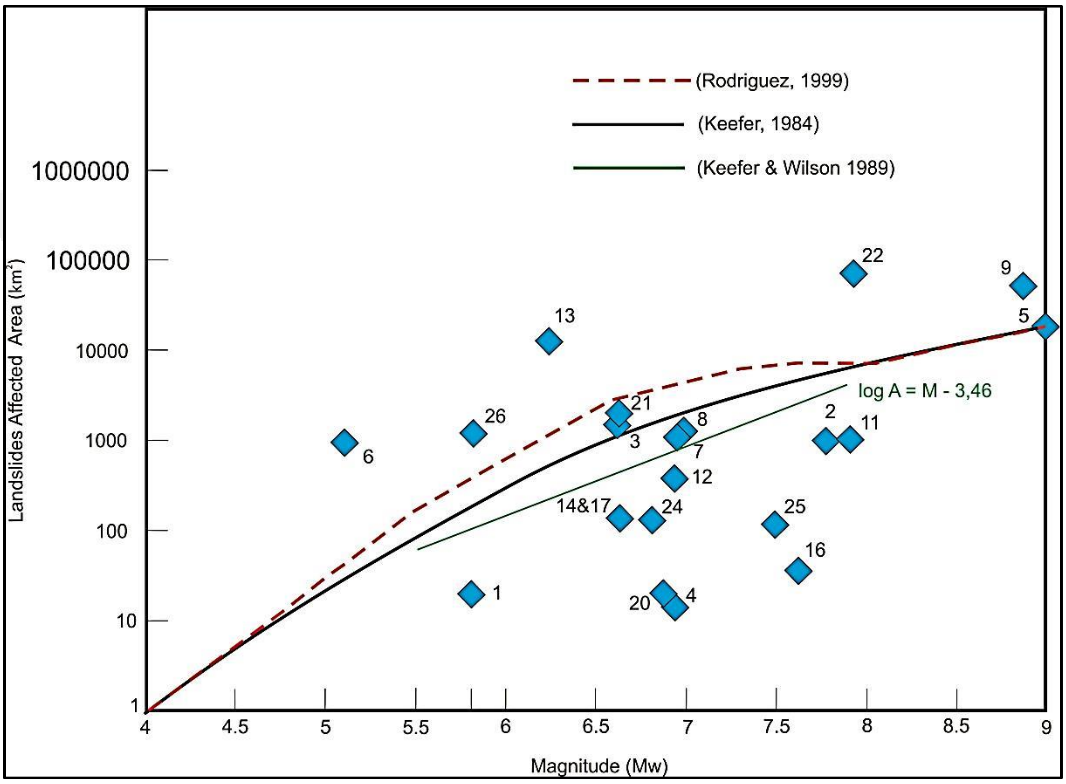

Figure 4.16 Relationship between earthquake magnitude and the area affected by landslides after (Numbers represent cases presented in Table 4.1)

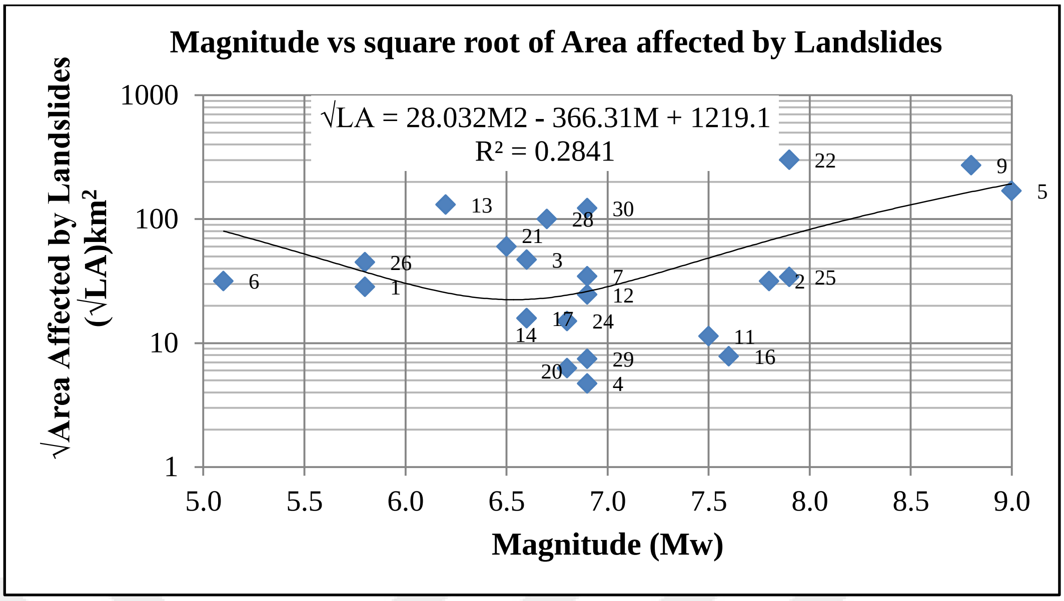

Figure 4.17 Relationship between earthquake magnitude and area affected by EI Landslides

An effort has also been made to establish a relationship between earthquake magnitude and the estimated volume of landslides. The estimated volume was obtained using the formula derived by Wartman, Dunham, Tiwari and Pradel (2013). The volume is estimated from the area affected by landslides using equation 4.3.

$$V = \alpha(A)^{\gamma} \tag{4.3}$$

Where:

V - Volume (m^3),

A- Landslides surface are (m^2)

α - 0.25 and γ - 1.36 are empirical constants.

The empirical parameter α = 0.25 and γ = 1.36 are taken into account when computing the volume of the landslides. According to Wartman et al. (2011), the empirical constants are based on a comprehensive review of the 150 published landslide area and volume relationships.

It can be observed that when a mathematical approach is adopted by taking a square root of the estimated volume, a very weak correlation is obtained (Figure 4.18). The coefficient of determination is noted to be $R^2 = 0.30$

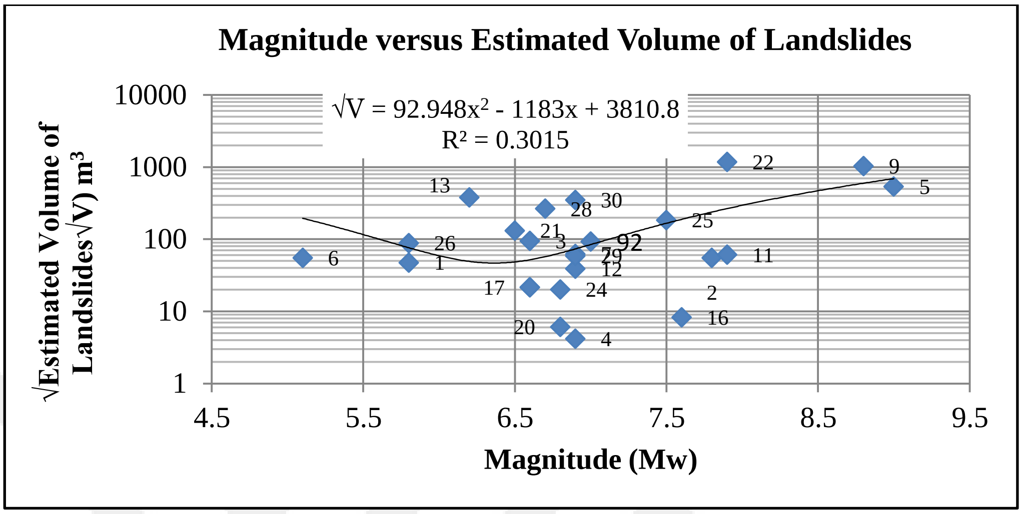

Figure 4.18 Relationship between earthquake magnitude and the estimated volume of landslides (Formula $\boldsymbol{V} = \boldsymbol{\alpha}(\boldsymbol{A})^{\boldsymbol{\gamma}}$ by Wartman et al., 2011) (Numbers in the Figure represent cases in Table 4.1).

4.3.1.2 Peak Ground Acceleration (PGA)

Khazai & Sitar (2004) defined PGA as a measure that describes the earthquake shaking reasonable to trigger landslides. The plot of PGA versus studied landslides is shown in Figure 4.21. A glance at the figure reveals that there is only one reported landslides event where PGA ≤ 0.3g. Scatter plot of the PGA of the major earthquakes against number of reported landslides has given a scatter pattern clustered between 0.35g to 0.8g. However, there is no correlation between PGA and reported number of landslides. For instance, while the Gorkhan, Nepal earthquake of 2015 with a PGA of 0.35g recorded 25,000 landslides while the Niigata, Chuetsu-Oki Japan earthquake of 2007 with a PGA of 1.01g only caused 70 landslides. Thus, a good relationship of the two variables can be made if comparisons are made in the same geological and topographic settings. Single case studies by Keefer (2000), Parise & Jibson (2000) Khazai & Sitar (2004), Collins et al. (2012a), revealed a strong positive correlation between PGA and EI landslides

Another point to notice is that there seems to be a threshold value of PGA ≥ 0.3g for landslides occurrence during studied earthquakes except for Matukutuki earthquake which had a PGA of 0.11g (Figure 4.19). This threshold PGA value is in agreement with the findings of Khazai & Sitar (2004) who made a comparative study of the Chi-Chi (1999), North Ridge (19994) and Loma Prieta (1989) earthquakes.

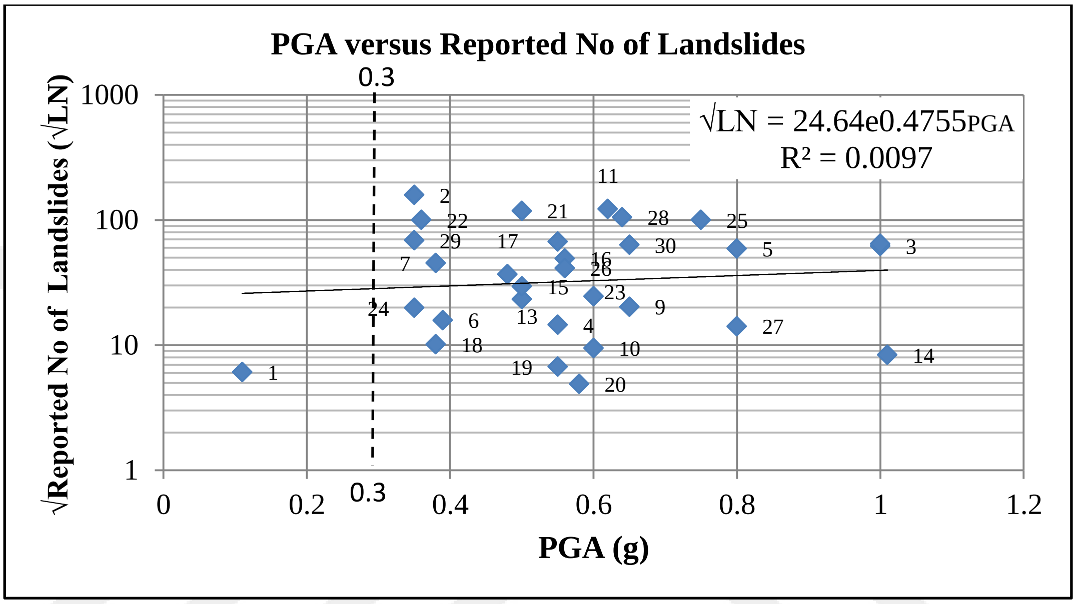

Figure 4.19 Relationship of PGA and number of landslides occurrence (Numbers inside the Figure represent cases presented in Table 4.1)

In order to understand the role of ground shaking duration in inducing landslides during and/or after an earthquake, PGA of earthquake was multiplied by duration of earthquake shaking and plotted against reported number of landslides. The plot of PGA*t versus reported number of landslides is given in Figure 4.20. It can be observed from Figure 4.20 that when the duration of earthquake shaking is integrated in the analysis a slight increase in the coefficient of determination value is obtained showing the impact of time taken by an earthquake. The R^2 value rose from as low as R^2 = 0.01 (PGA only) to R^2 = 0.03 after incorporating duration of earthquake.

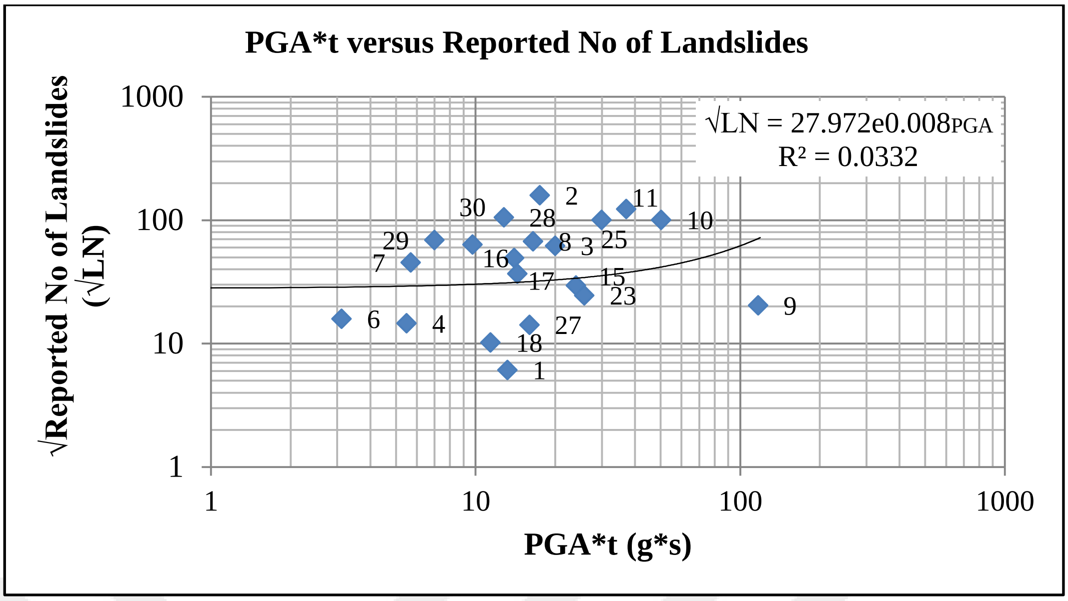

Figure 4.20 Relationship of PGA*t and number of landslides occurrence (Numbers inside the Figure represent cases presented in Table 4.1)

Attempt was also made to find out a relationship between PGA and the area affected by landslides and PGA times earthquake duration against the area affected by landslides (Figures 4.21 & 4.22). As it can be observed from Figure 4.21, there is no correlation between PGA and area affected by landslides. However, a weak linear positive correlation is obtained when the duration of earthquake shaking is incorporated (Figure 4.22). The coefficient of determination of $R^2 = 0.28$ clearly indicate that PGA*t has some influence on area affected by landslides. PGA*t gives the seismic shaking velocity. This velocity concept is reported by some investigators; (Saygili et al., 2008; Jibson, 2007) to characterise the earthquake properties.

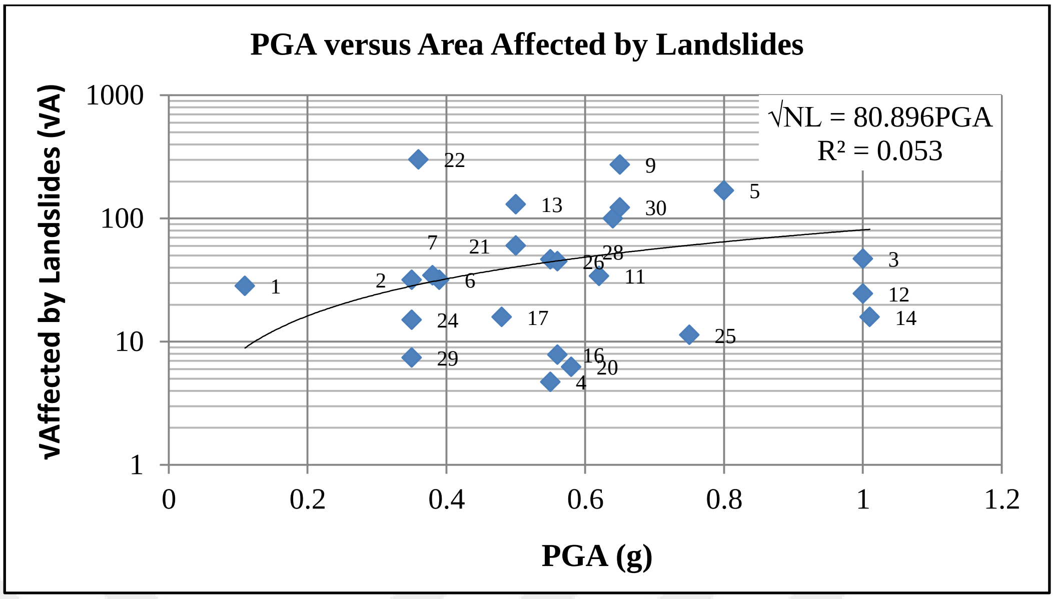

Figure 4.21 Relationship between PGA and area affected by EI landslides (Numbers inside the Figure represent cases presented in Table 4.1).

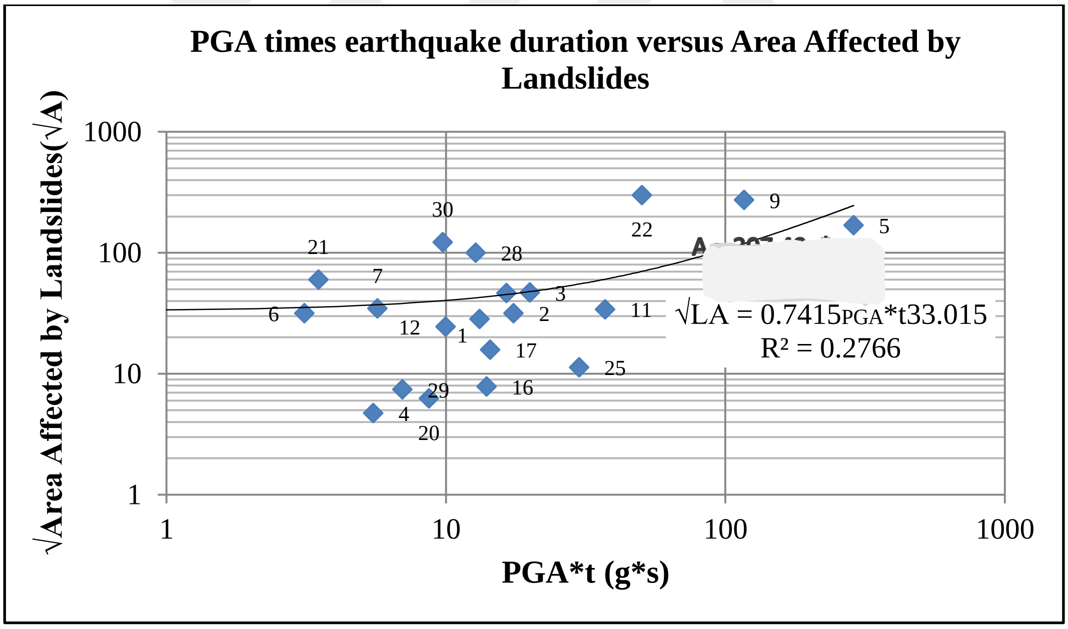

Figure 4.22 Relationship between PGA*t and area affected by EI landslides (Numbers inside the Figure represent cases presented in Table 4.1).

Furthermore, the study sought to understand the relationship between PGA and volume of landslides and PGA times time against volume of landslides (Figures 4.23 and 4.24). The estimated volume was derived from area affected by landslides using the formula given by Wartman et al. (2011). A similar trend, as in PGA and PGA*t against area affected by landslides, can be noted in a relationship between PGA and PGA*t and the estimated volume of landslides. It can be observed from Figure 4.25 that there is no relationship observed between PGA and estimated volume of EI Landslides. Nevertheless, when the duration of earthquake shaking is integrated a weak linear positive relationship is obtained (Figure 4.24). The coefficient of determination of R^2 = 0.26 value indicate that PGA*t has a significant effect on volume of landslides.

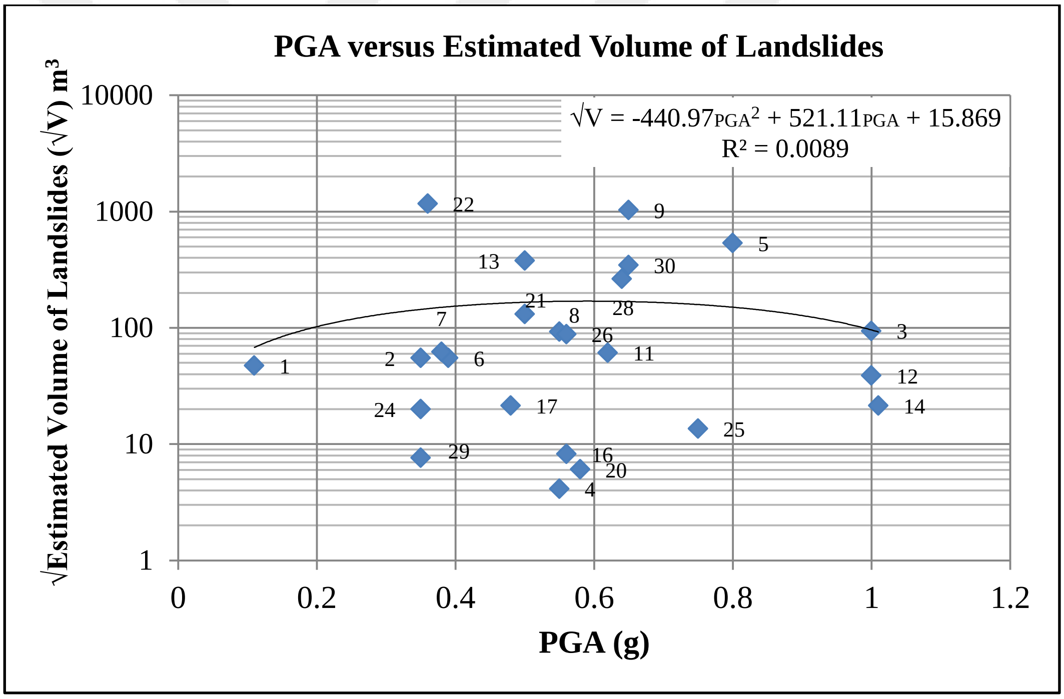

Figure 4.23 Relationship between PGA and estimated volume of landslides (Numbers inside the Figure represent cases presented in Table 4.1).

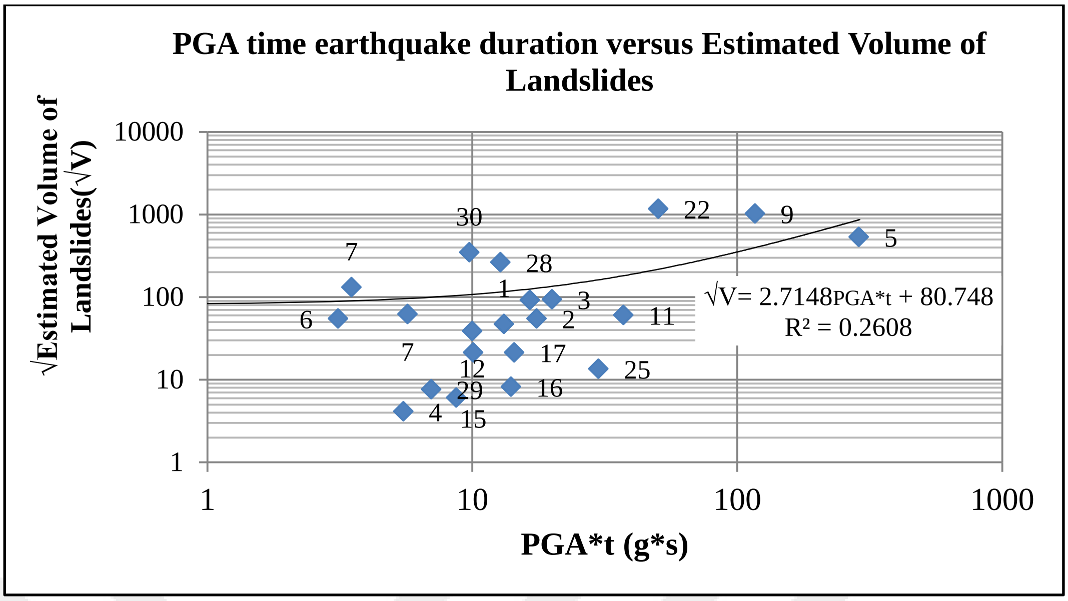

Figure 4.24 Relationship between PGA*t and estimated volume of Landslides (Numbers inside the Figure represent cases presented in Table 4.1).

4.3.1.3 Arias Intensity

To explore the role of earthquake duration further, another seismic parameter for ground shaking referred to as Arias Intensity was applied (I_A). The I_A is a measure of the strength of a ground motion developed by Arturo Arias in 1970. The measure was meant to determine the acceleration of transient seismic waves. Despite Arias's conviction that I_A is a more dependable parameter to interpret earthquake shaking needed to trigger landslides. The measure had not earned the support until the work of Wilson & Keefer (1993) who used the parameter. Although PGA is a widely used parameter to describe earthquake ground shaking, I_A is by far endorsed to be an improved seismic parameter (Chousianitis, Del Gaudio, Kalogeras, & Ganas, 2014 and Travasarou, Bray, & Abrahamson, 2003). Chousianitis et al. (2014) adds that the use of the I_A has been suggested to quantify the impact of seismic shaking on ground failure events more effectively.

I_A is derived after Wilson and Keefer (1993) as follows:

$$I_A = \frac{\pi}{2g}\int_0^{tf} \alpha(t)^2 \, dt \qquad (4.4)$$

Where:
g is acceleration due to gravity,
α (t) is recorded acceleration time-history and
tf is the duration of the ground motion.

The main advantage of I_A over PGA, according to Chousianitis et al. (2014), is that it measures the total acceleration content of the record other than just the peak value, offering a more complete characterisation of the shaking energy than PGA. Apart from that, I_A is recommended as objective and comparable from one earthquake to the other, making it a reliable indicator of the capacity of the earthquake shaking to trigger landslides. Hence, the study also attempted to assess the impact of I_A in inducing landslides and compare the results against the impact of PGA. The relationship between I_A and area affected by landslides is shown in Figure 4.25. The results indicate a good correlation between I_A and area affected by landslides with a coefficient of determination of R^2 = 0.46. In contrast, the relationship between PGA and area affected by landslides yielded a very low correlation with R^2 = 0.05. However, when PGA multiplied by duration of earthquake the coefficient of determination augmented to R^2 = 0.27 which indicates a fairly positive increasing trend against area affected by landslides. A critical look at the I_A equation reveals that it integrates time in its derivation. This evidently ascertains that time is a critical component in as far as magnitude and ground shaking is concerned.

A similar trend, as in I_A against area affected by landslides, can be noted in a relationship between I_A and the estimated volume of landslides. Figure 4.26 shows that there is a good correlation between I_A and estimated volume of landslides. The coefficient of determination for the relationship is R^2 = 0.45.

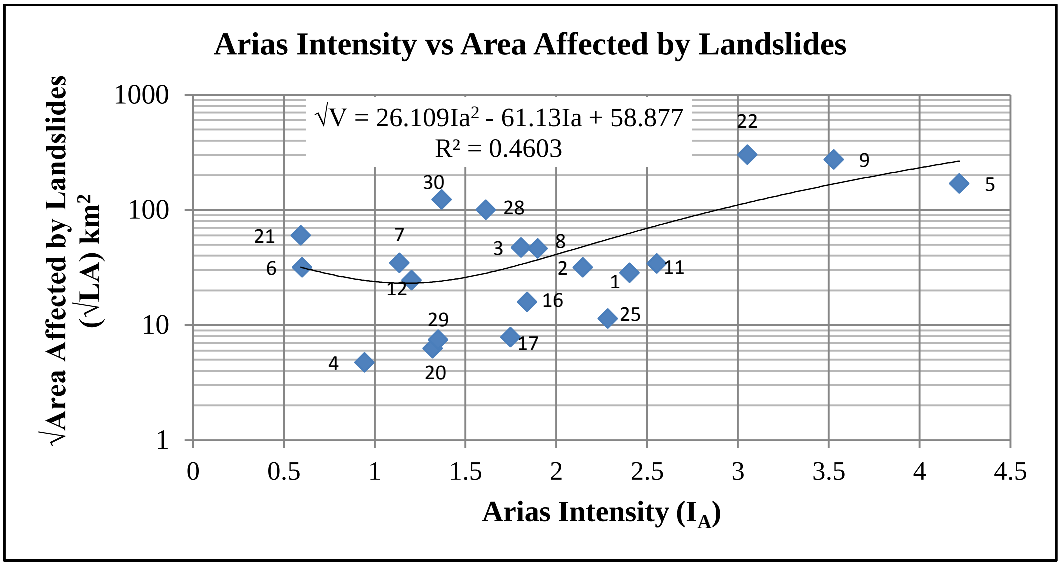

Figure 4.25 Relationship between I_A and area affected by EI landslides

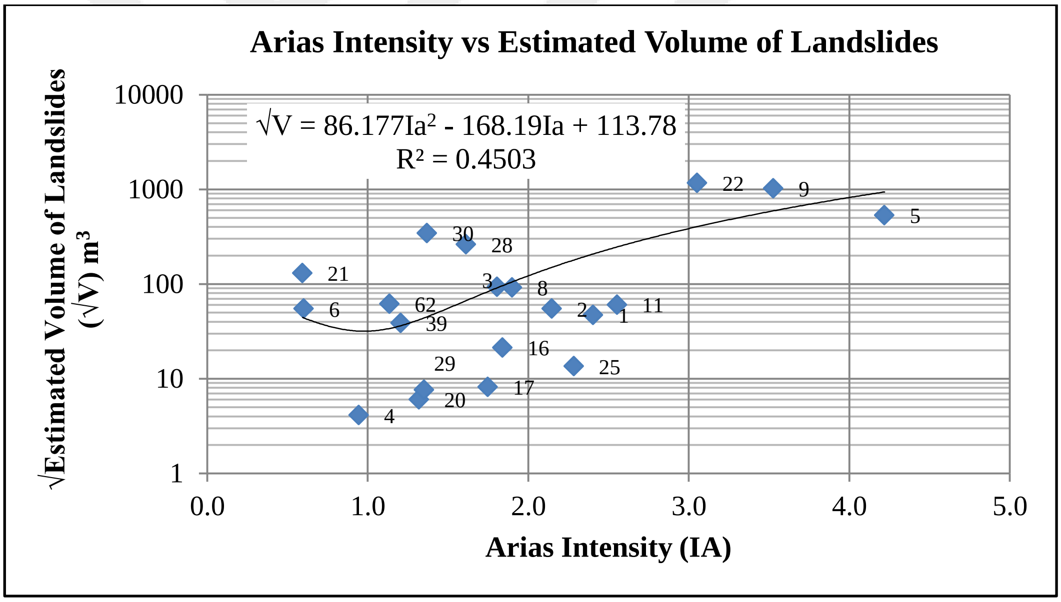

Figure 4.26 Relationship between I_A and estimated volume of EI landslides

4.3.1.4 Focal Depth

Focal depth describes the depth of an earthquake's focus or hypocentre to the epicentre. Keefer (1984) asserts that shallow focus earthquakes (≤ 35 km) are believed to generate widespread landslides that the deep seated focus earthquakes.

From Keefer's assertion, an effort was made to test the hypothesis. In the analysis of the studied earthquakes that caused landslides in the past two decades indicate that most of the EI landslides are concentrated within the focal depth ≤ 20 km and the occurrence of landslides is very sparse when the focal depth > 20 km. This supports the hypothesis that shallow earthquakes have a high likelihood of inducing landslides during and/or after an earthquake than earthquakes with seated hypocentre. The finding is in agreement with Keefer's (1984) findings who established a threshold of ≤ 35km after an analysis of 40 cases of earthquakes that induced landslides.

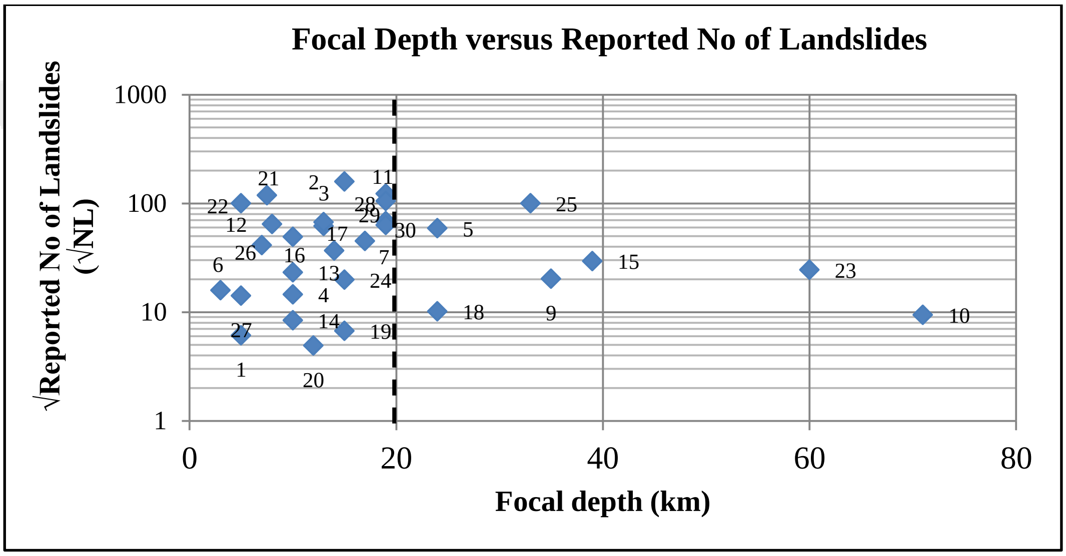

Figure 4.27 Relationship between focal depth and EI Landslides (Numbers inside the Figure represent cases presented in Table 4.1).

In the scope of the study, correlation between focal depth and area affected by landslides was also performed in order to understand the impact of focal depth on the extent of area affected by the landslides. The results of the relationship are presented in Figure 4.28.

It can be observed that the coefficient of determination ($R^2 = 0.01$) for correlation between focal depth and area affected by the landslides is extremely low. This is because landslides hardly occur at greater depth during and/or after an earthquake. It is also interesting to observe that landslides are concentrated within the depth ≤ 20 km. At depth > 20 km very few landslides have been recorded. This finding validates a study by Lei (2012). Lei (2012) produced a 3D diagram on earthquake magnitude, focal depth with landslides affected areas (Figure 4.30). He demostrated that most of the earthquakes that caused landslides had a focal depth of ≤ 30 km and as the magnitude of the earthquake increased, they seem to have caused landslides over wider area. However, Keefer and Wilson (1989) in their study found some earthquakes that had focal depth > 40 km. This emphasises the dominating influence of other factors other than just focal depth.

Since, estimated volume is computed from area affected by the EI Landslides, the results show similarities with results for area affected by landslides (Figure 4.29).

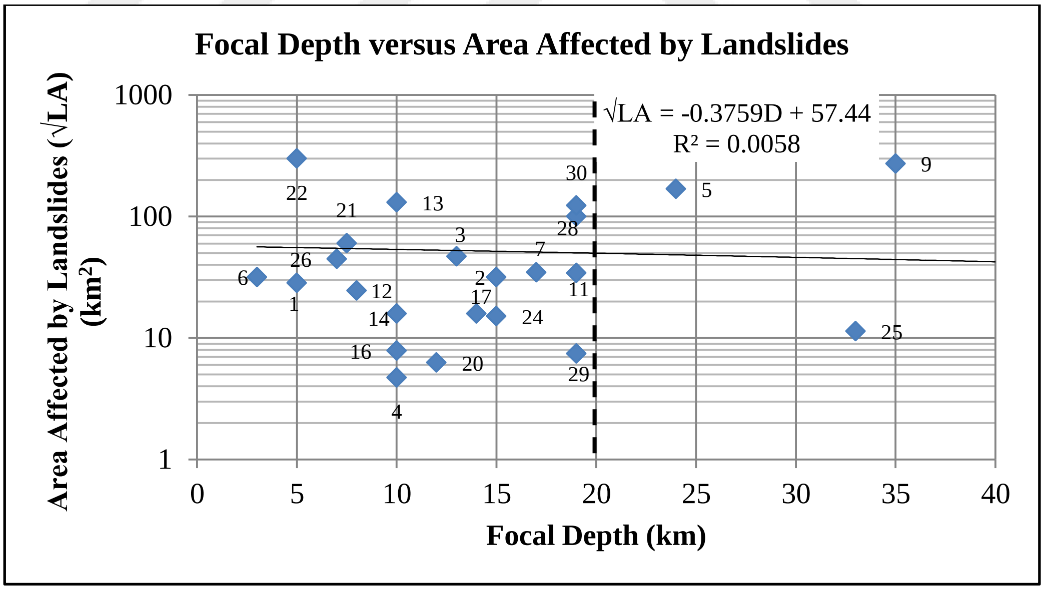

Figure 4.28 Relationship between focal depth and area affected by landslides (Numbers inside the Figure represent cases presented in Table 4.1).

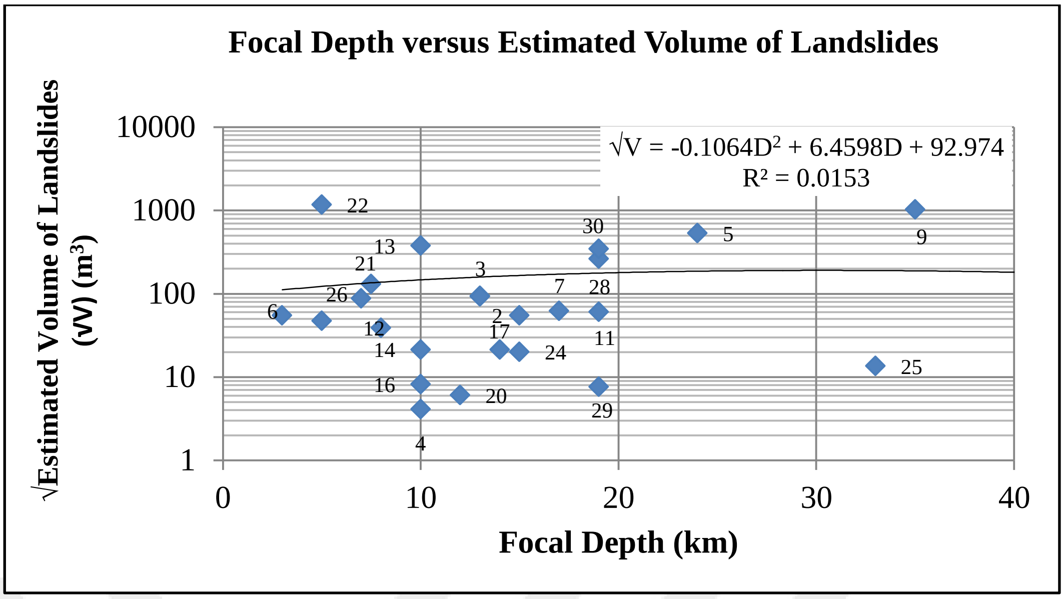

Figure 4.29 Relationship between focal depth and estimated volume of EI Landslides (Numbers inside the Figure represent cases presented in Table 4.1).

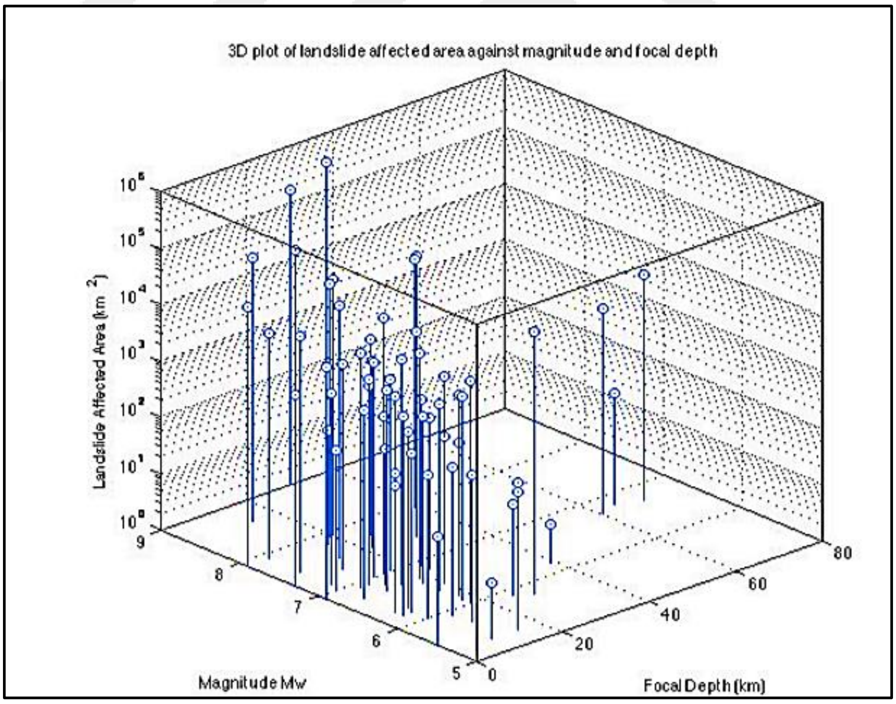

Figure 4.30 The 3D plot of earthquake magnitude and focal depth with landslide-affected area (Lei, 2012)

4.3.1.5 Fault Length

A relationship between fault length and EI landslides was also investigated. The results are presented in Figure 4.31. It would be anticipated that the longer the earthquake produced fault length is, the more violently the ground will be shaken, and the more landslides will occur during the earthquake. Nevertheless, there is no strong correlation obtained between the earthquake produced fault length and number of EI landslides generated. It can be observed in Figure 4.31 that there is no corresponding increase in landslides with respect to the fault length.

It can be appreciated that magnitude of the earthquake and of course other factors such as geology and morphology also play a key role in landslides occurrence during the earthquake. For instance, the Haiti 2010 earthquake (Mw 7.0) having a fault length of 65 km, recorded only 4,490 landslides (Gorum et al., 2013) lower than the landslides (10,000) triggered by Northridge 1994 (Mw 6.7) with a fault length of 15 km (Parise & Jibson, 2000). Thus it would not be prudent to expect a direct relationship between landslides occurrence and the fault length alone.

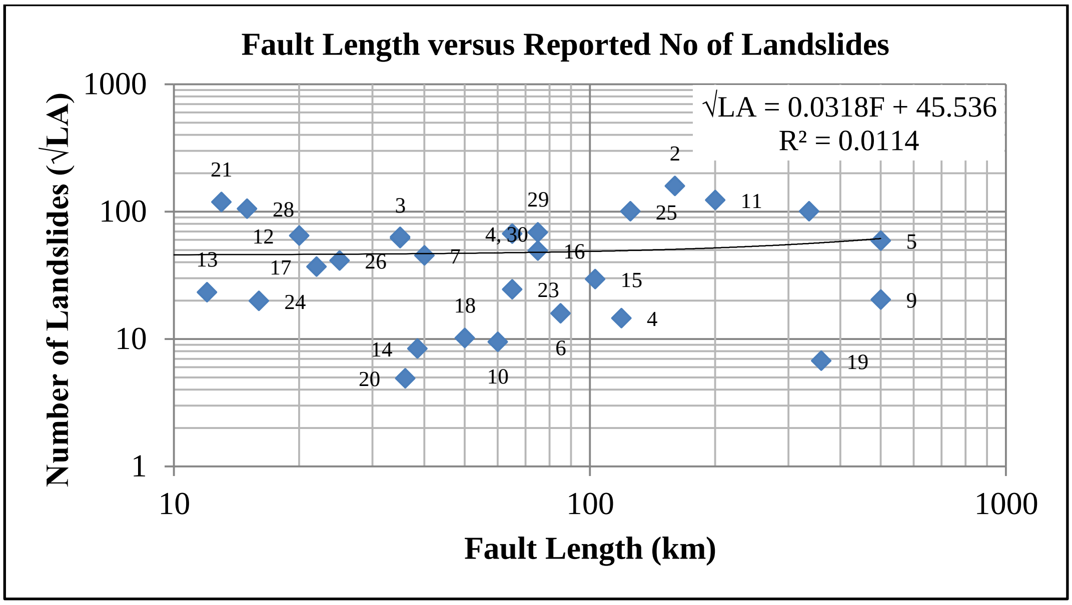

Figure 4.31 Relationship between fault length and landslides occurrence (Numbers inside the Figure represent cases presented in Table 4.1)

In the scope of the study, attempts were also made to investigate the relationship between fault length and the area affected by landslides and fault length against estimated volume of landslides (Figures 4.32 and 4.33). It can be observed from Figure 4.34 that there is a weak positive correlation between fault length and area affected by landslides. The coefficient of determination value for the correlation is $R^2 = 0.39$ which shows that fault length has somewhat a significant impact on the area affected by landslides. Similarly, a weaker positive correlation can be noticed between fault length and estimated volume of landslides (Figure 4.33). It can be observed from Figure 4.33 that the R^2 value recorded is $R^2 = 0.43$.

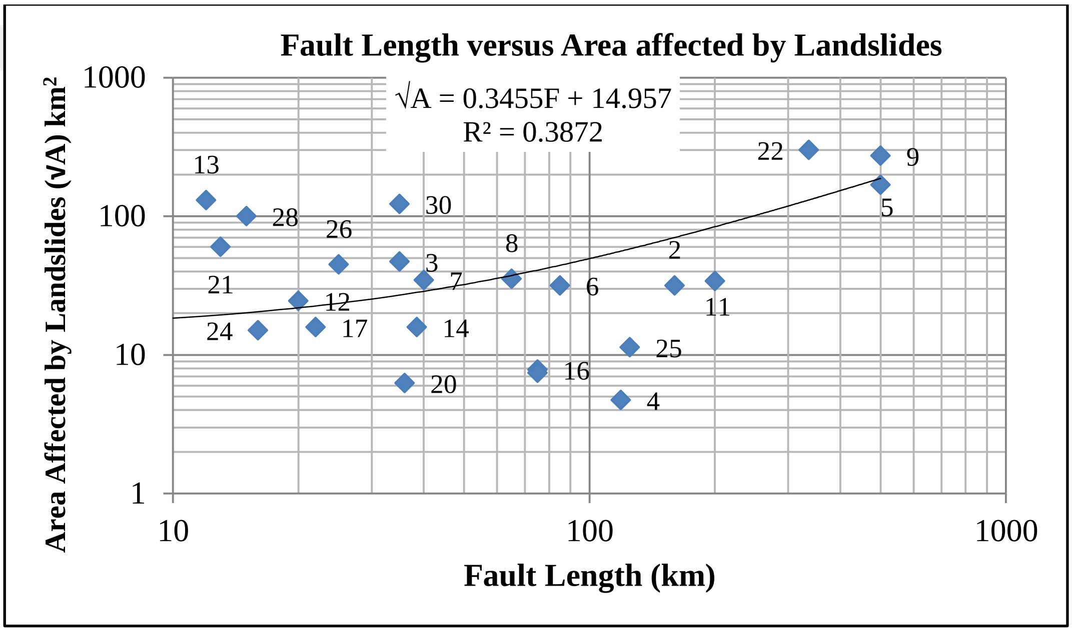

Figure 4.32 Relationship between fault length and area affected by landslides (Numbers inside the Figure represent cases presented in Table 4.1)

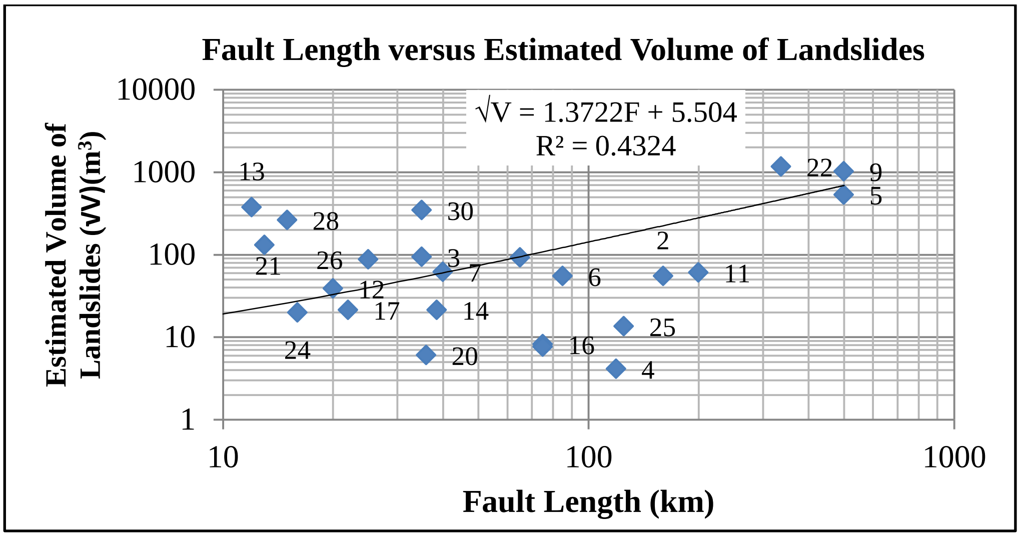

Figure 4.33 Relationship between fault length and estimated volume of landslides (Numbers inside the Figure represent cases presented in Table 4.1).

4.3.1.6 Distance from the Epicentre

The place on the earth's surface under which earthquake impact starts is so critical in understanding probable occurrence of landslides and the likely extent of the damage. In this respect, attempts were made to find the relationship between epicentral distance and landslides occurrence. From the study done by Keefer (1984) on 40 different landslides, shallow and disrupted slides generally occurred at greater distances than larger coherent landslides. Khazai & Sitar (2004) in a similar study noted that the greatest distance away for shallow disrupted slides was up 87 km from the epicentre while the greatest distance away from the epicentre for coherent slides was 46 km. Khazai & Sitar (2004) also observed that the number of landslides tend to decrease with distance away from the epicentre. In this study, landslides distribution as a function of distance from the epicentre indicates that most of the landslides occur within 50 km from the epicentre (Figure 4.34 - 4.35). For the Loma Prieta earthquake, based on 1280 landslides that were Mapped in an area of approximately 2000 km^2 in the southern Santa Cruz Mountains, landslide concentration values decrease from about 2.5 landslides/km^2 at a rate of 2 km to less than 1 landslides/km^2 at distances greater than 10 km (Keefer, 2000).

The landslide concentration value as a function of epicentral distance for the Chi-Chi earthquake based on 2507 landslides in an area of approximately 14,000 km^2 show a close agreement with the data for the Loma Prieta earthquake (Khazai & Sitar, 2003).

It can be observed that there is slow decline of landslide concentration as distance increases away from the epicentre, and landslide concentration values waning beyond the 50 km band (Figure 4.34). Similar results were obtained for the 2013 Lushan earthquake by Khazai & Sitar (2004) and in the Italian Catalogue of Earthquake –Induced Ground Failures (CEDIT) by Fortunato, Martino, Prestininzi, & Romeo (2012) (Figure 4.35).

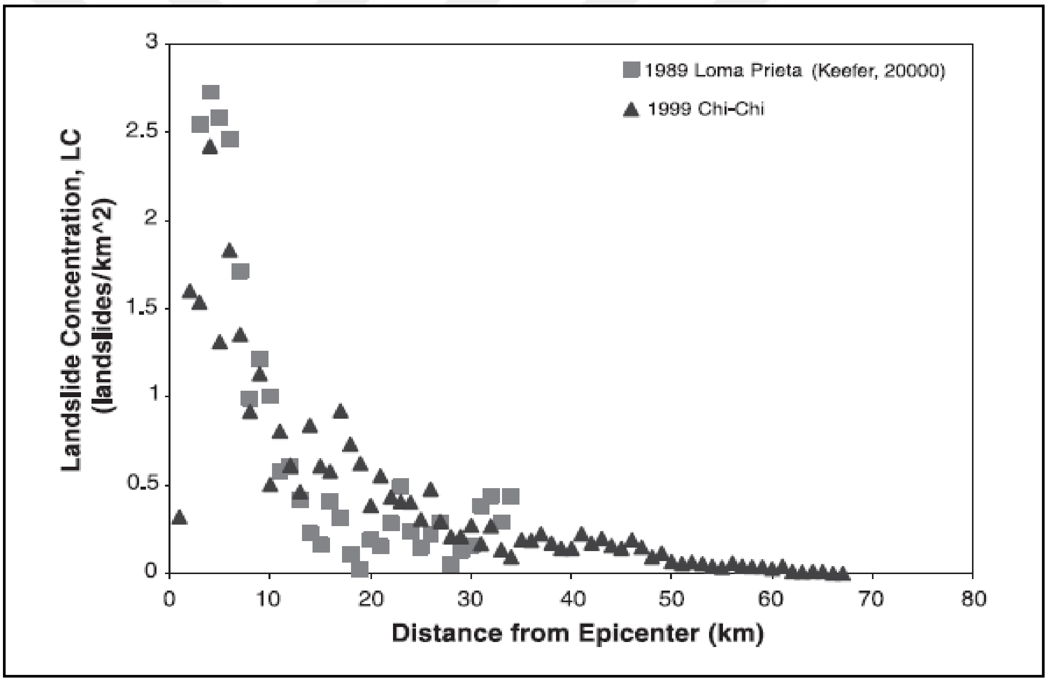

Figure 4.34 Distribution of landslide with respect to distance from the epicentre (Khazai & Sitar, 2004)

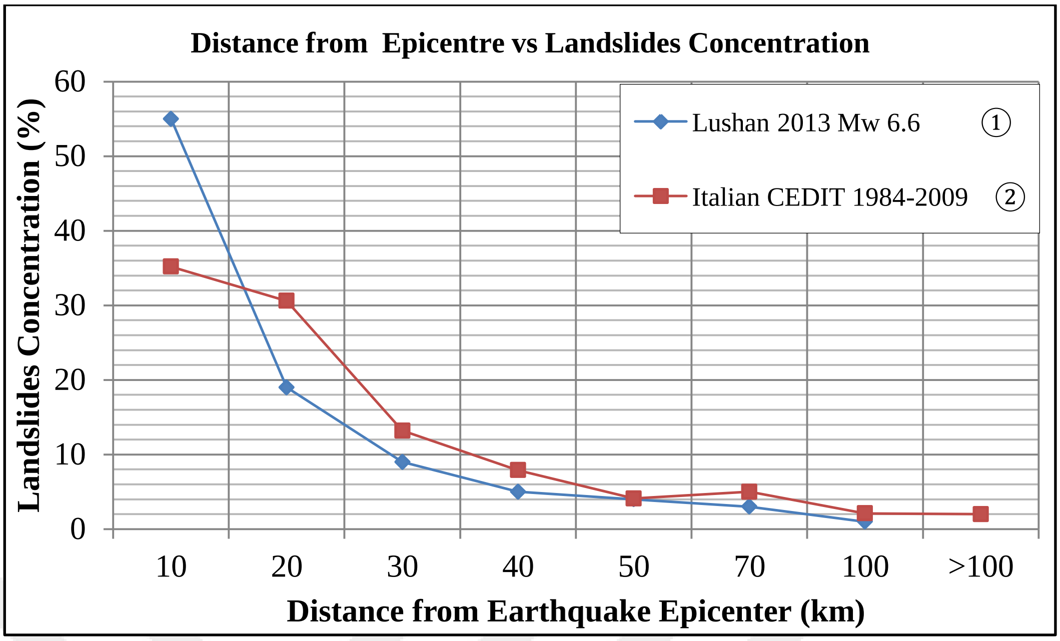

Figure 4.35 Distribution of landslide with respect to distance from the epicentre (Data from ①Khazai & Sitar, 2004 and ②Fortunato et al,. 2012)

4.3.1.7 Distance from the Fault Surface Rupture

Knowing that earthquakes are closely associated with faulting activities, efforts to understand the relationship between fault surface rupture and landslides occurrence were made. A plot of the distance from the fault plane against the EI Landslides concentration is shown in Figure 4.36 and 4.37. In the Loma Prieta 1989 earthquake, landslide concentration values rapidly decline with distance from the source, with highest values of about 2 landslides/km^2 instantly adjacent to the source (Khazai & Sitar, 2004, Figure 4.36). The landslide for the Chi-Chi 1999 earthquake also shows a much steadier decline with distance away from the surface projection of the fault. However, there is a sharp decline at about the 25 km band where landslide concentration values drop from about 0.4 landslides/km^2 to 0.1 landslides/km^2 (Figure 4:36). Khazai & Sitar (2004) attributed the less abrupt decrease in landslide concentration values with distance away from the surface projection of the fault to different faulting mechanism for the Chi-Chi 1999 and Loma Prieta 1989 earthquakes and the different definitions used for the surface projection of the fault in both analyses (Figure 4.36).

Data acquired from studies of Tang (2015), Xu & Xu (2014), Qi et al. (2010) and Harp & Crone (2006) were reworked and plotted in quest to further understand the relationship of the two parameters. The results are shown in Figure 4.37. A glance at Figure 4.37 shows that landslides tend to concentrate on the hanging wall of the thrust faults than on the foot wall but on both walls the landslides concentration decrease away from the fault plane except for the Lushan earthquake, 2013 where the major landslides occurrence took place in the footwall (Figure 4.37).

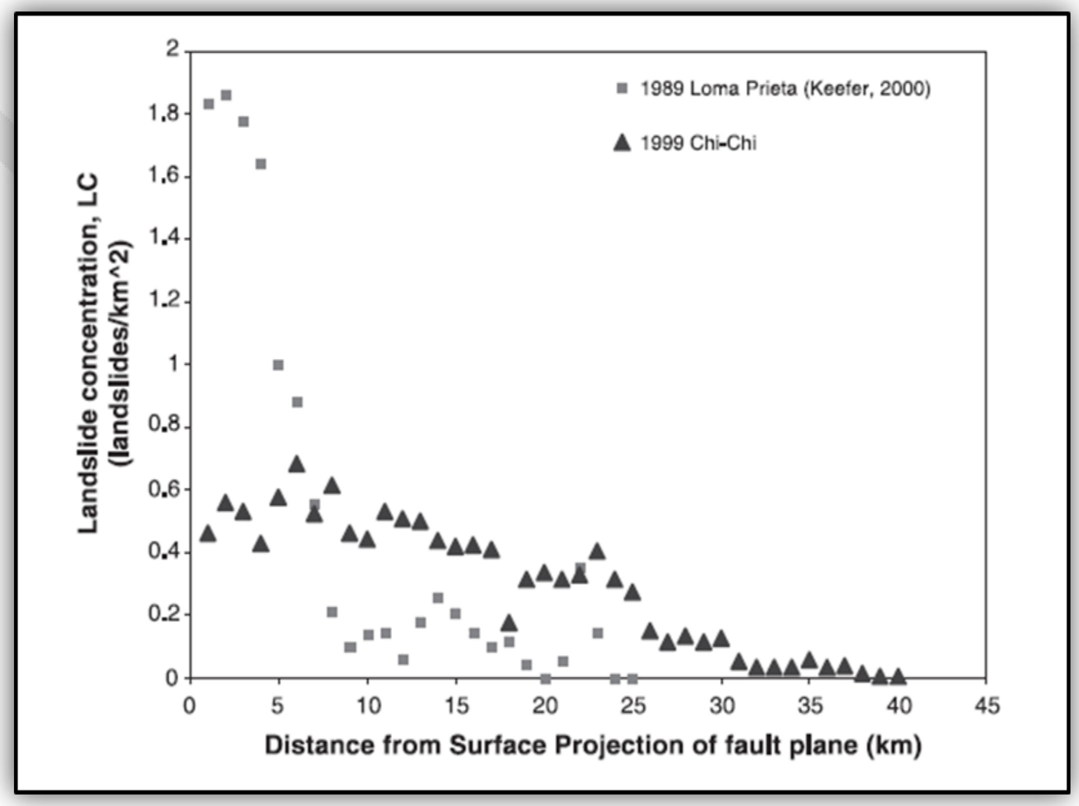

Figure 4.36 Distribution of landslide with respect to distance from the fault plane after (Khazai & Sitar, 2004)

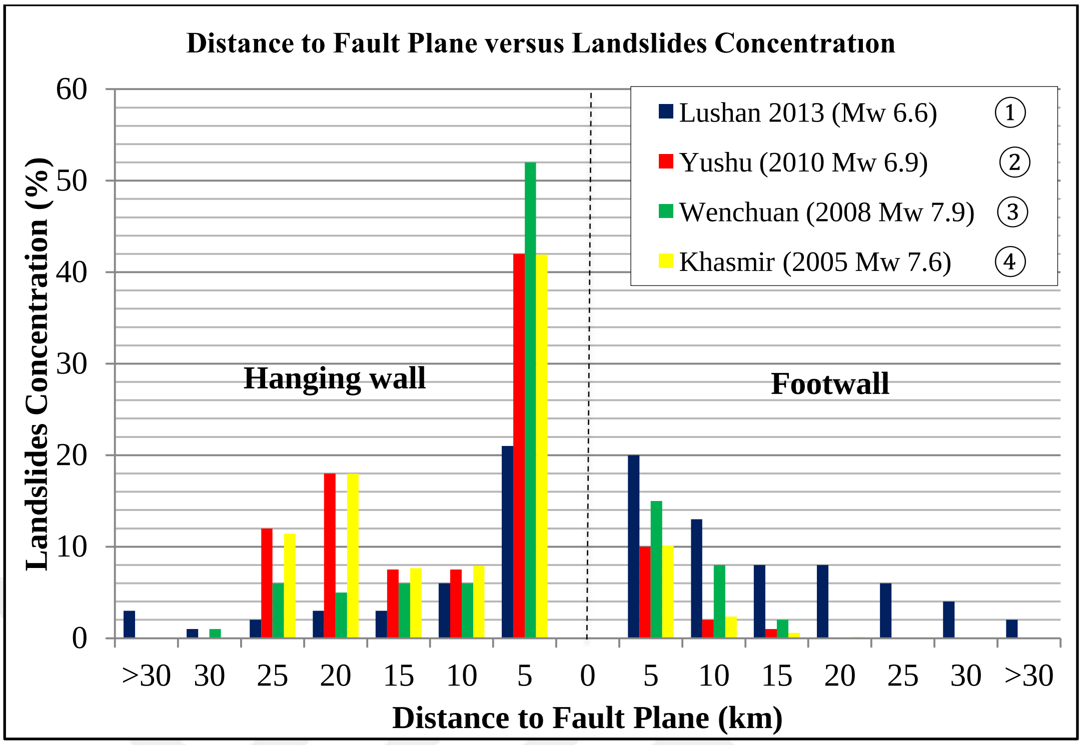

Figure 4.37 Distribution of landslide with respect to distance from the thrust fault plane (Data from ①Tang et al., 2015, ②Xu & Xu, 2014, ③Qi et al,. 2010 and ④Harp & Crone, 2006).

4.3.2 Geological Environments

4.3.2.1 Lithology

It is widely recognised that lithology plays a significant role in occurrence of EI landslides because strength, structure, composition and related soil and rock properties consisting the slope determine the likelihood of landslides occurrence. Although some EI landslides like rock falls occur in virtually all types of rocks, they probably tend to augment in closely jointed or feebly cemented and strongly weathered rocks. The presence of discontinuities, the presence of discontinuities, spacing and orientation and nature of joints and beddings in weathered rock greatly catalyse sliding. Shear zones, faults and bedding can have a great effect on the hydrological conditions. Keefer (1984) observed that rock falls were dominant in weakly cemented rocks such as pumice, tuff, shale, siltstone, sandstone and conglomerate.

Furthermore, boulders in moraine and in residual soil also produced rock falls as did in sheared and weathered rocks. Keefer's study also revealed that most well-cemented rocks that produced rock falls were broken by joints spaced a few centimetres apart. Joints were opened by physical weathering or stress relief or field with weak chemical-weathering products. Thus, most slopes that exhibit at least one of the following conditional signs of low strength or potential instability: (1) conspicuous planes of weakness; faults, master joints, bedding planes or foliation surfaces dipping out of the slope, (2) significant weathering of the rock, (3) weak cementation of the rock or geologic or historical evidence of landsliding are vulnerable to sliding (Keefer, 1984).

In order to understand the influence of geology on EI landslides, evaluation of the occurrence of EI landslides with respect to geology was done for 7 major landslides inducing earthquakes. Firstly, the relationship of lithology and landslides for the Lushan 2013 earthquake has been presented in Figure 4.38. It can be observed that the majority of landslides after the Lushan earthquake occurred in Paleogene sandy mudstone (21%) and Cretaceous sandstone and mudstone (19%) lithologic units (Figure 4.38).

The distribution of landslides after the Tohoku 2011 earthquake bears the same trend with the highest value recorded in the Neogene Sedimentary rocks (42%) followed by Quaternary Alluvium (Figure 4.39). During the Wenchuan 2008 earthquake, landslide concentrated in the Cambrian sandstone and siltstone (49.6%) followed the Silurian slate and phylite (23%) (Figure 4.40).

After the 2007 Niigata Chuetsu–Oki Japan Earthquake, several units indicate that they were particularly susceptible to landsliding, namely Pliocene (56%) and Miocene (16%) sedimentary units , typically consisting of sandstones and mudstones, and Pleistocene dune sands (Figure 4.41). Weakly cemented sands were also vulnerable to failure from seismic shaking. Neogene sandstone and shales after the Chi-Chi 1999 earthquake accounted for over 66% of the landslides induced by the ground shaking (Figure 4.42).

The value of landslides for Chi Chi 1999 is relatively lower than in 1994 Northridge earthquake, in which Tertiary sedimentary rocks accounted for 71% of the total landslides that occurred (Figure 4.43). For the 1989 Loma Prieta earthquake, sedimentary rocks were also most vulnerable to producing shallow disrupted landslides. More than 25% of the total landslides were concentrated in the formation, comprising of an interbedded sequence of sandstones, siltstones, and shales. It can be concluded from these cases that Sedimentary rocks, particularly Tertiary Sedimentary rocks, are highly susceptible to failure during earthquakes.

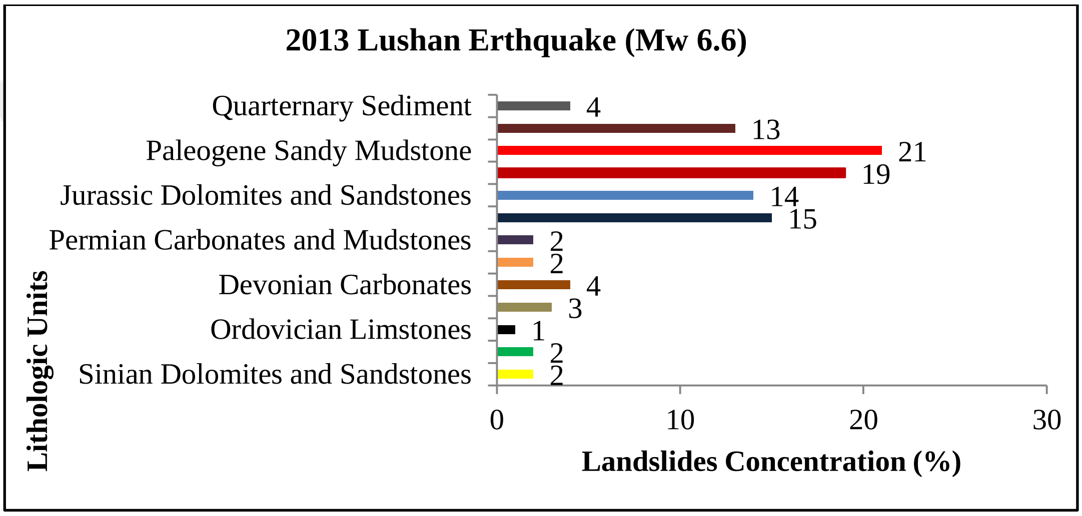

Figure 4.38 Distribution of EI landslides with respect to lithology after the 2013 Lushan earthquake (Data from Tang et al., 2015)

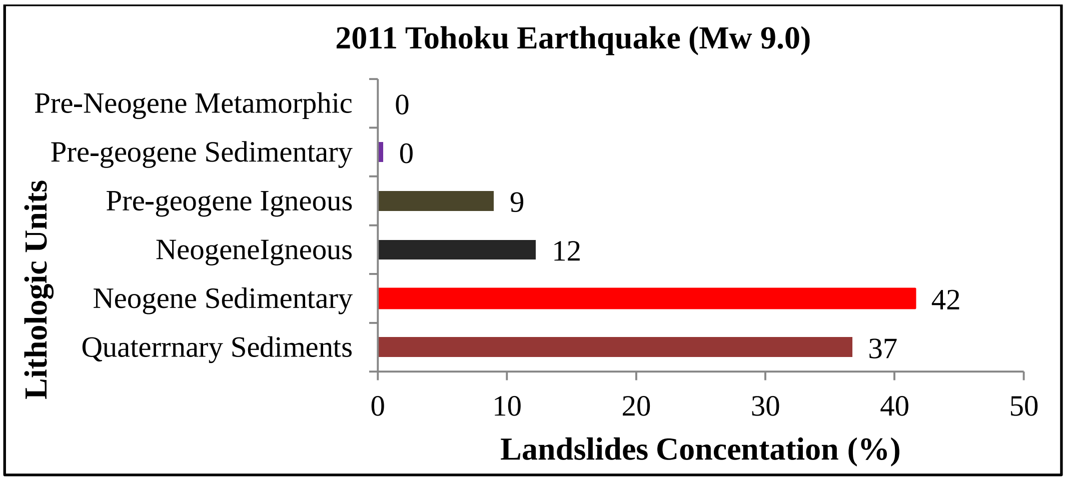

Figure 4.39 Distribution of EI landslides with respect to lithology after the 2011 Tohoku Japan earthquake (data from Hashimoto et al., 2012)

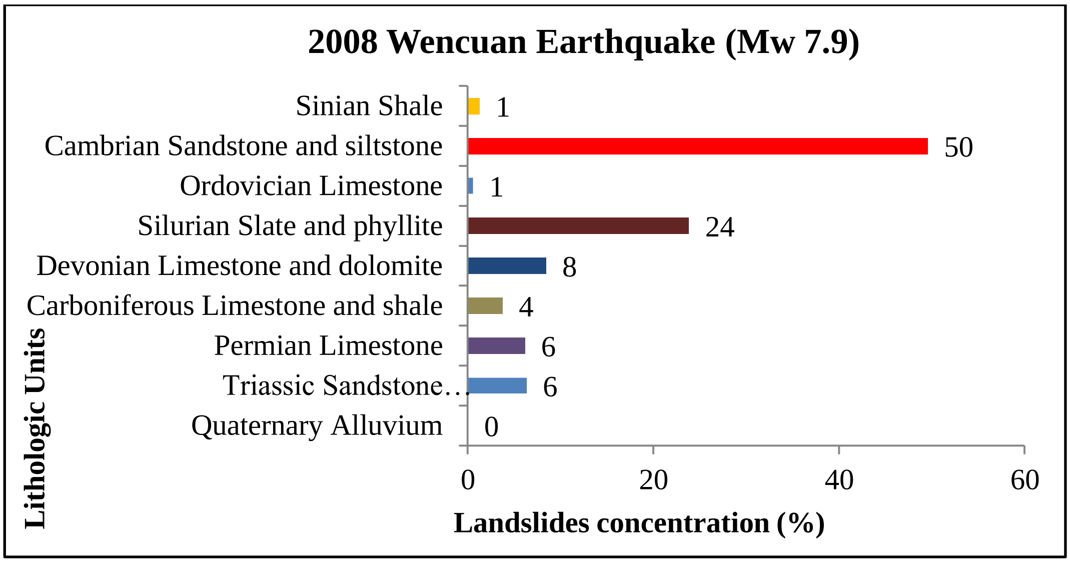

Figure 4.40 Distribution of EI Landslides with respect to lithology after the 2008 Wenchuan Earthquake (data from Qi et al., 2010b)

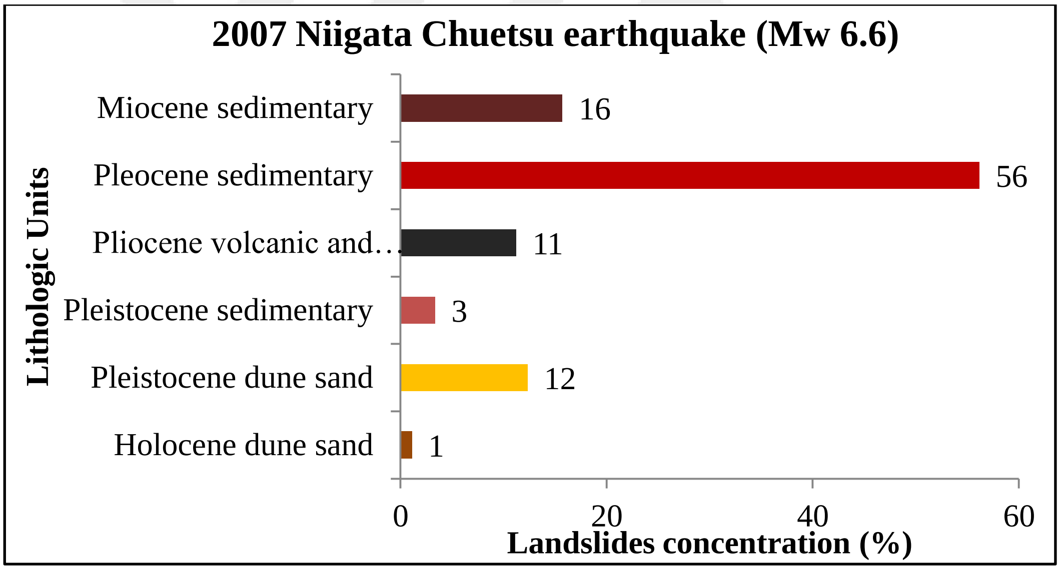

Figure 4.41 Distribution of EI Landslides with respect to lithology after the 2007 Niigata earthquake (Data from Collins et al., 2012b)

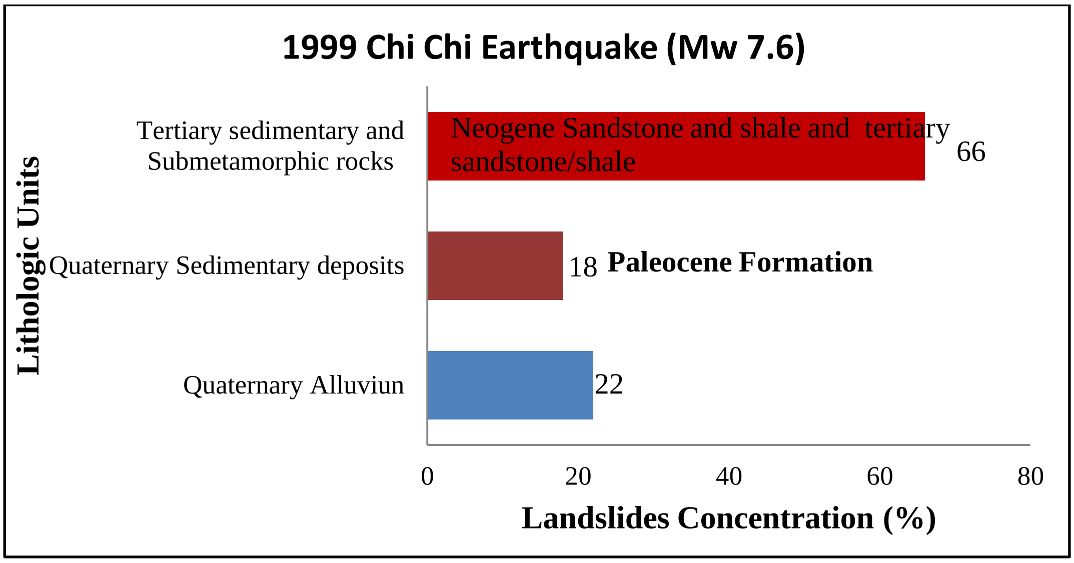

Figure 4.42 Distribution of EI Landslides with respect to lithology after the 1999 Chi Chi earthquake (Data from Khazai & Sitar, 2004)

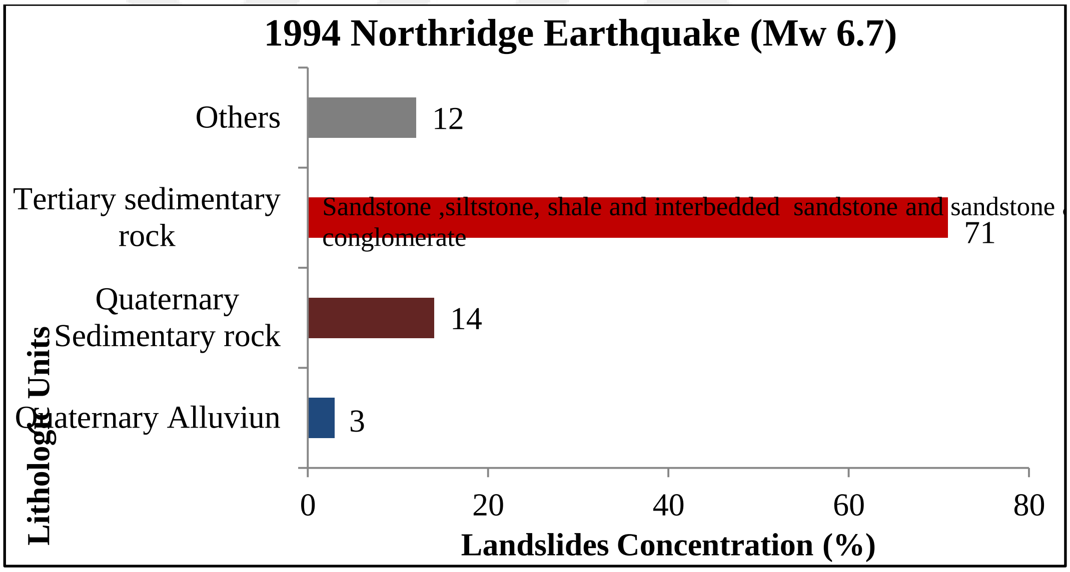

Figure 4.43 Distribution of EI Landslides with respect to lithology after the 1994 Northridge Earthquake (data from Parise & Jibson, 2000)

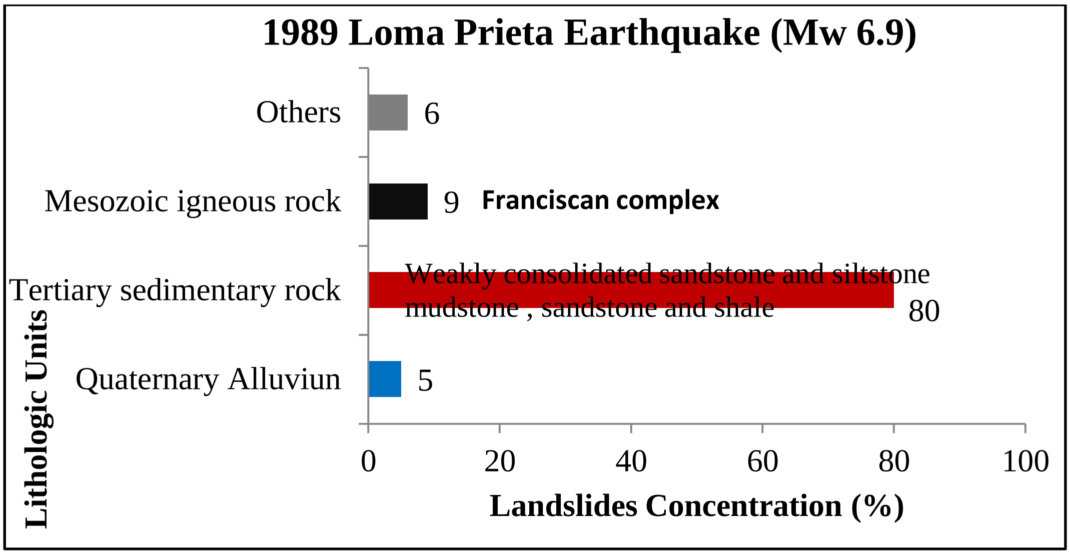

Figure 4.44 Distribution of EI Landslides with respect to lithology after the 1989 Loma Prieta Earthquake (Data from Keefer, 2000)

4.3.2.2 Fault Type

Earthquakes are closely associated with plate boundaries along which active faulting takes place. To understand the dynamics of fault type regarding EI landslides, an analysis was performed. A study of global distribution of earthquakes with respect to fault type was done by Johnson, Bürgmann and Pollitz (2015). Data on occurrence of earthquakes was compiled by Global Centroid Moment Tensor (GCMT).

GCTMT catalogued 39,989 earthquakes between January 1976 and December 2013. Johnson et al. (2015) analysed occurrence of earthquakes using data from the GCMT catalogue between January 1976 and December 2013 containing 39,989 earthquakes of which 122 were identified as main shocks with the rest categorised as minor shocks. Johnson et al. (2015) demonstrated that majority of the earthquakes occurred on thrust or reverse fault followed by strike slip faults and normal faults record the least of the earthquakes (Figure 4.45).

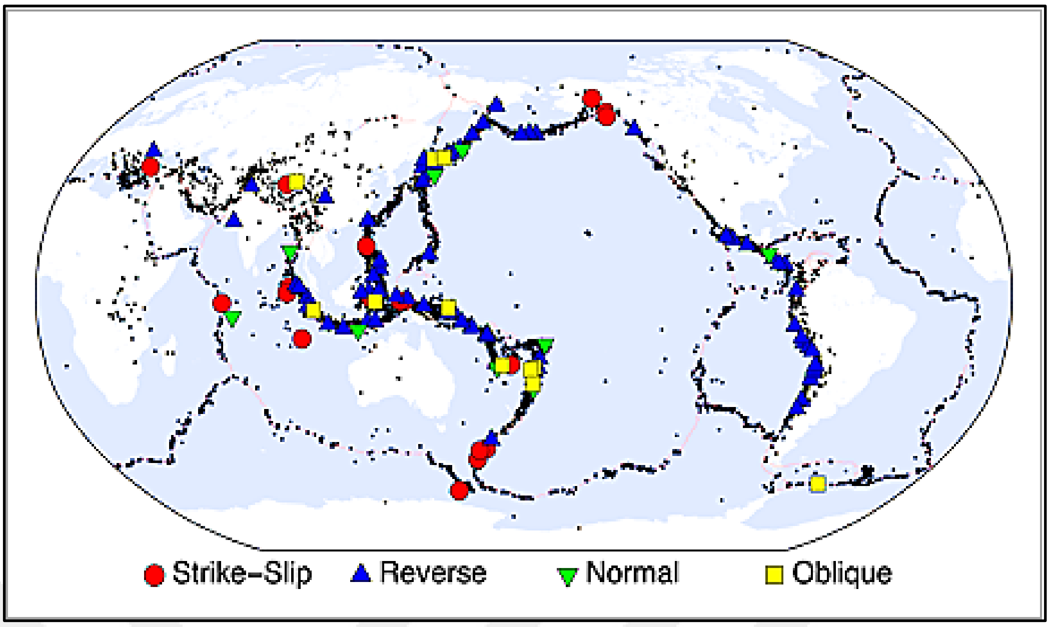

Figure 4.47 Locations of the 122 main shocks between 1977 and 2012 in the GCMT catalogue (Johnson et al., 2015). The bigger icons represent the main shocks and the small black dots represent minor shocks

Information on fault type is presented in Table 4.3 for the studied landslides produced by earthquakes. Additionally, the relationship between fault type and landslides is presented in Figure 4.48 using the cases from Table 4. 2. An analysis of the earthquakes that induced landslides indicate that landslides occurrence due to earthquakes is controlled by fault type. It can be observed in Figure 4.48 that occurrence of landslides is strongly correlated to thrust fault type.

Earthquakes on thrust faults recorded a frequency of 67% and have caused a greater proportion of EI landslides with a proportion of 87% of the total landslides reported followed by earthquakes that occurred on strike slip faults (13%) with a frequency of 29% (Figure 4.46). At thrust faults, compressional forces cause the blocks on the fault plane to collide violently as the hanging wall runs over the foot wall during the upward movement along the fault plane. Unsurprisingly, a very small proportion of EI landslides (2%) have been reported to have occurred on normal fault for the studied cases.

The trend on normal faults is evidently attributable to non-violent nature of the extensional forces operating on normal faults that might merely induce ground breaking and imperceptible deep seated failures with creeping effect. Table 4.1 presents the distribution of landslides with respect to fault type.

Table 4.3 Distribution of landslides with respect to fault type (Data from Table 4.1).

FAULT TYPE AND LANDSLIDES							
Thrust fault	**No of Landslides**	**Strike Slip Fault**	**No of Landslides**	**Oblique Fault**	**No of Landslides**	**Normal Fault**	**No of Landslides**
Gorkha,	25,000	Matukutuki	2,036	Loma Prieta	4,000	Elsavado	600
Lushan	3810	Lorca	250			Umbria	1700
Sikkim	210	Yushu	2,036				
Tohoku	3477	Haiti	4490				
Maule	410	Aysen Fjord	538				
Sumatra	89	Bingöl	45				
Wenchuan	15,000	Christchurch	200				
Iwate-Miyagi	4161						
Niigata - Oki	70						
Pisco, Peru	866						
Kashmir	2,424						
Mid-Niigata	1,353						
Tecoman	103						
Boumerdes	24						
Avaj, Iran	14000						
Denali	10,000						
Garhwali	394						
Chi-Chi	10,000						
Northridge	11,000						
Finisterre	4700						
TOTAL 20	**107,091**	**7**	**9,595**	**1**	**4,000**	**2**	**2300**

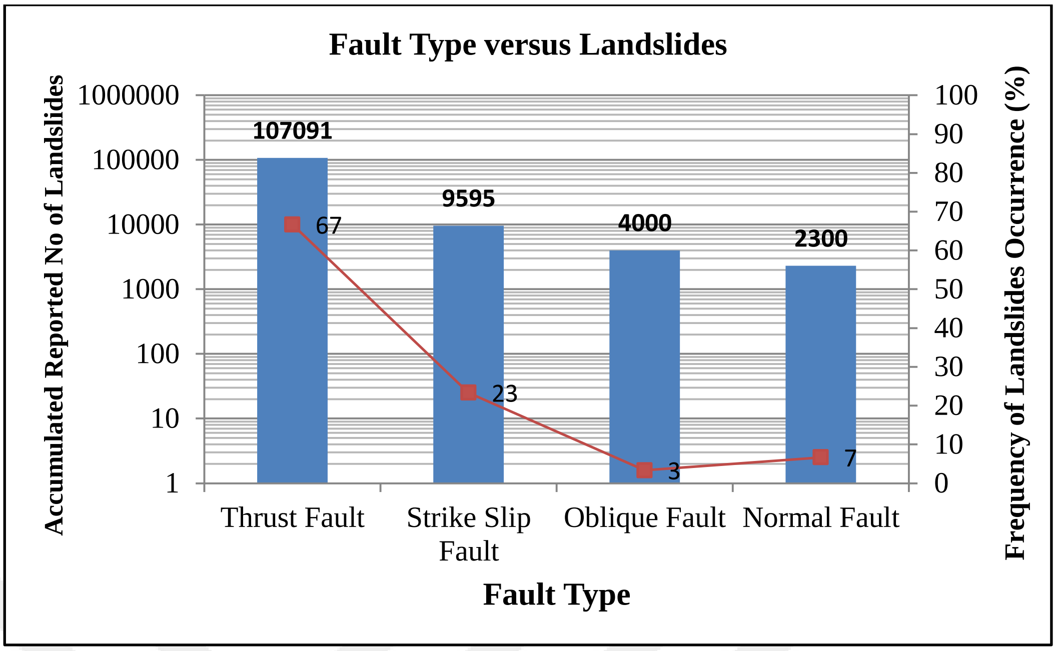

Figure 4.46 Relationship between fault type and landslides (Data from Table 4. 2)

4.3.3 Topography

Landslides occurence is evidently terrain dependent. Meunier , Hovius, & Haine (2008) argue that of all the attributes of topography, slope angle is probably the strongest controlling parameter to landslides. In agreement, Messaoudi, Laouami, & Mezouer (2012) propounded a generalised statement that "the steeper the slope is, the more the effects of topography are accentuated". The influence of topographic parameters that have been investigated in this study include; slope angle, slope aspect and slope height and elevation. Additionally, a relationship between slope angle and geology has also been analysed.

4.3.3.1 Slope Angle

According to Meunier et al. (2008), hillslope failures happen as the shear stress over a likely failure plane increases above the substratum strength. Essentially, the stability of a hillslope is determined by its surface gradient, the density, cohesion and fractional properties of its substrate, the depth of potential failure plains and the gravitational acceleration. Thus, a change in any of these parameters can cause the destabilisation and failure of slope.

It was also demonstrated by Meunier et al. (2008) that topographic site impacts on seismic waves are known to cause significant gradients in ground acceleration in individual mountain ridges. Using landslide maps from the epicentral areas of earthquakes after the Chi-Chi 1999, Northridge 1994, California, Taiwan, and the Finisterre Mountains of Papua New Guinea 1993, Meunier et al. (2008) realised that earthquake-triggered landslides clustered near ridge crest where the vulnerability to landslides occurrence was greatest. It can be said that slopes on which landslides occur can range from overhanging cliffs in well-indurated bedrock to unconsolidated sediments with nearly a fat surface. According to Keefer (1984) and Parise & Jibson (2000), minimum slopes for various types of landslides ranges from 1^0 to 40^0, although certain landslide types occur at greater slope angle and that the most abundant landslides (rock falls, disrupted rockslides, disrupted slides in earth and debris) initiate on slope greater than 15^0.

The relationship between slope angle and EI landslides drawn from 8 major landslides inducing earthquakes is presented in Figure 4.47. It can be observed from Figure 4.47 that the trend line for Lushan 2013 earthquake shows that the peak for landslides concentration was registered in the 40^o-50^o category and then declined with increase in slope angle. For Yushu 2010 earthquake, landslides are concentrated in the 40-50^o category. This is due to data truncation, that is; the data on slope angle and landslides concentration for Yushu 2010 earthquake as presented by Xu & Xu (2014) was clumped in the 40-50^o band for slope angles ≥ 40 degree.

The trend line for Wenchuan 2008, Niigata Chuetsu Oki 2007, Kashmir 2005 and Northridge 1994 earthquakes show a common trend where landslides concentration increases with increasing slope angle until the maximum is attained in the 30°–40° category, and then decreases generally with increasing slope gradient. This implies that if the data for Yushu 2010 earthquake was provided for 40^o-50^o category alone the trend line would have declined just as the other trend lines for Wenchuan 2008, Niigata Chuetsu Oki 2007, Kashmir 2005 and Northridge 1994 earthquake.

In other cases, after the Chi-Chi 1999 earthquake, 90% of failures occurred in slope angles greater than 45^0, while 83% and 90% of failures occurred on slopes less than 50^0 in the Northridge 1994 and Loma Prieta 1989 earthquakes, respectively. Khazai & Sitar (2004) attribute the deviant trend of the Chi Chi 1999 landslides distribution to the fact that the steep slope angles of the young mountain ranges in Taiwan reflected the predominant type of failure since disrupted slides and toppling/rock falls typically happen on such kind of steep slopes. However, the general trend of landslides distribution with respect to slope angle is such that landslides concentration increases with increasing slope angle until the maximum is reached in the 30°–40° category, and then decreases generally with increasing slope gradient. In few cases, the landslides concentration peak were recorded in the, 40^o-50^o, 60^o-75^o and 20^o-30^o category as noted for Lushan 2013, Chi Chi 1999 and Loma Prieta 1989 earthquakes respectively. It is also worth mentioning that the undercutting action of a river, distances from drainage and road cuts expose slopes to failures as discussed by Kıncal, Akgun, & Koca (2009).

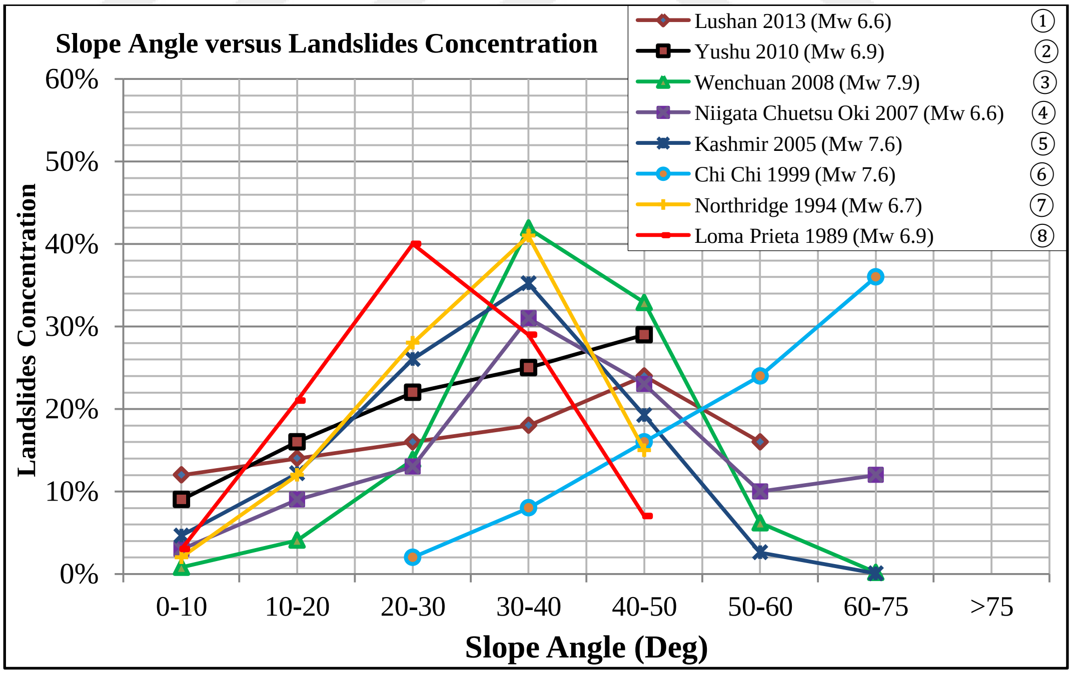

Figure 4.47 Distribution of landslides with respect to slope angles in degrees (Data from ①Tang et al., 2015, ②Xu & Xu, 2014, ③Qi et al., 2010, ④Collins et al., 2012, ⑤Harp & Crone, 2006, ⑥Khazai & Sitar, 2004, ⑦Parise & Jibson, 2000 and ⑧Keefer, 2000)

4.3.3.2 Slope Angle and Geology

A study by Hancox, Perrin, & Dellow (2002) revealed a strong correlation between slope angle and rock type in causing EI landslides after an earthquake. The study involved a critical analysis of the 22 historical earthquakes in New Zealand in 1997. The outcome of the intensive study demostrated that failures in well-jointed hard rocks such as greywacke and granite occur principally on moderate to steep slopes (15^0-45^0). Slope failures in the Tertiary sandstone and mudstone occur mainly on gentle to steep dip slopes (10^0-40^0), whereas landslides in limestone occur principally on cliffs and escarpments (Table 4.3).

Table 4.4 Relationship between slope angle and geology with respect to earthquake intensity (after Hancox, Perrin, & Dellow, 2002)

Slope Range	Approx % EIL* Slope Failures	Typical Slope and Rock Type
1-10^0	<1%	Few failures, several low angle dip slope slides in Tertiary mudstone.
11-25^0	10%	Mainly dip slope slides in interbedded Tertiary sandstone and mudstone and limestone.
26-35^0	30%	Dip slope failures in bedded Tertiary rocks; steeper slopes in hard rocks (greywacke, schist, granites etc).
36-45^0	40%	Steep cliffs, escarpments, and gorges in Tertiary limestone; scarp slopes in hard rocks (greywacke, schist, granites etc).
>45^0	20%	Steep cliffs, scarps, gorges in tertiary sediments, greywacke, schist, granites etc.

Thus, Hancox, Perrin, & Dellow (2002) inductively concluded that lithology and geological structure are regarded as key factors, which together with slope configuration and steepness control the distribution of rock falls, slides and avalanches during the earthquakes.

The inclusion of ground shaking to slope angle and geology, shows that failures at lower Mercali Modified (MMVI) intensities occured in weakly cemented Tertiary sandstone and limestone, and had been common during several earthquakes. Closely jointed volcanic rocks appear to be vulnerable to widespread landsliding solely during earthquakes of $M_w \geq 6.0$, and shaking intensity of MMVII or greater. A study of landslides during the Lushan earthquake by Tang et al. (2015) revealed a similar correlation. Landslides composed of Paleogene, Cretaceous, and Jurassic rocks mainly occurred on slopes over 25° steep, having the highest concentration at slope 45°–55° in all geologic units. In addition, Neogene silty mudstones and conglomerates and Quaternary sediments were mainly distributed in places with relative gentle slopes.

4.3.3.3 Slope Aspect

Xu et al. (2014) clarifies that aspect is related to factors such as exposure to sunlight, drying winds, rainfall (degree of saturation) and discontinuities, which may control landslides occurrence. The occurrence and distributions of landslides has been found to be influenced by orientations of slopes as revealed in a comparative study on the topographic site effects and EI Landslides by Meunier et al. (2008). It was discovered that in the Finisterre Mountains, New Zealand most landslides took place to the east of the earthquake epicentre such that slopes facing to the South East (SE) and away from the seismic source were four times more likely to fail than slopes dipping toward the epicentre (Figure 4.50) (Hancox et al., 2002).

In Taiwan during the Chi Chi 1999 earthquake, Khazai & Sitar (2003) discussed that most of the landslides were located to the south of the earthquake epicentre, and in slopes facing to the south-south west (SSW), away from the epicentre.

These strongly oriented landslide distributions indicate that topographic site effects dominate the location of EI Landslides in central west Taiwan and the southern Finisterre Mountains, and that the rate of failure of the steepest slopes in mountain ranges is set by the local PGA. Similarly, Landslides in the Northridge 1994 epicentral area have occurred preferentially on south-facing slopes in the Santa Susanna and San Miguel Mountains (Figure 4.48). Ridge clustering of landslides was found to be strongest in the region, implying a considerable topographic site effects on seismic waves, but the focus was locate to the south of the Santa Susanna Mountains.

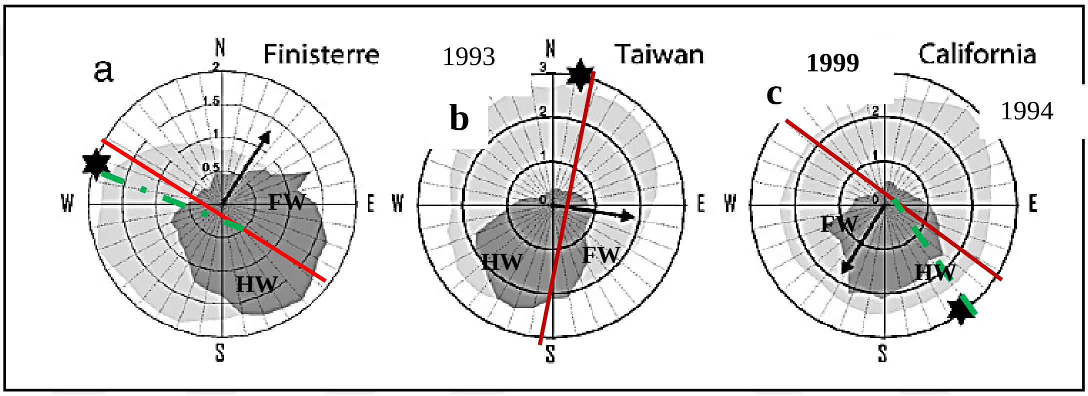

Figure 4.48 Distribution of orientation of the slopes (in %, light grey) and normalized distribution of orientation of the landslides (dark grey) (after Meunier et al., 2008). Arrows indicate the direction of the fault dip. Stars indicate the relative mean position of the epicentre.

It is also interesting to note that the Figures 4.48a-c, the fault planes strike at almost an angle of 10^{o} to the epicentres for the studied 3 major earthquakes. This suggests that earthquake caused on thrust faults occur at a constant angle of tearing to the epicentre. Similar scenario has been also observed for the Kashmir 2005 earthquake having been produced at thrust fault. The radar plot for Yushu 2010 and Kashmir 2005 earthquakes are presented in Figure 4.49.

The Yushu 2010 earthquake occurred on a strike slip fault while Kashmir 2005 took place at the thrust fault type. It can be noted in Figure 4.49 that the distribution pattern of the landslides for Yushu 2010 is spread around the fault plane almost equally whereas the pattern of landslides distribution for the Kashmir is high in the direction parallel to the fault plane on the hanging wall side.

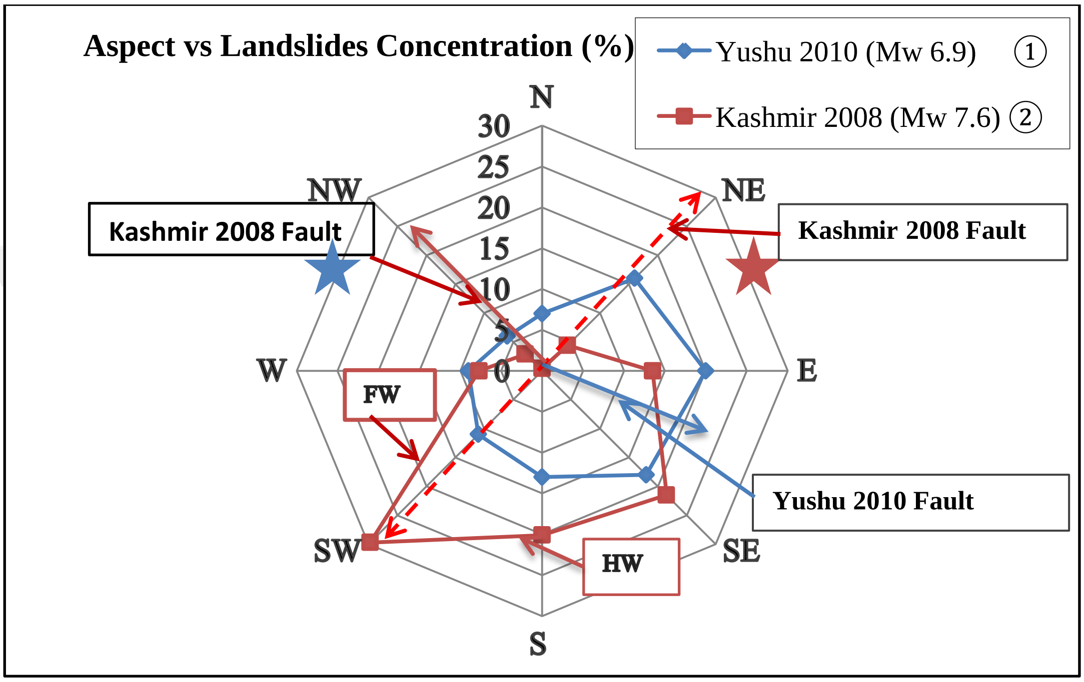

Figure 4.49 Distribution of landslides with respect to orientation of slopes (data from Xu & ①Xu, 2014 and ② Mahmood et al., 2015). The stars represent earthquake epicentres, HW stands for hanging wall and FW stands for foot wall.

4.3.3.4 Slope Height

The impact of slope height cannot be ignored in the study of EI landslides. Meunier et al. (2008) discussed that elevation diparities and associated vegetation, weathering, slope material misture content, and seismic wave amplification effect have a tendency to control seismic landslides. In view of this, an effort was made to assess the influence of slope hieght on EI landslides. The histogram in Figure 4.50 reveals that Landslides increase with increasing the slope elevation until the maximum is reached in the region of 1000–1250 m and then decline at very high elevations.

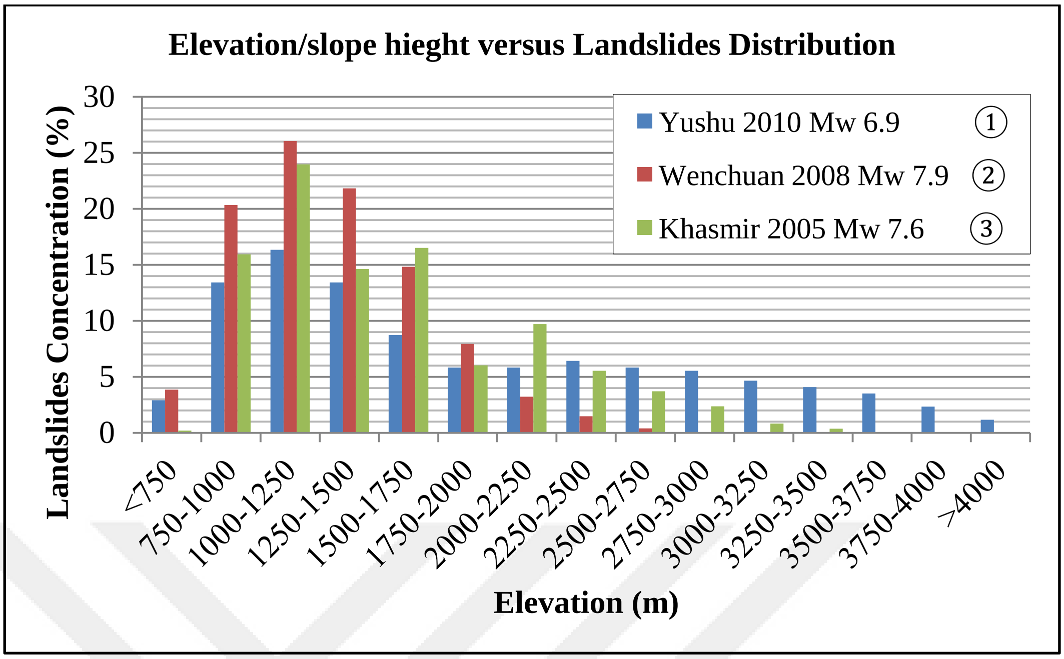

Figure 4.50 Distribution of landslides with respect to elevation (Data from ①Xu & Xu, 2014,② Qi et al., 2010, and ③Kamp, 2008)

4.3.3.5 *Slope Curvature*

Slope curvature, which gives a measure of the convexity or concavity of the slope of an area, has the potential to determine the occurrence of landslides. Basically; negative curvatures represent concave surfaces, a zero curvature denotes a flat surface and positive curvatures denote convex surfaces. To understand the impact of slope curvature, a relationship between slope curvature anİzmird EI landslides was evaluated. The relationship is shown in Figure 4.51. The slope curvature map shows that 50% of EI landslides occurred on concave slope (-1 - -0.001) for the Khasmir 2005, to which Ray et al. (2009) suggested it was a result of the depletion of mass. Data for Yushu 2010 shows a similar trend as that of Khasmir. High values of occurrence of landslides are observed to be concentrate in concave slopes (-1– -0.001 and -0.001 – 0) (Figure 4.51). Thus, concave slopes might be said to be greatly associated with EI landslides.

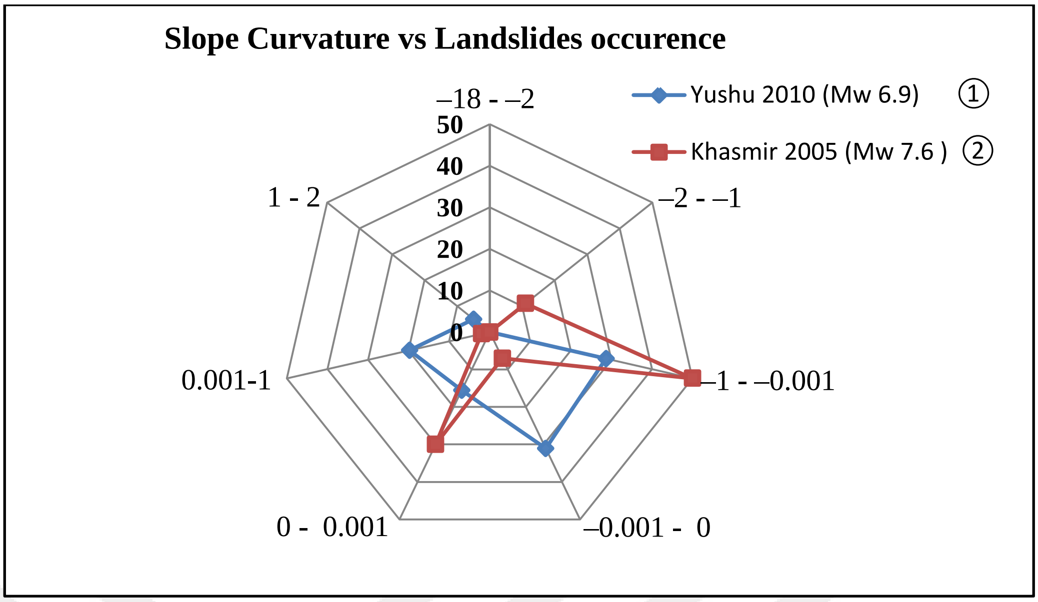

Figure 4.51 Distribution of landslides with respect to slope curvature (Data from Mahmood et al., 2015)

4.4 Discussion

In this section of the study, the principal features of the landslides caused by major earthquakes have been investigated. The list of the investigated earthquakes ($m_w \geq 5.0$) which caused landsliding are given in Table 4.1. The relative frequency of occurrence of EI landslides from these and other historical earthquakes indicate that rock falls, disrupted soil slides, soil slumps and rock slides appear to be the most common types of landslides whereas subaqueous landslides, slow earth flows, rock block slides, and rock avalanches tend to be least common (Figures 4.11 - 4.13).

A quantitative technique of data analysis employed in this study to correlate variables so as to establish their relationship indicate that covariates found to be significantly associated with EI landsliding were; PGA times earthquake duration or Arias intensity, proximity to the epicentre and/or fault rapture, geology, slopes angle, aspect and elevation.

The study has shown that earthquake magnitude has a negligible influence on occurrence of landslides. However, a very weak positive correlation between magnitude and the total area affected by the landslides was obtained with a coefficent of correlation of 0.28. It was also noted that earthquakes with Mw $\leq$ 6.0 hardly induce landslides.The occurrence of EI landslides as a function of earthquake ground shaking reveals that PGA alone has no significant influence unless it is combined with earthquake duration. The occurrence of EI landslides was significantly higher in locations where PGA*t is greater than 12 g*s.

Depth of the focus also has an impact on the occurrence of landslides. Swallow depths can be considered as a significant ingredient for occurrence of landslides. Earthquakes at greater depth in the ground virtually do not cause imminent landslides as the energy becomes lethargic upon reaching the surface of the earth (Lei, 2012). In this regard, it has been observed that earthquakes with a focal depth of $\leq$ 35 km are likely to cause landslides than deep seated ones although outliers (earthquakes with Mw > 35) might cause landslides on rare occasions.

Furthermore, the influence of epicentral distance and fault rupture distance was investigated to gain an understanding of their impacts. Landslides distribution as a function of distance from the epicentre and distance from the surface projection of the fault plane show that most of the landslides occur 30 km from epicentre and/or fault plane and considerably reduce further away. This is attributable to the attenuation of energy as seismic waves travel through the ground.

Notwithstanding the correlation between earthquake parameters and landslides, the ostensible conclusion that earthquake magnitude, PGA*t, are good criteria for predicting seismically induced landslides is not very adequate and could be misleading. As noted in Figure 4:16, there are variations in the scatter values of the affected area and the magnitude of the earthquakes. The parameters significantly contributing to such a scatter are probably the geology and variation in the geographical environments where the earthquakes occurred.

Therefore, interrelationship between geology, topography and seismically triggered landslides were also brought into play to come up with a conclusive trend. The study revealed that geological setting has a great influence on occurrence of landslides after an earthquake. The main lithologic unit prone to landsliding due to seismic effect are the Tertiary sedimentary rocks with at least over 50% of landsliding concentration (Figures 4.38 – 4.44). Landslides also occur in metamorphıc and igneous rocks if they could be weakened enough by discontinuities and/or weathering. Quaternary lithologic units recorded low landslides because they are usually located in flat areas. However they could be prone to liquefaction. It can be inductively said that, seismically induced landslides predominantly occur in tectonic mountain ranges and along active faults particulary along mobile marginal zones of continental blocks.

Another interesting observation from the study is that earthquakes that cause landslides have been observed to be controlled by fault type. It has been discovered that occurrence of EI landslides is strongly correlated to thrust fault type. Earthquakes on thrust faults recorded a frequency of 67% and have caused a greater proportion of EI landslides with a proportion of 87% of the total landslides reported followed by earthquakes that occurred on strike slip faults (13%) with a frequency of 29% (Figure 4.46). This is because, at thrust faults, compressional forces cause blocks on the fault plane to collide violently as the hanging wall runs slides over the foot wall during its upward movement along the fault plane. And it is not schocking that a very small proportion of EI landslides (2%) have been reported to have occurred on normal fault for the studied cases. The phenomenon is attributtable to non-violent nature of the extensional forces operating on normal faults.

Geographical environments cannot be ignored when considering seismically induced landslides. On slope angle, the study showed that in general, landslides tend to increase with increasing slope angle until the maximum is reached in the 30°–40° category, and then decreases generally with increasing slope gradient (Figure 4.47). Kıncal et al. (2009) add that the propensity of the slope to sliding is heightened by undercutting action of rivers, proximity to drainages and roads. Regarding elevation, the results have also shown that landslides increase with increasing slope elevation until the maximum is reached in the 1000–1250 m range and then decrease as such heights are surpassed (Figure 4.50). However the influence of orientations of slopes is complex as it is not consistent and generalizable. This is because the location of the epicentre determines the distribution of the seismic waves.

It is however recommendable to realise that most earthquakes do not record landslides imminently, but the shaking impact of the earthquakes could have caused slopes to become unstable by inertial loading they impose or by causing a loss of strength in in the slope materials. If rainfall comes, although the ground shaking impact by earthquakes might have created conducive conditions for landsliding, landslides that follow are attributed to precipitation. Consequently, Long-term landslides susceptibility assessment has typically put emphasis on rainfall-induced landslides events to model susceptibility as they occur more frequent than EI landslides leading to under-representation of earthquake triggered landslides risk.

CHAPTER FIVE
CASE STUDY OF İZMİR; KARABURUN

5.1 Background Information

Turkey lies in the tectonically and seismically active region that experiences innumerable destructive earthquakes and İzmir is no exception (Figure 5.1). Kandilli Observatory and Earthquake Research Institute (KOERI) has recorded thousands of earthquakes in Turkey since it was established 1868. However, the reporting of the aftermaths of the earthquakes that have been taking place has greatly focused on fatalities and destruction of properties and structures with little or no focus on occurrence of landslides. Unsurprisingly, information on landslides associated with earthquakes is scanty. According to Korup (2010) this is attributable to the propensity to less plainly attempt to understand the contribution of seismic shaking to decrease slope stability and the general limitation of predicting the magnitude, location, and timing of large landslide-triggering earthquakes. In addition the complexity of the analysis of the assessment of ground stability due to earthquakes which involves other disciplines like geology, geophysics, seismology and geotechnics may be limiting the research work in the EI landslides area.

From this background I made an effort to apply the understanding of the landslides controlling factors during earthquakes and relate the knowledge to assess the possibility of occurrence of landslides after the 1949 İzmir- Karaburun earthquake in the absence of landslides information during and/or after the earthquake.

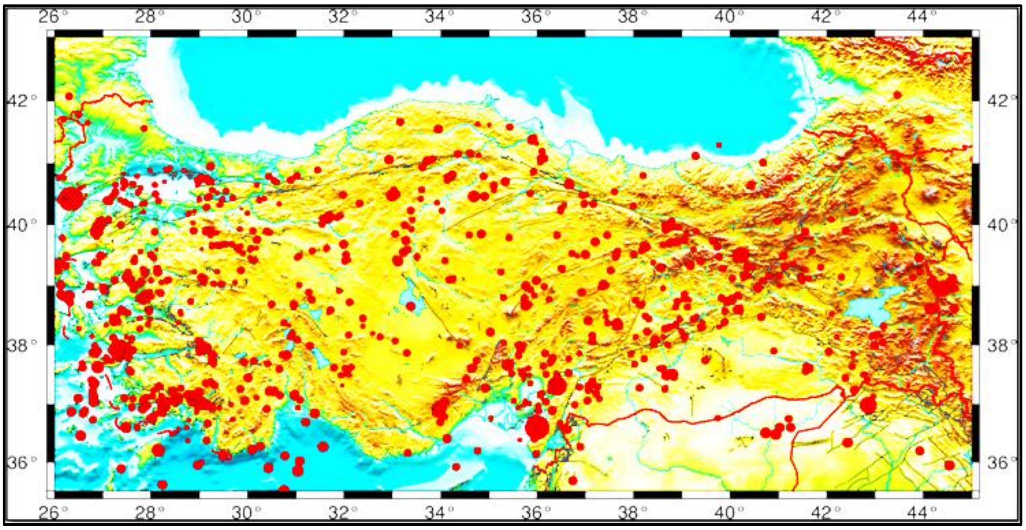

Figure 5.1 Earthquake distribution across Turkey (Kandilli Observatory and Earthquake Research Institute - KOERI). The bigger the dot the higher the earthquake magnitude

5.2 General Geology of İzmir

İzmir has a complex and fascinating geology. The İzmir metropolitan area's lithology encompasses the upper Cretaceous and Palaeocene Bornova melange rocks which predominantly consist of a flysch matrix of limestone olistolithes with clasts of different age sizes in the matrix. According to Kıncal et al. (2009) the flysch matrix is also comprised of sandstone-shale intercalations and conglomerate with shales, approximately 60–65% of the matrix, as the dominant component of the matrix and sandstones are found as lenses and interlayers between the shale layers.

The Bornova melange is highly folded and fractured by the strong impact of the tectonic activities. The rocks are intensively fractured, and two to four sets of joints have been identified (Kıncal et al., 2009). Neogene sedimentary rocks discordantly lie over the Bornova Melange rocks .These Neogene sedimentary rocks have been observed to comprise of conglomerate, sandstone, laminated marl and limestone from the base to the top respectively. The upper Miocene and Pliocene volcanic rocks are widespread in and around the city of İzmir and discordantly overlie all the sedimentary lithologic units.

The volcanic rocks, in ascending order, chiefly consist of dacitic tuff, dacitic lava, andesitic tuff and conglomerate and lava subunits. Andesitic volcanics in the southern part of İzmir Bay superimpose the clayey and marly levels of sedimentary rocks. These volcanics are generally described to have tuffs at the base and are perpetual with agglomerate and andesitic lavas, in that order.

On structural geological aspect, the main trends of the fault in the area are the NE–SW and E–W. The İzmir, Tuzla, Ciğli, Bornova, and Menemen fault zones are extremely crucial as they form the present morphology of the region. The Tuzla fault, which is a left lateral strike slip fault, runs along the contact between the Bornova Melange and the Neogene units. The Tuzla fault was apparently reactivated during the 2005 earthquake (Kıncal et al., 2009).

The other main fault group with a dominant E–W trend made up of the horst-graben structures, crosses the residential area of the city. The Kemalpas¸İzmir branches of the Gediz and Bornova grabens are two of the distinctive instances of the E–W depression in the Aegean region. Slope failures in natural slopes in the critical balance have been observed as a result of seismic activity in the region. According to KOERI (2008), 275 earthquakes occurred in the Aegean region in 2005 only. It is believed that the seismo-gravitational phenomena could cause serious slope instability after earthquakes in mountain slopes in weak rocks such as shale and marl. On the other hand, the Quaternary units comprise of wash and alluvium unconformably covering other geological units and alluvial soils are alluvial fan deposits formed in the sediments brought by the Gediz River.

5.3 Tectonic Setting

Tectonic framework of the Mediterranean is predominated by collision of Arabian and African Plates with Eurasia. Western extrusion of Anatolia along dextral North Anatolian Fault (NAF) in the north and sinistral East Anatolian Fault (EAF) in the south turns into an N–S extension in Western Anatolia.

According to seismological records of KOERI, İzmir, a metropolitan area of 2.5 million people, is subject to catastrophic earthquakes with potential to induce landslides. This is justifiable based on the historical earthquakes with intensity of IX–X that have occurred in the area with a death toll of 15,000 people as reported by KOERI. The most seismically active fault, based on the KOERI report, is the Tuzla fault, the activity of which has been agreed by majority of researchers Tuzla Fault forms the lineament trending NE–SW between Menderes Town and Doganbey Cape. Geological observations reveal a right-lateral offset of 200–700 m at young river beds of Holocene age along Tuzla Fault as the earthquake, Ms 6.0, 1992, shows a right-lateral focal mechanism (Aktuğ & Kılıçoglu, 2006).

Other potentially active faults are: Manisa Fault trending NW–SE between Manisa and Turgutlu with a length of about 25 km and Kemalpasa Fault of about 20 km length located on the southwestern side of E–W trending Gediz Graben. İzmir Fault, in the south of İzmir Gulf, which is two-segmented and E–W trending, and Gülbahçe-Karaburun Fault taking place in the Karaburun Peninsula are supposedly to be predominantly strike–slip faults with a relatively small dip–slip component (Aktuğ & Kılıçoglu, 2006).

5.4 Seismicity of İzmir

The accompanying effect of İzmir being tectonically active is that some of Agean sea are seismically sensitive. The İzmir city has a complex, active and rapidly changing tectonic pattern due to the relative motions of sorrounding tectonic plates. According to Kutluca & Ozdemir (2008), İzmir has recorded at least 20 devastating earthquakes with magnitudes greater than six. The author highlights that the most damaging earthquakes in the last century with potential of causing landslides include: the 1928 Torbalı, 1949 Karaburun and the 1992 Seferihisar earthquakes which mostly affected the southern part of İzmir.

Gediz graben, western part of İzmir, possesses several morphologically prominent active with nearly East-West strike and NE-SW and NW-SE trending faults, whose kinematic characteristics differentiate, form north to south, take major roles on the tectonic regime of the region (Kutluca & Ozdemir, 2008). However, there is no evidence on the active faults that could create a high earthquake activity except Gediz Graben.

Table 5.1 Summary of some of major earthquakes in İzmir (Kutluca & Ozdemir, 2008)

No	Date	Mag(M_s)	# of deaths	Lat	Long	City Area
1	03/31/1928	7.0	50	38.1	27.4	İzmir-Torbalı
2	22/09/1939	7.1	60	39.07	26.94	İzmir-Dikli
3	30/07/1949	7.0	1	38.62	26.45	İzmir-Karaburun
4	06/04/1969	5.6	None	38.47	26.41	İzmir-Karaburun
5	01/02/1974	5.2	2	38.55	27.22	İzmir
6	16/12/1977	4.8	None	38.41	27.19	İzmir
7	09/12/1977	5.3	None	38.35	27.23	İzmir
8	14/06/1979	5.9	None	38.79	26.57	İzmir-foça
9	06/11/1992	5.2	None	38.16	26.99	İzmir
10	04/17/2003	5.4	None	38.24	26.86	İzmir-Urla
11	10/04/2005	5.9	None	38.21	26.79	İzmir-Urla
12	20/10/2005	5.9	None	38.40	26.594	İzmir-Urla

5.5 Landslides in İzmir

Studies by Kutluca & Ozdemir (2008) and Avşar (1997) indicate that İzmir built up area is prone to landslides. Kutluca & Ozdemir (2008) divided the landslides vulnerability into two different regions. The first region is observed in the bed of Kocaçay stream, Karagöl and Yamanlar village and their surroundings in north of İzmir Gulf and the other region is the Cretaceous detritics in the South of İzmir Gulf outcrop in the South line of Balçova- Güzelbahçe.

Rock fall events were also evaluated using the disaster working reports registration data in which 17 rock fall events (Table 5.2) were recorded from the Disaster Working İzmir City Head Office reports between 1950 and 1998 (Kutluca & Ozdemir, 2008). The Landslide and rock fall areas were noted by Kutluca & Ozdemir (2008) to be around the metropolitan city, especially, squatter areas.

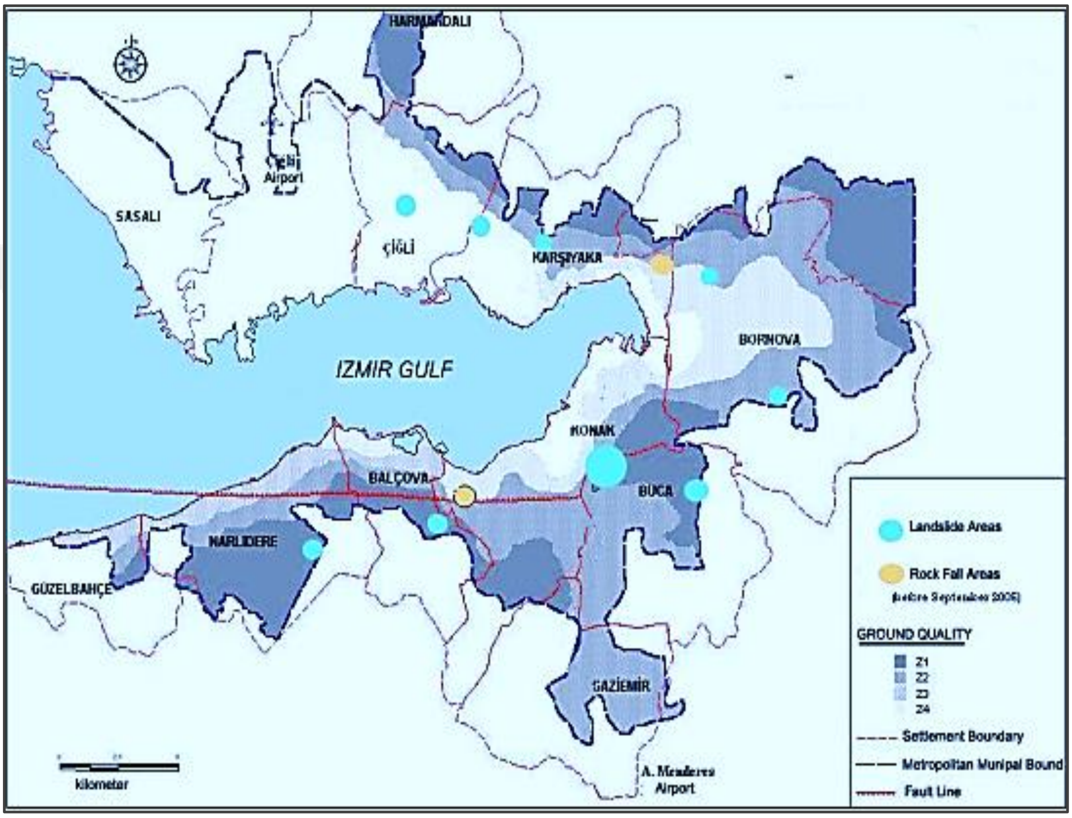

Figure 5.2 Landslide and Rock fall areas of İzmir Metropolitan Area (Kutluca & Ozdemir, 2008)

Table 5.2 Major Landslides and Rock Fall Areas in İzmir City (Kutluca & Ozdemir, 2008)

No	Region	Damaged Buildings	Natural Hazard Type
1	Çiğli-Güzeltepe	440	Landslides
2	Çigli-Örnekköy	250	Rock fall
3	Karşıyaka-Örnekköy	50	Rock fall
4	Bayraklı-Çiçekköy	20	Rock fall
5	Buca-Sakarya	44	Rock fall
6	Konak-Kocakapı	28	Rock fall
7	Konak-Gürçeşme	10	Landslides
8	Asansör	54	Rock fall
9	Kadifekale	31	Landslides
10	Altındağa-Merkez	62	Landslides
11	Altındağa-Kuyu	11	Landslides
12	Altındağa-Camdibi	13	Landslides
13	Hakimiyeti Milliye	64	Landslides
14	Narlidere-Narkent	800	Landslides

As indicated in Figure 5.2, the landslides susceptibility analyses in İzmir have not been extended to Karaburun which is officially regarded as part of İzmir. The area is also within earthquake prone zone just as İzmir, Aydın and Denizli. This work attempts to address this gap and infer the probability of landsliding in Karaburun.

5.6 Study Area

5.6.1 Location and Geological Setting of the Study Area

Karaburun Peninsula comprises of clastic Karaburun rock association and is tectonically overlain by Maastrichtian –Danian Bornova melange (Oberhänsli & Chen, 2011). The clastic sequence is pointed out to have been intruded by the Karaburun granitoid (Figure 5.3). Oberhänsli & Chen (2011) divided the clastic sedimentary sequences of the Karaburun Peninsula into two subunits; Küçükbahçe Formation and the upper clastic unit. The Küçükbahçe Formation, which outstandingly appear in the Western part of the study area has a monotonous composition and consists mainly of sandstone and shale alteration.

The sandstones in Karaburun are strongly sheared and characteristically have pronounced schistosity. Along the high-strain zones, newly formed fine-grained white mica can be recognised in the field. This unit, according to Oberhänsli & Chen (2011), was previously assigned, without any fossil evidence, to the Ordovician or Devonian but now it is dated as Early Carboniferous age based on newly found microfossils. The upper clastic unit is predominated by shales, sandstones and fine-to-medium grained conglomerate horizons. The presence of *in situ* black chert layers up to 3 m thick and extinction of the pronounced schistosity are the most diagnostic features of these clastic rocks. Oberhänsli & Chen (2011) also presented that the clastic sequence is tectonically overlain by a melange consisting of polygenetic blocks, up to 2 km across, entrenched in a highly-sheared sandstone-shale matrix. Erdoğan, Altinler, Güngör and Özer (1990) demonstrated that the blocks are predominantly limestone derivative from underlying platform-type Mesozoic carbonates, reddish chert, pelagic carbonate, mafic volcanics and serpentine constitute the other block. Based on the similarities of the internal stratigraphy of the blocks and palaeontological data, this blocky unit was correlated with the Maastrichtian–Danian Bornova melange.

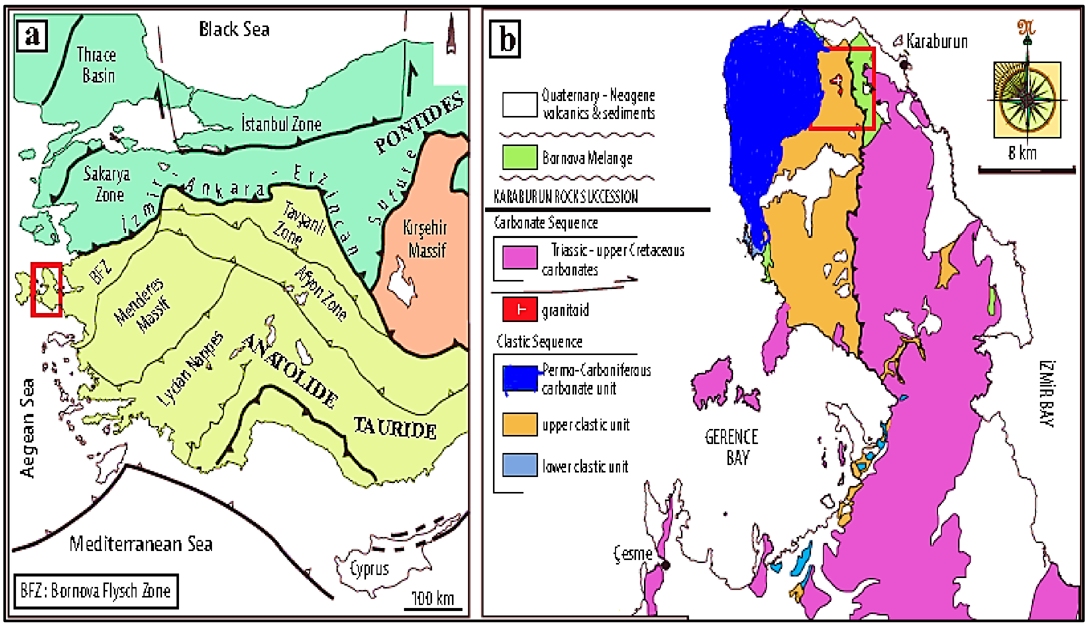

Figure 5.3 Geological Map of the Karaburun Peninsula (Oberhänsli & Chen, 2011)

5.6.2 Structural Geology

The Karaburun area comprise of the Karaburun and Karareis fault zones, NNE-striking conjugate faults and a number of folds (Uzel et al., 2013). Karaburun fault zone (KbFZ) was calculated by Uzel et al. (2013) to be 2–4 km wide, 25 km long, approximatelyN50◦W-striking and NE-dipping fault zone comprising several synthetic faults that display a well-developed step-like morphology with concave/curvilinear range-front (Figure 5.4). Further the authors explain that the fault zone controls the South West margin of the İzmir Bay at the North Eastern side of the Bozdağ high. Uzel et al. (2013) also discovered a couple of relatively small SW dipping antithetic faults in the North West of Karaburun village.

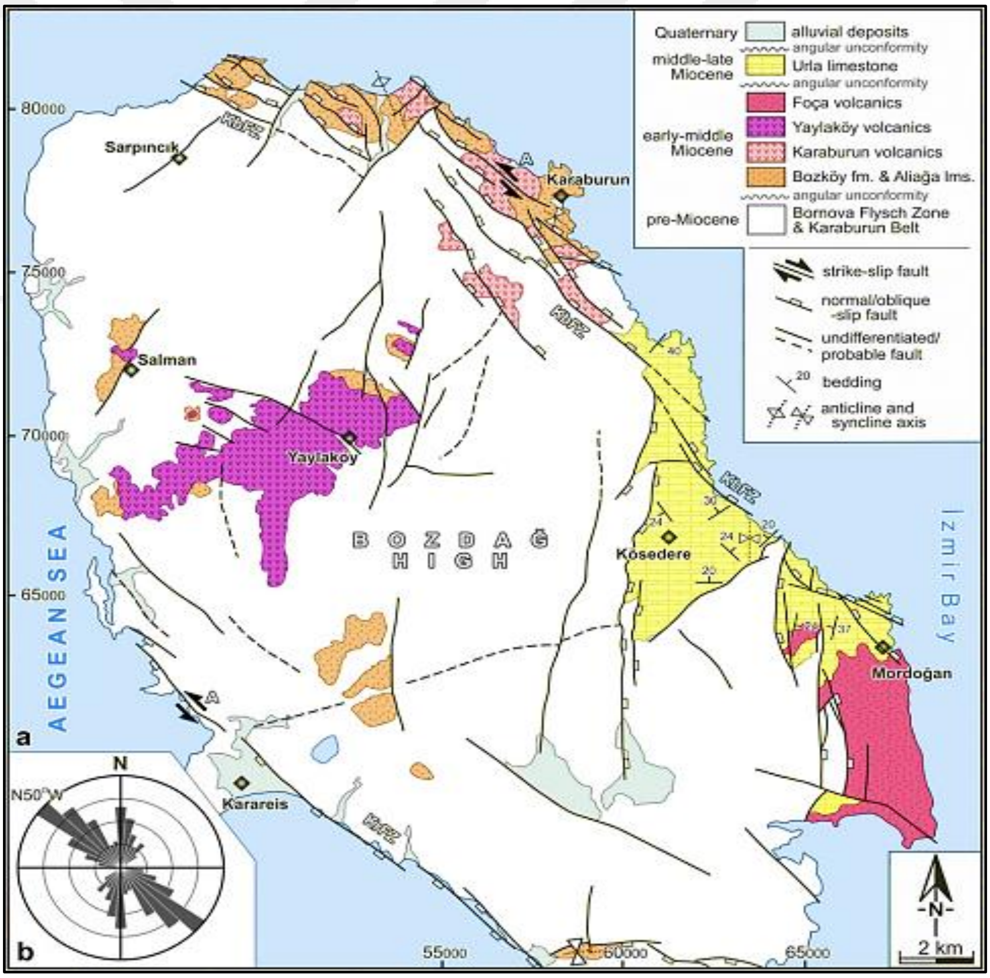

Figure 5.4 Structural setting of the study area (Uzel et al., 2013)

5.6.3 Seismicity of Karaburun

Karaburun peninsula is one of the earthquake-prone areas in the eastern central Aegean sea of İzmir bay. On 23rd July 1949 an earthquake with a surface wave magnitude (Ms) 7.0 (Mw 6.7) occurred at Karaburun, İzmir. The earthquake had a focal depth of 15 km (USGS) and it lead to 2 fatalities, 9 injuries and damage of 407 houses (Gazioglu, 2005). Due to the topographical characteristics of the Karaburun, Gazioglu (2005) is convinced the 1949 earthquake induced some landslides.

However, Gazioglu (2005) laments that the lack of information on the occurrence of landslides in the area is a serious drawback although his study of image drape-LANDSAT (7/5/36) of the region provides some scanty clues on landslides that might have occurred after the 1949 earthquakes. According to Gazioglu’s study findings of image drape-LANDSAT analysis, the landslides suspected to have been experienced in Karaburun Peninsula took place on a thick Mesozoic platform which is made up of sheared tectonic slices due to the active extensional regime in the region where the Neogene deposits on the platform are mainly composed of sandstone, clay and limestone. Apart from the 1949 Karaburun earthquake the area also experienced other strong earthquakes that occurred in the years 14th June 1979, 06th April 1969 and 02nd May 1953 (Utku, 2003). The magnitudes of the earthquakes were 5.9, 5.8 and 5.6 respectively. And recently in 2005 several minor earthquakes (≤ Mw 4.0) were recorded by KOERI.

5.7 Methodology

Work undertaken to achieve the second objective, which is to assess a possibility of landslides occurrence in the selected case study areas in the absence of EI landslides data, outlined in this study involved obtaining a Digital Elevation Model (DEM) Map, reviewing literature for study areas and application of CAMEL program which is embedded in GIS.

5.7.1 Review Data

Relevant information on EI landslides during historical earthquakes in the world was reviewed in order to form the basis of the study. Reviewed sources include; scientific and technical papers, technical reports, seismological and landslides data by USGS and university theses. Valuable data was also obtained from internet sites and relevant books on EI landslides.

5.7.2 Data Collection

A Digital Elevation Model (DEM) Map for Karaburun was extracted from Advanced Space borne Thermal Emission and Reflection Radiometer (ASTER) Global Digital Elevation Model (GDEM) Version 2(V2) (https://asterweb.jpl.nasa.gov/gdem.asp**).** The DEM has a 30 x 30 meter resolution. GIS was applied to analyse the DEM in order to calculate slope angle, aspect and curvature**.** Data on earthquake was downloaded from KOERI site (http://www.koeri.boun.edu.tr/new/) and United States Geological Survey (USGS) http://earthquake.usgs.gov/earthquakes/. The data set obtained from KOERI comprised of earthquake information since 1900 up to 2015. The data was cleaned for the minimum desired earthquake magnitude of 4.5 M_w. Earthquakes with Mw ≤ 4.5 were considered irrelevant to the study because they would not cause a significant ground shaking enough to induce sliding.

5.7.3 Approach

There are different approaches for landslides susceptibility analysis that have been propounded and implemented. The approaches may be distinguished into two main classes: qualitative and quantitative approaches (Yalcin, 2008 and Ayalew & Yamagishi, 2005). The hazard levels for the qualitative approaches are somewhat subjectively presented by descriptive terms based on expert opinion.

Yalcin (2008) explains that the most common types of qualitative methods merely use landslides inventories to identify sites of similar geological and geomorphological properties that are susceptible to failure but some qualitative approaches may incorporate the concept of ranking and weighing, and may evolve to be semi-quantitative in nature. Thus, the predictive power of the approaches varies in the weights of the parameters. However, weights evaluated by the experts are highly personal and may contain a degree of virtual admission.

Quantitative approaches on the other hand, minimise the personality and bias in the weight assessment processes and analyse the relationship between landslides occurrence and its dependency on environmental factors more objectively. The quantitative approaches fall into two categories: deterministic and statistical methods. According to Chowdhury and Flentje (2010), deterministic methods analyse the slope stability using physical based models and are slope stability using physically based models and are expressed by the FS. However, deterministic methods are limited for predicting potential landslides on a regional scale because of the need for more detailed geotechnical data.

Statistical approaches are applied to analyse landslides-contolling factors associated with landslides occurrence and rank the factors by using some statistical models. Yalcin (2008) discussed bivariate statistical analysis which deals with one dependent variable (in this case the occurrence of landslides) and one independent variable and the significance of each factor is analysed separately and combined with the landslide distribution Map, then weighting values based on landslide densities are calculated for each parameter class. The author father mentions that Statistical approaches have recently become common for evaluating landslide.

In this study a quasi-quantitative approach using fuzzy logic embedded in CAMEL are applied. CAMEL is a new, regional computer model for EI landslides hazards developed by Scot Miles and David Keefer (2004) using fuzzy logic systems, a component of the computing with words (CW) methodology. The objective of CAMEL is to deal with some of the current limitations in other EI landslides hazard models and create hazard maps that are more detailed and useful regulatory decision making (Miles & Keefer, 2009).

5.7.3.1 CAMEL Design

CAMEL was designed and implemented as a fuzzy logic system (Miles & Keefer, 2007). Fuzzy logic systems are a subset of CW, which refer to a large body of methods and frameworks and numerically representing natural language for the purpose of characterising uncertainty and propagating it using some calculus of logic. According to Schernthanner (2004) fuzzy sets can be thought of as a concept expressing a degree of belonging ranging from zero (0) and one (1). Basically, zero denotes certain not belonging and one denotes certain belonging. Fuzzy logic system refer to a configuration of IF-THEN rules that relate fuzzy sets of one or many input variable to fuzzy sets of one or more output variables.

CAMEL consists of two modules; the possibility and hazard module each of which are made up of numerous fuzzy IF-THEN rule-blocks (Miles & Keefer, 2009). The modules distinguish possibility – referred to as “indicators” – from the knowledge about relative hazard – referred to as – “intensifiers” – for each landslide type (Figure 5.5). According to the developers (Keefer and Miles, 2007; 2009), the possibility module determines whether the occurrence of each respective landslide type is feasible and it applies landscape attributes while the hazard module determines the relative hazard, expressed as a real landslide concentration, for each possible landslides type. This study adopts the possibility module to determine the feasibility of occurrence of landslides after the 1949 (Mw 7.0) İzmir-Karaburun earthquake.

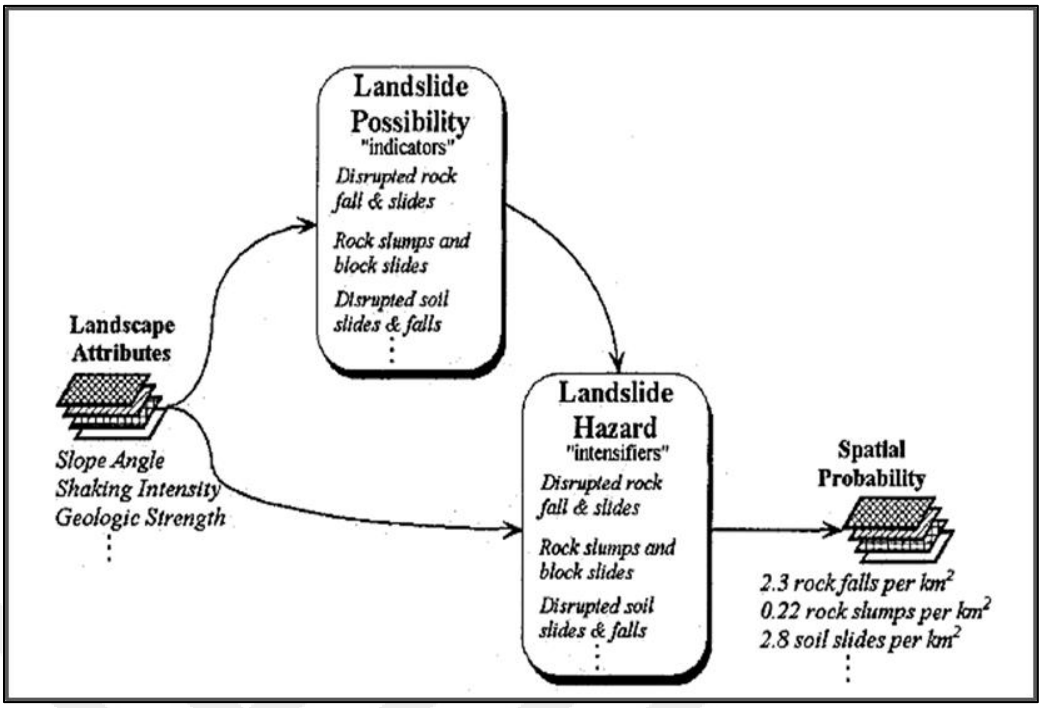

Figure 5.5 The two module framework of CAMEL; the possibility and hazard modules (Miles & Keefer, 2007)

5.7.3.2 Possibility Module

The structure and data flow of the possibility module is given in Figure 5.6. According to Miles & Keefer (2007) the possibility module comprises of seven input variables, together with seven corresponding rule blocks that are recognised in series. Each rule block consists of rules associated with a particular variable to collectively determine the degree to which each landslide type is possible. If one indicator variable specifies that a certain landslide type is not possible, the overall results of this chain of rule-blocks will be that landslide type is impossible. If one indicator variable specifies that a particular landslide type is not possible, the overall result of this chain of rule-blocks will be that the particular landslide type is impossible. If all variables show that a landslide type is possible, the minimum truth-value across these rule blocks is the output truth-value for the possibility module.

Furthermore, the developers explain that when the magnitude of the output truth-value indicates the degree to which the user-supplied input data suggests that each landslide type is possible based on the knowledge presented by the IF-THEN rules of the module. The AND operator is used for all rule blocks in the possibility module. Thus, the possibility design implies that CAMEL presumes landslide type is possible in the face of uncertainty. Miles & Keefer (2007) add that all rules in the possibility module are assigned an equal Degree of Support (DoS) weight of 1.0 and each landslide type is expressed through variable. If a truth-value is zero (0) for a particular landslide type, that type is regarded to be impossible based on the inputs provided to CAMEL. Positive possibility values then denote that the particular landslide type is possible to the degree indicated.

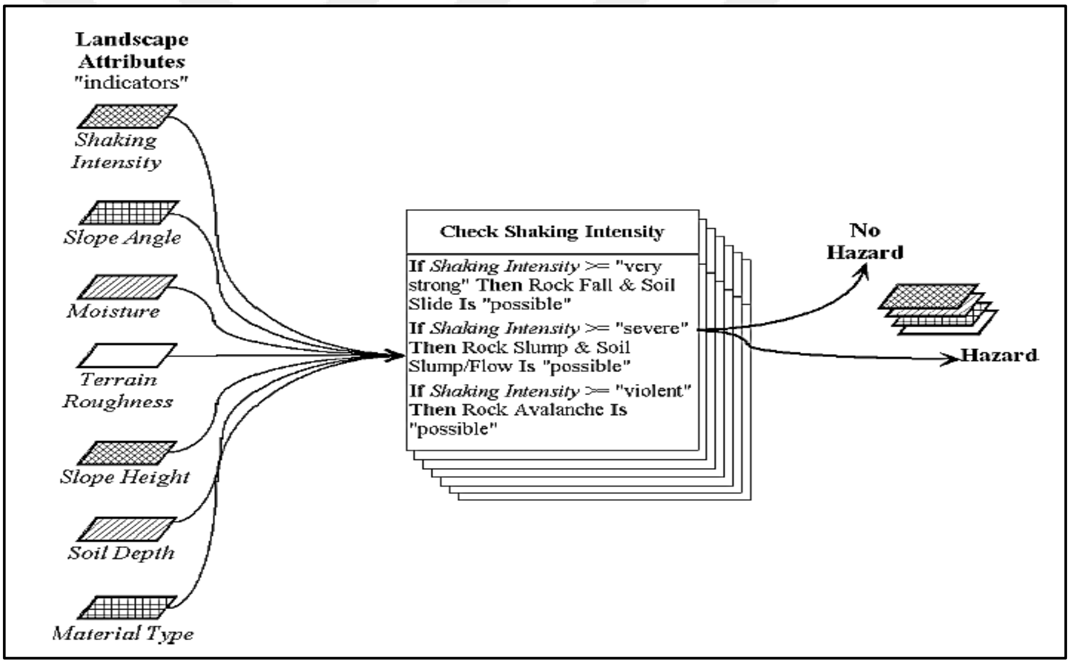

Figure 5.6 Design of the possibility module of CAMEL (Miles & Keefer, 2007)

The possibility module of CAMEL comprises of inputs as indicator variables. The variables are defined with the quantitative units, the domain, and the number and label of the fuzzy values for each variable.

Miles and Keefer (2007) also clarify that, variables that have a domain defined by a minimum value of -1 have an actual minimum of 0 where the negative value is a designed technique to track whether the user has provided input value. For negative variables, “missing” (data) is a valid data value. The design and specification of each indicator variable and associated rule block is described in Table 5.3 after Miles & Keefer, (2007)

Table 5.3 CAMEL Possibility Module Input Variables (Miles & Keefer, 2007)

Variable Name	**Units**	**Min**	**Max**	**Fuzzy Variable Labels**
pTerrainRough	Slope of slope angle	0	40	planar rough
pShapeIntensity	Shake map intensity (MMI)	-1	12	missing_than_7 greater_than_8 greater_than_9
pSoilDepth	Meters	-1	10	missing shallow deep
pSlopeHieght	Meters	-1	300	missing low height
pMaterialType	(linguistic)	-	-	missing rock soil
pMoisture	Percent	0	100	more_than_moist about_saturated
pSlopeAngle	Degrees from the horizontal	0	90	between_5 and 40 between_15 and 40 greater_than5 greater_than_15 greater_than_25 greater_than_35

1. Terrain Rough

In order to measure slope curvature, Miles & Keefer (2007) developed *pTerrainRough* variable. Although quantitative knowledge about slope curvature and EI landslide hazard is relatively sparse, a study by Liao et al. (2002) found that a variable they referred to as “terrain roughness” correlated exceptionally well with the occurrence of landslides from the 1999 Chi-Chi, Taiwan earthquake (Miles & Keefer, 2007). Khazai & Sitar (2004) established that landslides triggered during this event were primarily disrupted falls and slides. Terrain roughness is thus, the unsigned slope curvature in profile and it is second derivative of elevation in the down-slope direction, with all calculation done in degrees.

The two fuzzy values for *pTerrainRough*—“planar” and “rough”—lie on either side of second-derivative value of 15 (Figure 5.7). Miles and Keefer (2007) argued and justified the use of Liao et al. (2002) data to come up with pTerrainRough variable by stating that Liao et al. (2002) found a significant increase in landslide concentration above 15 value and that they observed that there is some small possibility of having a landslide at terrain roughness values of as low as 5. An s-shaped membership function is applied rather than a straight line curve because it results in very low truth values near a *pTerrainRough* of zero. This being the case, no accommodation for missing data is made for *pTerrainRough* because slope curvature can be computed from elevation data, which is likely to be used to calculate regional slope angle values.

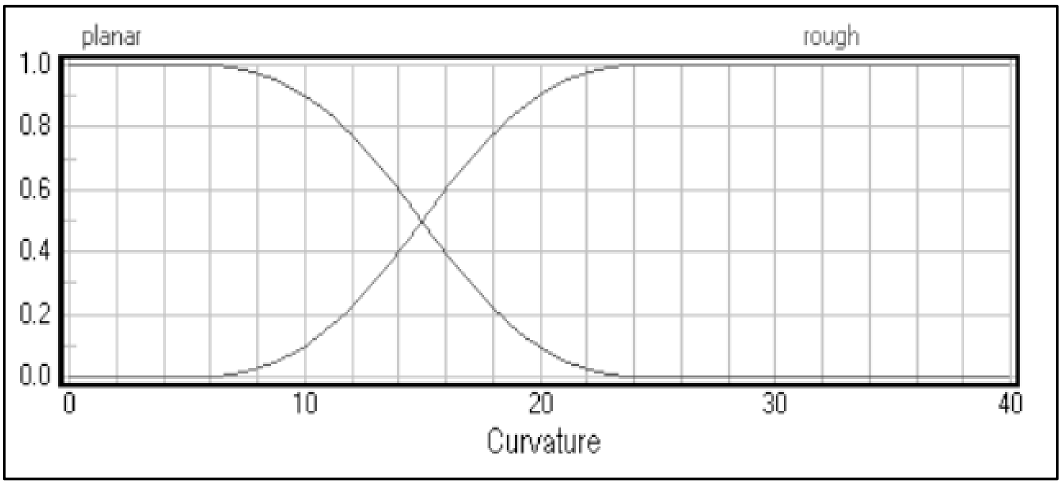

Figure 5.7 Membership functions for *pTerrainRough* (Miles & Keefer, 2007)

The rules that determine possibility based on *pTerrainRough* are given in Table 5.4 after Miles and Keefer (2007). For Category I landslides, possibility is true only if *pTerrainRough* is “rough.” It is assumed that terrain roughness is not a significant indicator for the remaining landslide types of CAMEL, and so possibility is true for either fuzzy value. Miles and Keefer (2007) highlight that this rule block is currently first in the sequence of the possibility module. Therefore, it has to consider all input combinations. Even though it is not important whether, for example, soil slumps have a “rough” *pTerrainRough*, thus fuzzy value must be checked for as recommended by developers.

Table 5.4 Possibility module rule block expressing knowledge about pTerrainRough (Miles & Keefer, 2007)

IF	THEN	
pTerrainRough	DoS	LandslidesType7
rough	1.00	rock_fall
rough	1.00	rock_avalanche
rough	1.00	soil_slide
rough	1.00	rock_slump
rough	1.00	soil_slump
rough	1.00	soil_flow
planar	1.00	soil_slide
planar	1.00	rock_slump
planar	1.00	soil_slump
planar	1.00	soil_flow

2. *Shake Intensity*

Shake intensity variable is based on the USGS ShakeMap intensity scale which is similar to the Modified Mercalli Intensity (MMI) scale, but is a ratio scale (Miles & Keefer, 2007). The minimum required shaking intensity for each respective landslide type is represented by the indicator *pShakeIntensity* (Figure 5.8).This simplifies the use of ShakeMap outputs, which are available in GIS data formats from actual or scenario events at (http://earthquake.usgs.gov/shakeMap/).

According to Miles & Keefer (2009), the *pShakeIntensity* variable consists of three fuzzy values: “missing”, “greater_than_7”, “greater_than_8”, and “greater_than_9.” The lowest value represents Category I landslides, excluding rock avalanches. The middle value represents Category II (coherent slides) and Category III landslides (rapid soil flows).

The highest value of shake intensity is related to the occurrence of rock avalanches. MMI threshold values for rock avalanche were determined from minimum magnitude and distance information in Hancox et al. (2002) and Keefer (1984), which were then converted to MMI. The other values are based on Rodriguez et al. (1999) and Keefer (1984). Each membership function augments from a truth-value of zero (0) at the lowest recorded minimum MMI threshold to a truth of one (1) at the maximum-recorded minimum MMI value. If no intensity data is provided, CAMEL will compute static susceptibility for each landslide type.

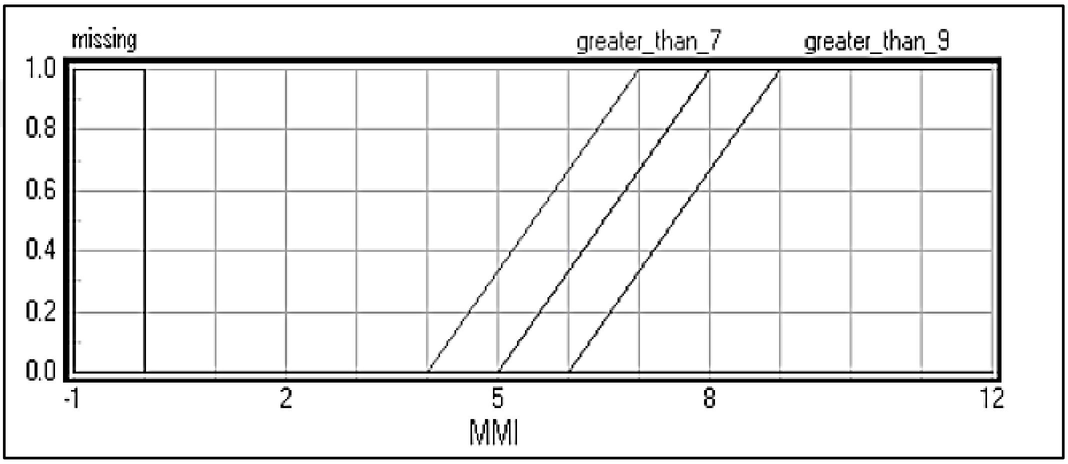

Figure 5.8 Membership functions for *pShakeIntensity* (Miles & Keefer, 2007)

3. Soil Depth

The variable pSoilDepth is based on knowledge from Keefer (1984) and Bommer and Rodriguez (2000). The two fuzzy values lie on either side of 3 meters (Figure 5.9). This fuzzy threshold gives knowledge regarding whether there is sufficient soil for a deep-seated failure to occur (Miles & Keefer, 2007). The developers further explain that if data regarding slope depth is missing CAMEL will presume that Category I landslides in soil are possible. Table 5.5 shows the associated rules.

It can be noticed in Figure 5.9 that the truth-values for all of the fuzzy values are simply passed on to the next rule block, except for”soil_slump.”

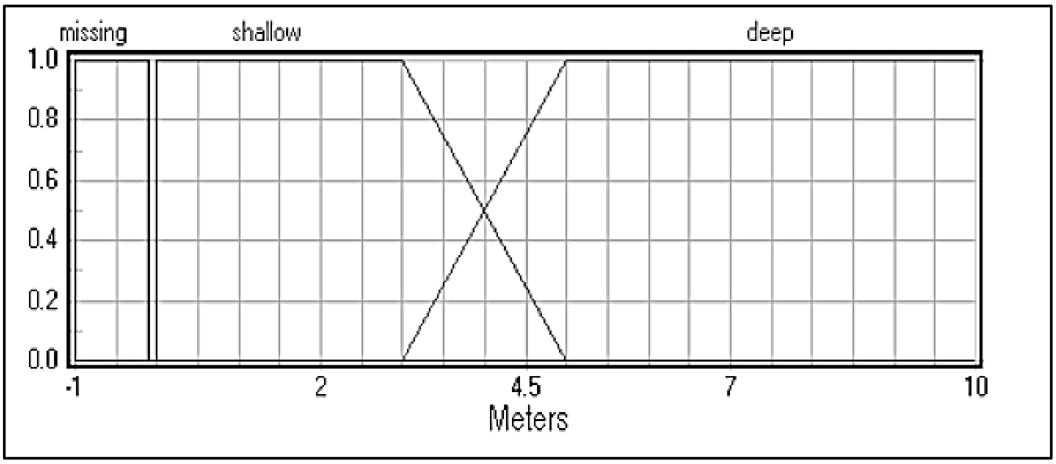

Figure 5.9 Membership function for *pSoilDepth* (Miles & Keefer, 2007).

Table 5.5 Possibility module rule block expressing knowledge about pSoilDepth (Miles & Keefer, 2007)

IF		**THEN**	
LandslidesType6	pSoilDepth	DoS	LandslidesType5
soil_slump	deep	1.00	soil_slump
soil_slump	missing	1.00	soil_slump
rock_fall		1.00	rock_fall
rock_avalanche		1.00	rock_avalanche
soil_slide		1.00	soil_slide
rock_slump		1.00	rock_slump
soil_flow		1.00	soil_flow

4. Slope Height

Keefer (1984) observed that for the occurrence of rock avalanches the local slope height must be greater than or equal to 150 meters. This knowledge is reflected in the variable *pSlopeHeight* which is comprised of two fuzzy values, “low” and “high.”(Figure5.10). The latter value is defined so that the truth-value is one (1) at a slope height value of 150 meters. The other membership function is simply inverse.

The steepness of the membership functions is warranted because 150 meters is an extreme minimum for the avalanche dataset of Keefer (1993). A fuzzy value of “missing” is also possible and is used to assume that rock avalanches are possible in the event of missing slope height data values. Table 5.6 lists the associated rules and shows that calculations are only performed on the fuzzy value “rock_avalanche.” Otherwise, truth values associated with other landslide types are passed to the next rule block.

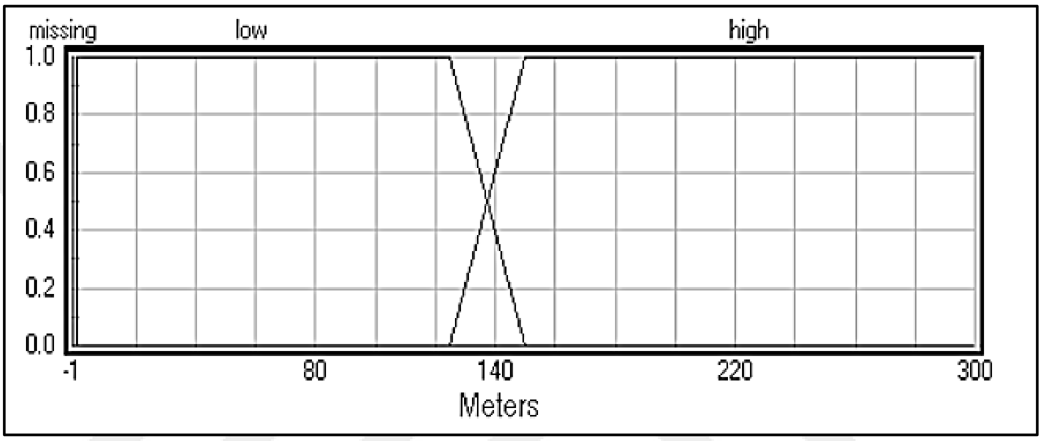

Figure 5.10 Membership functions for pSlopeHeight (Miles & Keefer, 2007)

Table 5.6 Possibility module rule block expressing knowledge about *pSlopeHeight* (Miles & Keefer, 2007)

IF		THEN	
LandslidesType5	pSlopeHeight	DoS	LandslidesType4
rock_fall		1.00	rock_fall
rock_avalanche	high	1.00	rock_avalanche
rock_slide		1.00	rock_slide
rock_slump		1.00	rock_slump
soil_slump		1.00	soil_slump
soil_flow		1.00	soil_flow
rock_avalanche	missing	1.00	rock_avalanche

5. Material Type

For input material type Miles and Keefer (2004) came up with the *pMaterialType* variable which is a nominal variable. This variable designed to take nominal values; “rock”, “soil”, and “missing.” Hence, the material type variable serves as a binary switch to denote whether material properties inputs given refer to a rock or soil. If the indication is given, the fuzzy system will apply the same material properties to both rock and soil landslides Table 5.7. Further, the developers clarify that both rock and soil landslides are assumed possible.

Table 5.7 Possibility module rule block expressing knowledge about *p*MaterialType (Miles & Keefer, 2007)

IF		THEN	
LandslidesType4	pMaterialType	DoS	LandslidesType3
rock_fall	Rock	1.00	rock_fall
rock_avalanche	Rock	1.00	rock_avalanche
soil_slide	Soil	1.00	soil_slide
rock_slump	Rock	1.00	rock_slump
soil_slump	Soil	1.00	soil_slump
soil_flow	soil	1.00	soil_flow
rock_fall	missing	1.00	rock_fall
sock_avalanche	missing	1.00	sock_avalanche
soil_slide	missing	1.00	soil_slide
rock_slump	missing	1.00	rock_slump
soil_slump	missing	1.00	soil_slump
soil_flow	missing	1.00	soil_flow

6. Moisture

When developing CAMEL Miles and Keefer (2007) also considered the *pMosture* variable to acquire knowledge about different categories of landslides with respect to ground moisture content or water table depth.

The *pMosture* variable describes the degree to which the analysis layer is saturated, relative to depth of the layer. Conceptually, *pMoisture* variable is the ratio of the ground water height over the depth of the ground layer under analysis, multiplied by 100% (Miles & Keefer, 2007). The knowledge for this variable is based on Keefer (1984). The lowest value, “more_than_moist”, is related to Category II landslides, assuming that the occurrence of coherent slides require some ground water. The membership function shape indicates that above 0 percent layer saturation some possibility exists. The high value, “about_saturated”, is related to rapid soil flows, which require high moisture content (Keefer, 1984).

A threshold value of 75% (indicating truth value of 1) was assumed as a conservative value describing that the entire layer saturated (Miles & Keefer, 2007). A higher threshold would reduce possibilities assigned to less-saturated slopes. Looking at the corresponding rules listed in Table 5.11, it can be noticed that “rock_fall”, “rock_avalanche”, and “soil_slide” are possible regardless of moisture conditions (Keefer, 1993; Keefer, 1984).

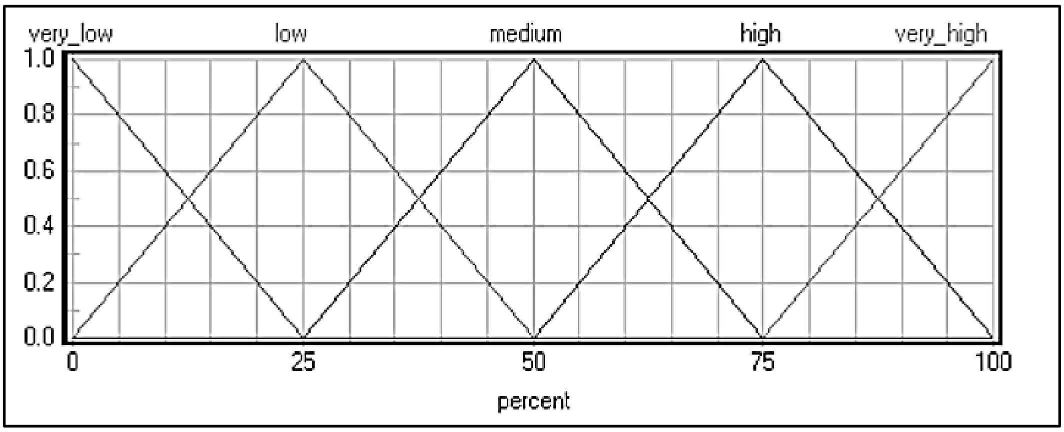

Figure 5.11 Membership functions of pMoisture (Miles & Keefer, 2007)

Table 5.8 Possibility module rule block expressing knowledge about *pMoisture* (Miles & Keefer, 2007)

IF		THEN	
LandslidesType3	pMoisture	DoS	LandslidesType2
rock-fall		1.00	rock-fall
rock_avalanche		1.00	rock_avalanche
rock_slide		1.00	rock_slide
rock_slump	more_than_moist	1.00	rock_slump
soil_slump	more_than_moist	1.00	soil_slump
soil_flow	about_saturated	1.00	soil_flow

7. *Slope Angle*

Miles and Keefer (2007) collected considerable data to have a better knowledge for describing the minimum slope angle required for the occurrence of each landslide type represented by the variable *pSlopeAngle*. The five membership functions, shown in Table 5.9, are based on Hancox et al. (2002), Rodriguez et al. (1999), and Keefer (1984). In defining the membership function for rapid soil flows, Miles and Keefer (2007) rounded up the (highest) minimum value found in the literature from 2.3 degrees to 5. The majority of flows in the data set of Keefer (1984) are greater than 5 degrees. This simplifies definition of *pSlopeAngle* membership functions.

The fuzzy value "greater_than15" is applied to Category I landslides in soil and is founded on the published values for disrupted soil slides. This implies that the possibility for soil avalanches is presently over-predicted by CAMEL because the general minimum slope angle for this landslide type is 35 degrees. Disrupted soil slides are very common (Keefer, 1984); so the variable is designed to reflect this priority. The fuzzy value "greater_than35" is defined based on knowledge about disrupted rock falls and slides. Knowledge about soil block slides was used to define the fuzzy value "between_5and40" and is applied to both soil block slides and soil slumps.

The fuzzy value “between_15and40” is based on knowledge about all coherent rock slides. Further, Miles and Keefer (2007) discuss that the slope angle maximum of 40 degrees for the Category II landslides is based on Hansen and Franks (1991), Cruden and Varnes (1996), and the data set of Keefer (1984). Because of uncertainty in this maximum, the membership function attenuates slowly until it reaches a truth-value of zero (0.0) at 90 degrees (Figure 5.12).

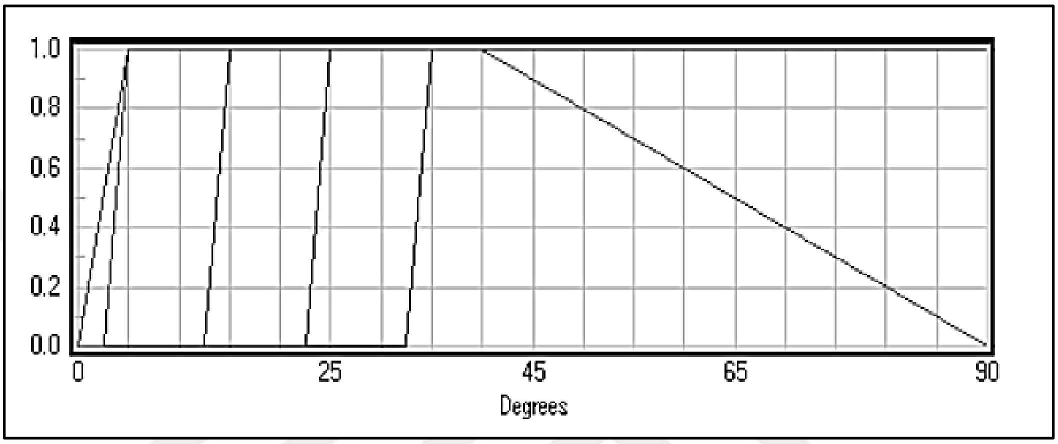

Figure 5.12 Membership functions for *pSlopeAngle* (Miles & Keefer, 2007)

Table 5.9 Knowledge about minimum slope angles required for particular types of landslides (Miles & Keefer, 2009)

Landslides Type	Minimum Slope Angle (degrees)		
	Keefer (1984)	Rodriguez et al. (1999)	Hancox et al. (2002)
Disrupted rock falls and rock slides	35-40	35	40
Disrupted soil slides/soil falls	35/40	55	25-35
Rock avalanches	25	n/a	25-35
Rock slumps and soil block slides	15	15	15
Soil slumps and soil block slides	5-10	8	15
Rapid soil flows	2.3	0	2

Table 5.10 Possibility module rule block expressing knowledge about *pSlopeAngle* (Miles & Keefer, 2007)

IF		THEN	
Landslides Type2	pSlopeAngle	DoS	Landslides Type
rock_fall	greater_than_35	1.00	rock_fall
rock_avalanche	greater_than_25	1.00	rock_avalanche
rock_slide	greater_than_15	1.00	rock_slide
rock_slump	between_15and40	1.00	rock_slump
Soil_slump	between_5and40	1.00	Soil_slump
Soil_flow	greater_than5	1.00	Soil_flow

5.8 Results

This section presents the findings obtained from the application of GIS and CAMEL to assess the possibility of occurrence of EI landslides during and/or after the 1949 Karaburun earthquake

5.8.1 Structure of CAMEL for Analysis

CAMEL was designed to operate through a GIS-based program. As a typical ArcGIS Map, CAMEL contains a number of layers (with or without connected database) that are stack on top of each other (Figure 5.13). When implementing CAMEL on a possibility module, the following layers are used:

1) Slope Height
2) Slope Angle
3) Terrain Roughness
4) Material Type
5) Soil Depth
6) Moisture
7) Shake Intensity

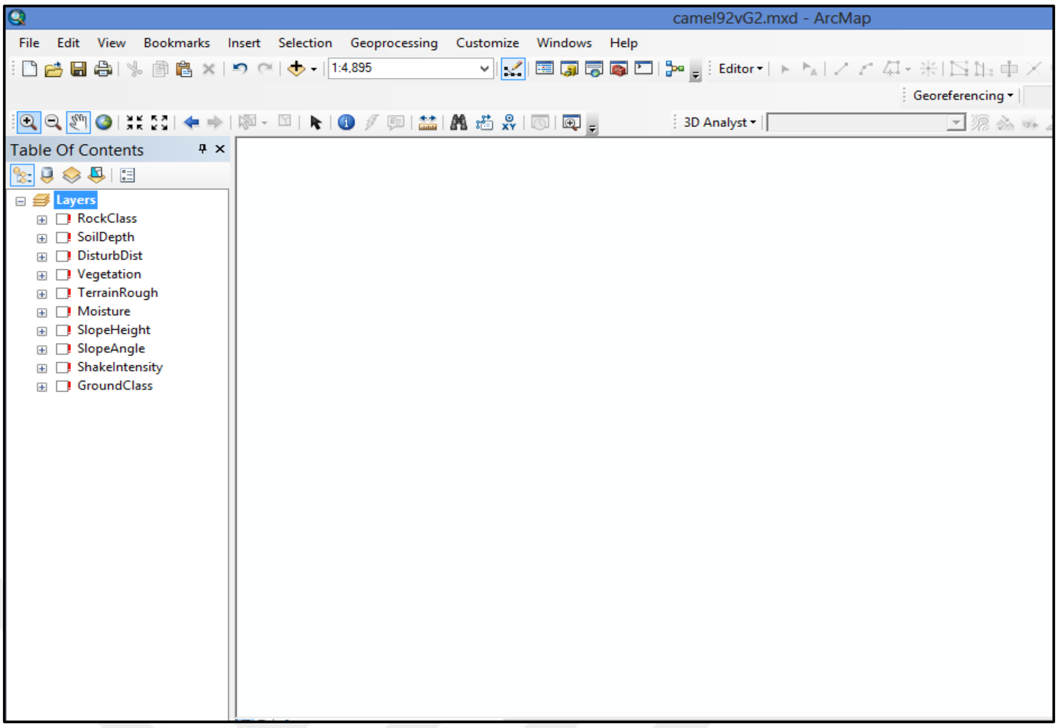

Figure 5.13 The structure of CAMEL in ArcGIS

In an attempt to assess the possibility of the occurrence of landslides after the 1949 İzmir Karaburun earthquake, the four topographical parameters; elevation, slope angle, slope aspect and slope curvature were used for correlation with susceptibility of landslide occurrence. The topographic parameters: Slope height, slope angle, slope aspect, and slope curvature were extracted from the Karaburun DEM at 30m×30m resolution which was obtained from ASTER GDEM V2 and downloaded from http://gdex.cr.usgs.gov/gdex/. To extract the weighted value of the topographic parameters, the Karaburun DEM was run in CAMEL which is embeded in Arc GIS (Figure 5.14).

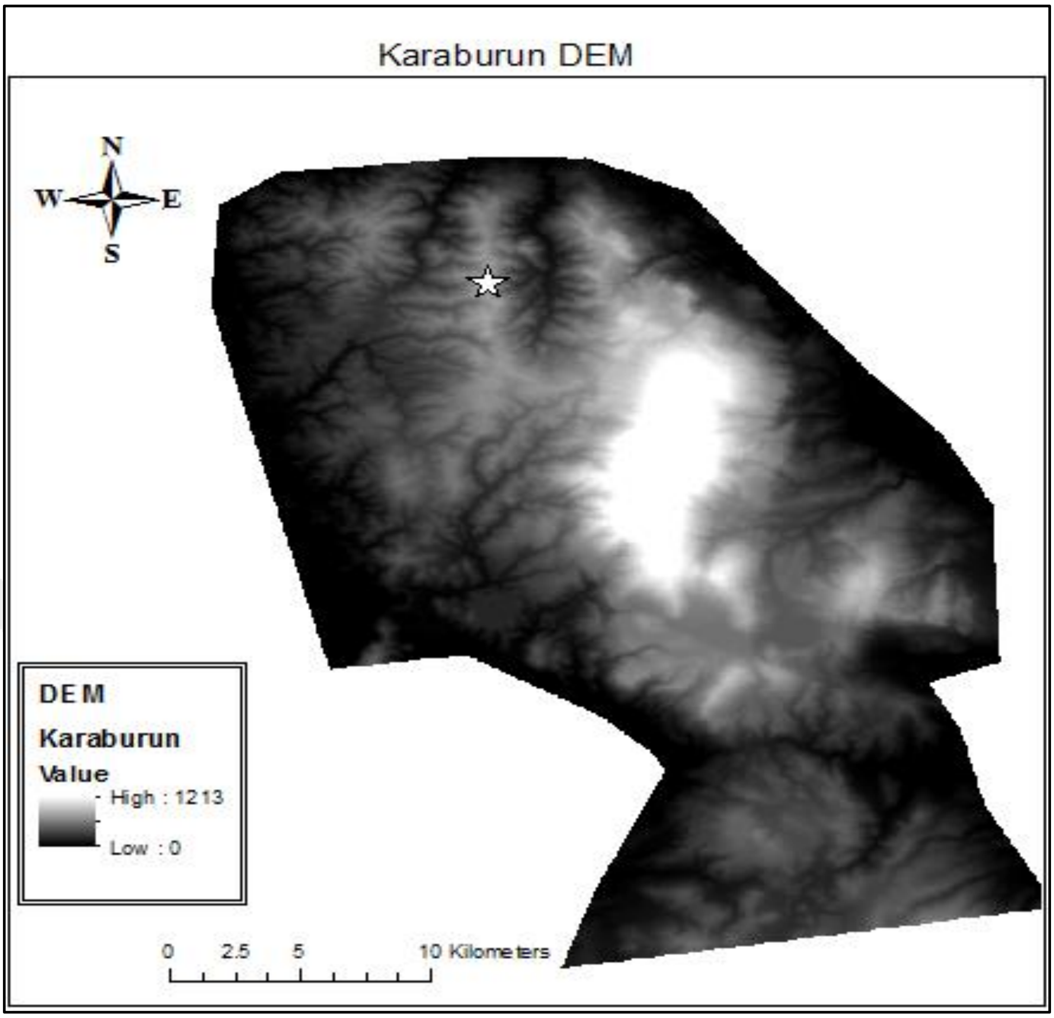

Figure 5.14 Digital elevation model for Karaburun (The star is the epicenter of the 1949 İzmir-Karaburun earthquake

5.8.2 Slope Height

Slope height was directly calculated from the Karaburun DEM in ArcGIS through the Spatial Analyst Tools “surface analysis. Before running the slope height layer, a fill command in Spatial Analyst Tools “hydrology” was run to correct surface irregularities. After calculating the slope height, I reclassified the slope angle at intervals of 200m (Figure 5.15). As noted in the review, slope heights between 750m and 1500m have high susceptibility of landslide occurrence in an event of a strong ground shaking. The star inside the slope height map denotes the approximate epicentre of the Karaburun earthquake.

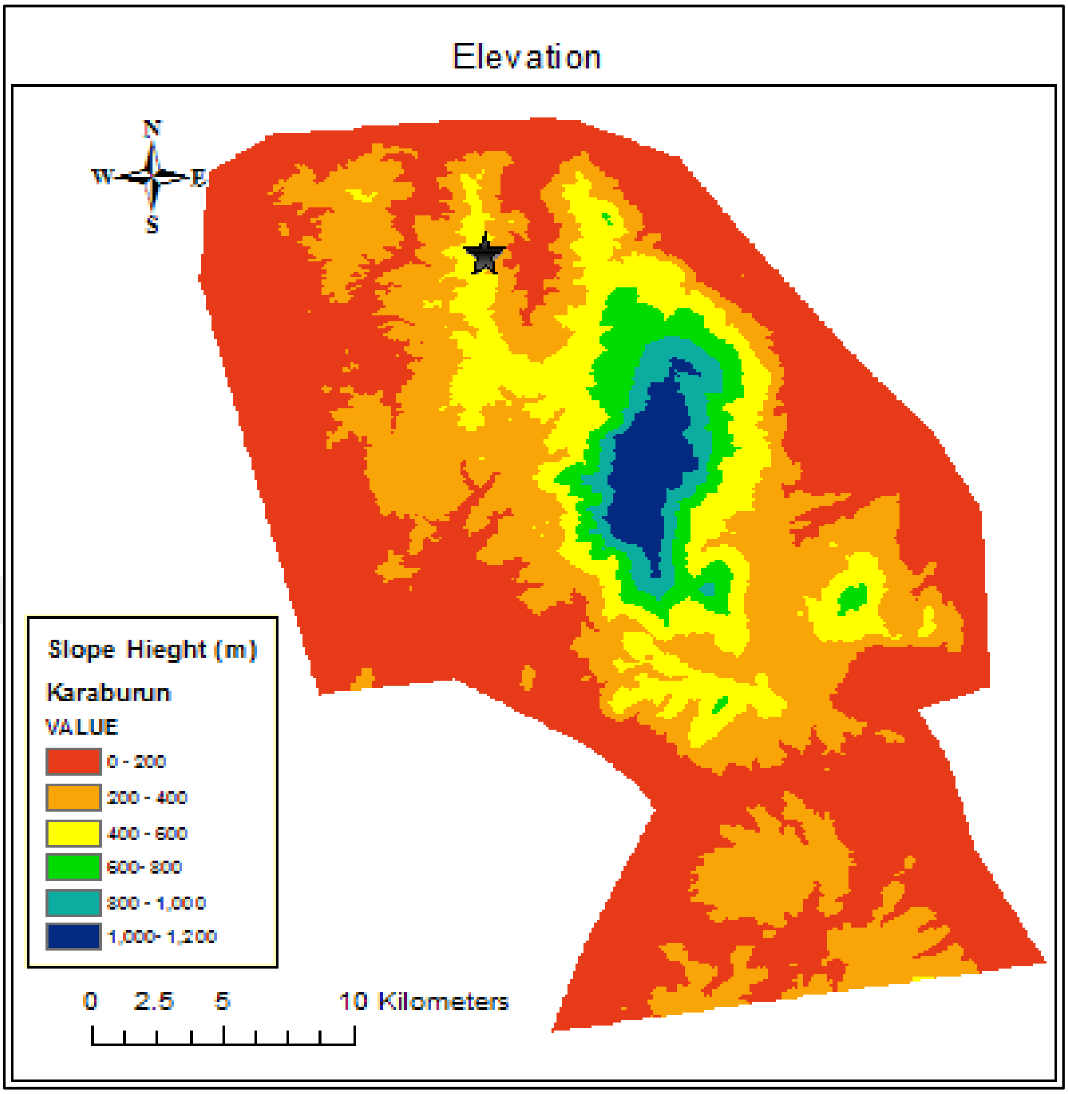

Figure 5.15 Slope height Map derived from the Karaburun DEM

To assess the significance of the slope height variable, the layer of slope height was then run in CAMEL integrated in ArcGIS to test for the variable's fuzzy membership. The fuzzy membership was obtained by running the slope height layer calculated from the Karaburun DEM in ArcGIS through the Spatial Analyst Tools using 'surface analysis'(Figure 5.16). It can be observed that the epicentre of the Karaburun earthquake lies in the slope height membership value of 0.4 – 0.6 (Figure 5.16). This implies some probability of occurrence of landslides.

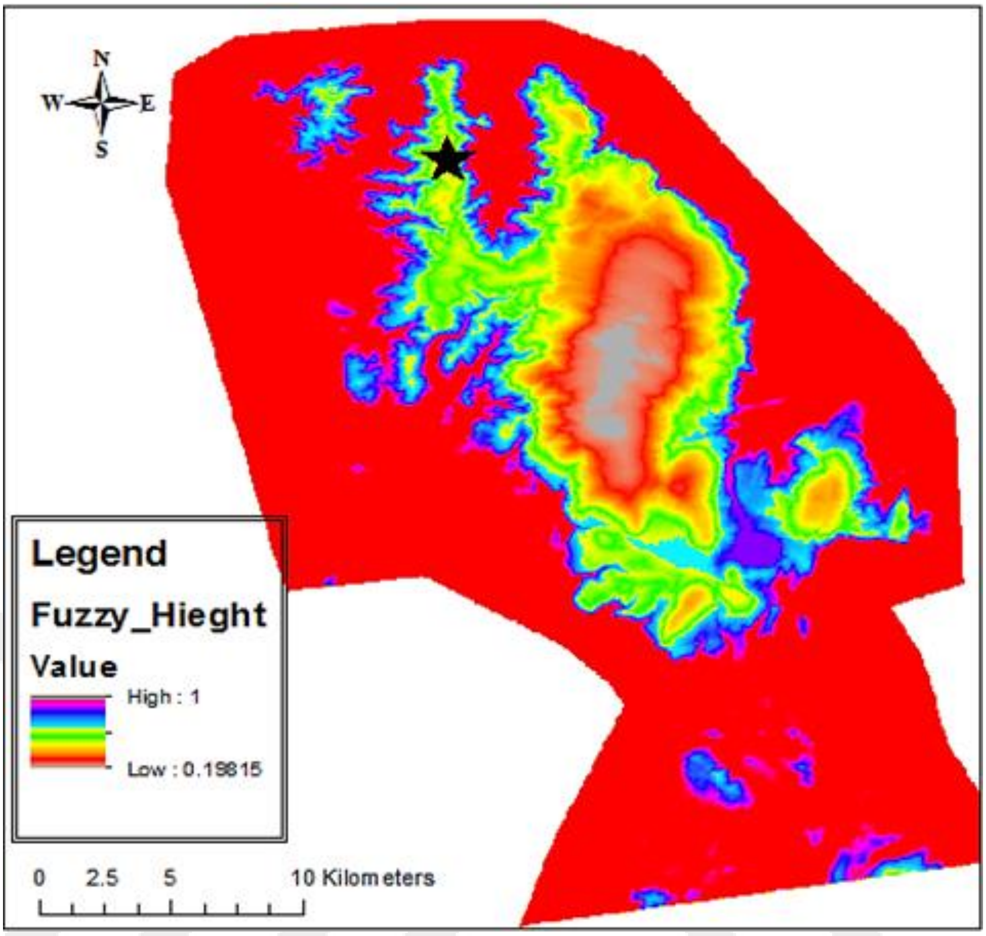

Figure5.16 Fuzzy membership Map of slope height derived from a calculated elevation

5.8.3 Slope Angle

The slope angle was directly calculated from the Karaburun DEM in ArcGIS through the Spatial Analyst Tools “surface analysis. Then I reclassified the slope angle at intervals of 10°. Generally, “the steeper and higher slopes are the higher susceptibility for landslide occurrence, even when the slope failure is not triggered by an earthquake” (Xu et al., 2014) . From the possibility module rule block expressing knowledge about *pSlopeAngle* developed by Miles and Keefer (2007), the susceptibility values generally increase with the slope angle, but slopes exceeding 35° (classes 8– 13) are more susceptible to landsliding. It can be noted from the slope angle Map that categories 20-30^{o}, 30-40^{o} and 40-50^{o} are dominant (Figure 5.17).

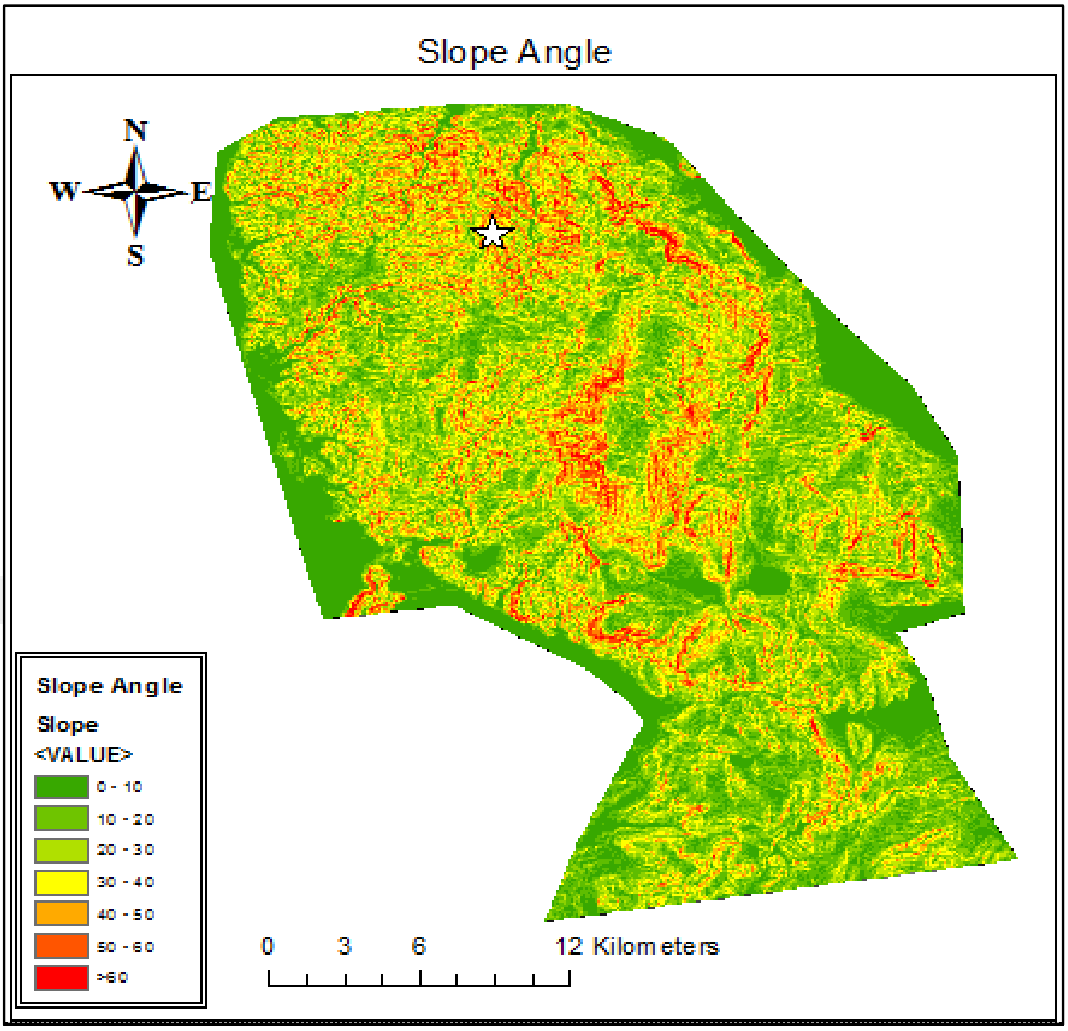

Figure 5.17 Slope angle Map derived from the Karaburun DEM

After calculating slope angle from the Karaburun DEM in ArcGIS through the Spatial Analyst Tools using 'surface analysis', the layer of slope angle was then run in CAMEL embedded in ArcGIS to test for its fuzzy membership. It can be observed that the epicentre of the Karaburun earthquake lies in the slope membership value 0.2 – 0.6 (Figure 5.18). The region around the epicentre is characterised by slopes ≥ 50. However, there are a few areas with a fuzz membership value ≥ 0.6 and are characterised by slope angle values ≤ 50. Generally, the finding implies that there is a low probability of landslides occurrence within the region.

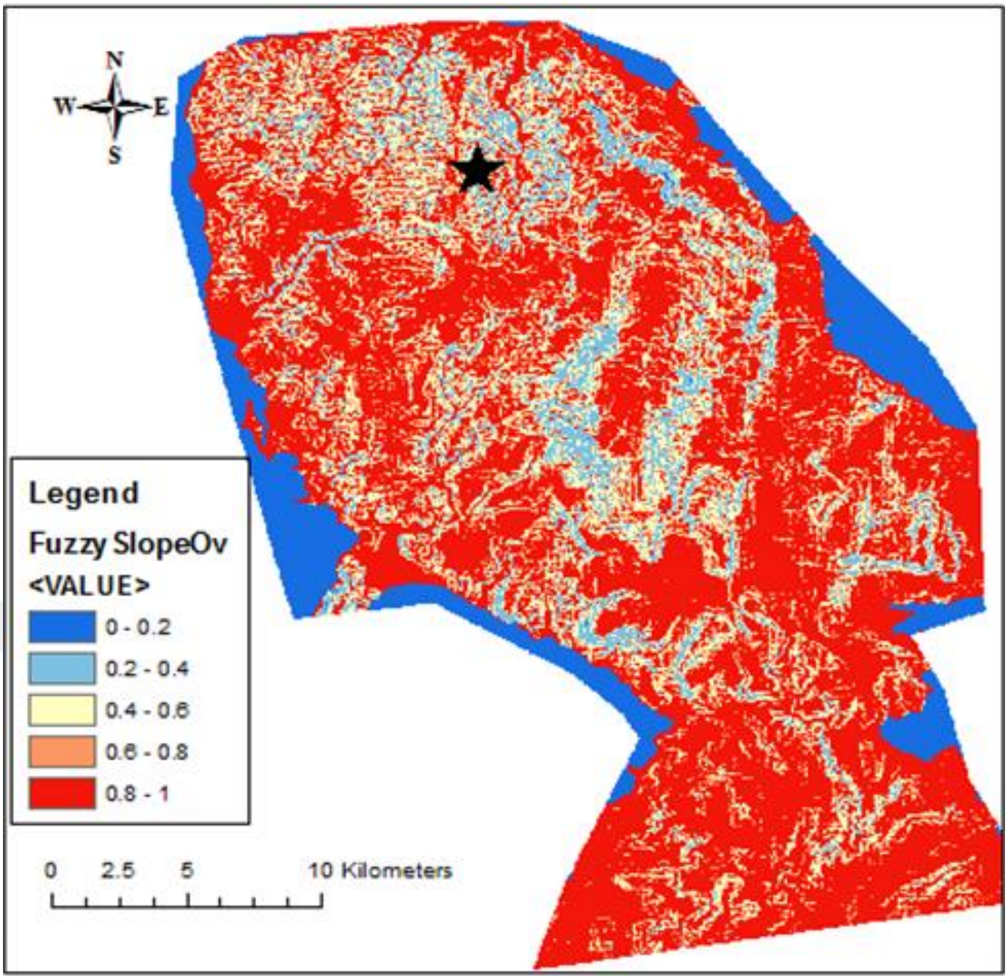

Figure 5.18 Fuzzy membership Map of slope angle derived from a calculated slopes angle

5.8.4 Slope Aspect

The slope aspect is defined as the direction of the maximum slope of the terrain surface and is related to factors such as exposure to sunlight, drying winds, rainfall (degree of saturation), and discontinuities, which may control landslide occurrence (Yalcin, 2008). The slope aspect may also have an effect on landsliding because it is related to factors such as directional PGAs (Dai et al. 2011). With this knowledge in mind, I calculated Slope aspect values from the Karaburun DEM in ArcGIS through the Spatial Analyst Tools "surface analysis.

The slope aspect was separated into nine classes for the study, including flat, N, NE, E, SE, S, SW, W, and NW as presented in Figure 5.19. It can be observed that the earthquake epicentre fall in the predominant W and a little of N trending slopes

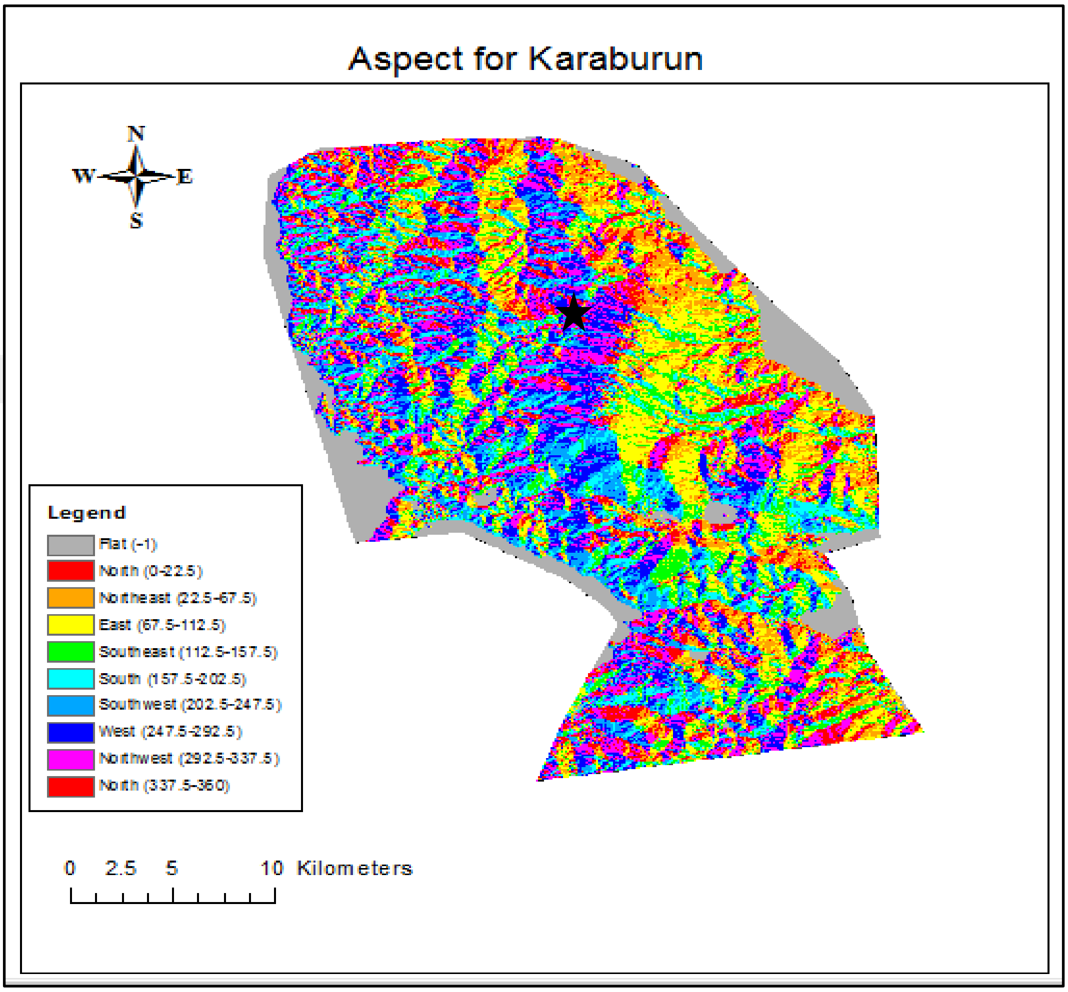

Figure 5.19 Aspect Map for Karaburun

An attempt to extract a fuzzy membership of slope aspect was done to relate probability of occurrence of landslides with respect to slope orientation. Figure 5.20 presents a Map of the fuzzy membership of aspect. The slope aspect values were obtained after running the calculated slope aspect values which were calculated from the Karaburun DEM in ArcGIS through the Spatial Analyst Tools "surface analysis.

The fuzzy slope aspect values in this case offer less meaning because the occurrence of EI landslide is affected by the position of the epicentre, PGA and seismogenic fault (Dai et al. 2011).

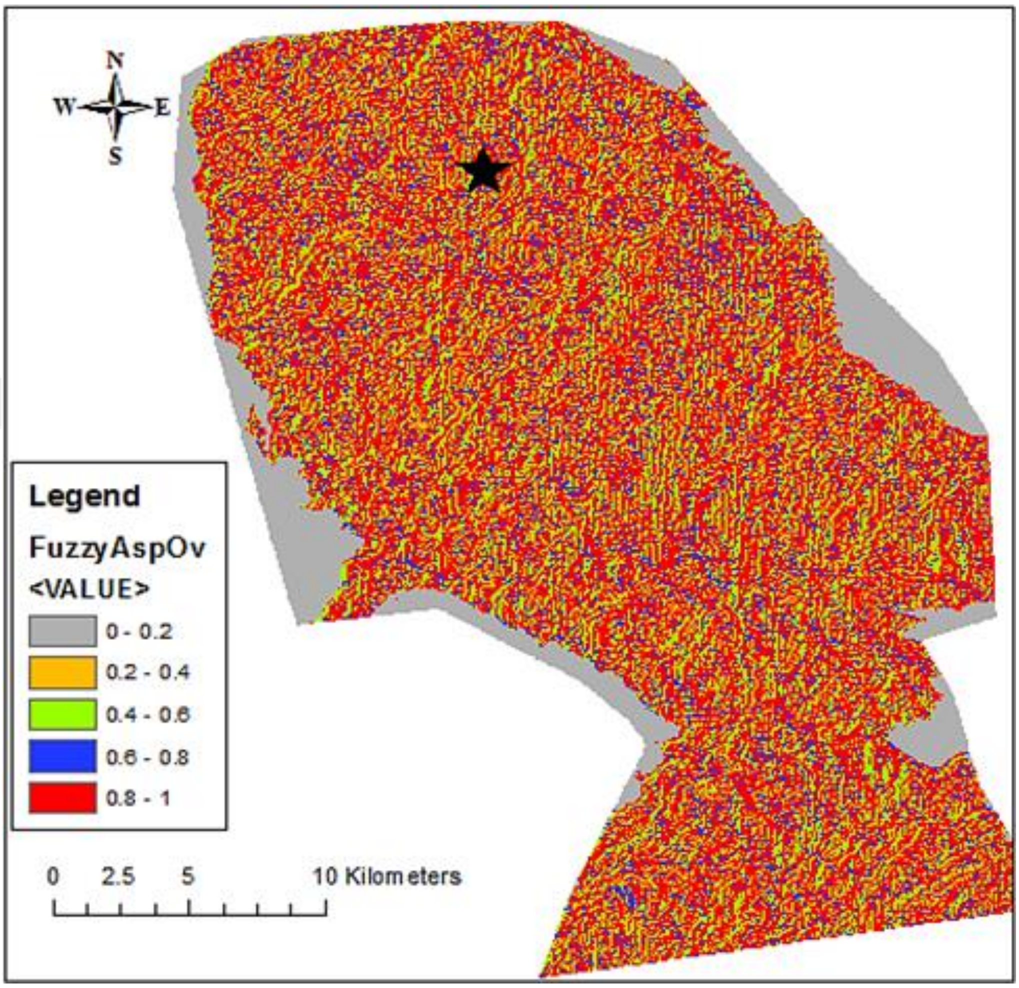

Figure 5.20 Fuzzy membership Map of slope aspect derived from a calculated slope aspect layer

5.8.5 Terrain Roughness

The terrain roughness is a measure of the convexity or concavity of the slope of an area. In this respect; negative curvatures represent concave surfaces, a zero curvature represents a flat surface, and positive curvatures represent convex surfaces. Terrain roughness can be considered as simply slope curvature in profile.

This terrain roughness variable is the second derivative of elevation in the down-slope-direction, with calculations done in degrees. The terrain roughness layer is obtained by merely running the curvature component in spatial analyst tool. Figure 5.21 presents the terrain roughness Map. Figure 5.21 indicates that there is dominance of convexity over concavity as the dominating values are in the range of 0-5 and -0.5 – 0 respectively.

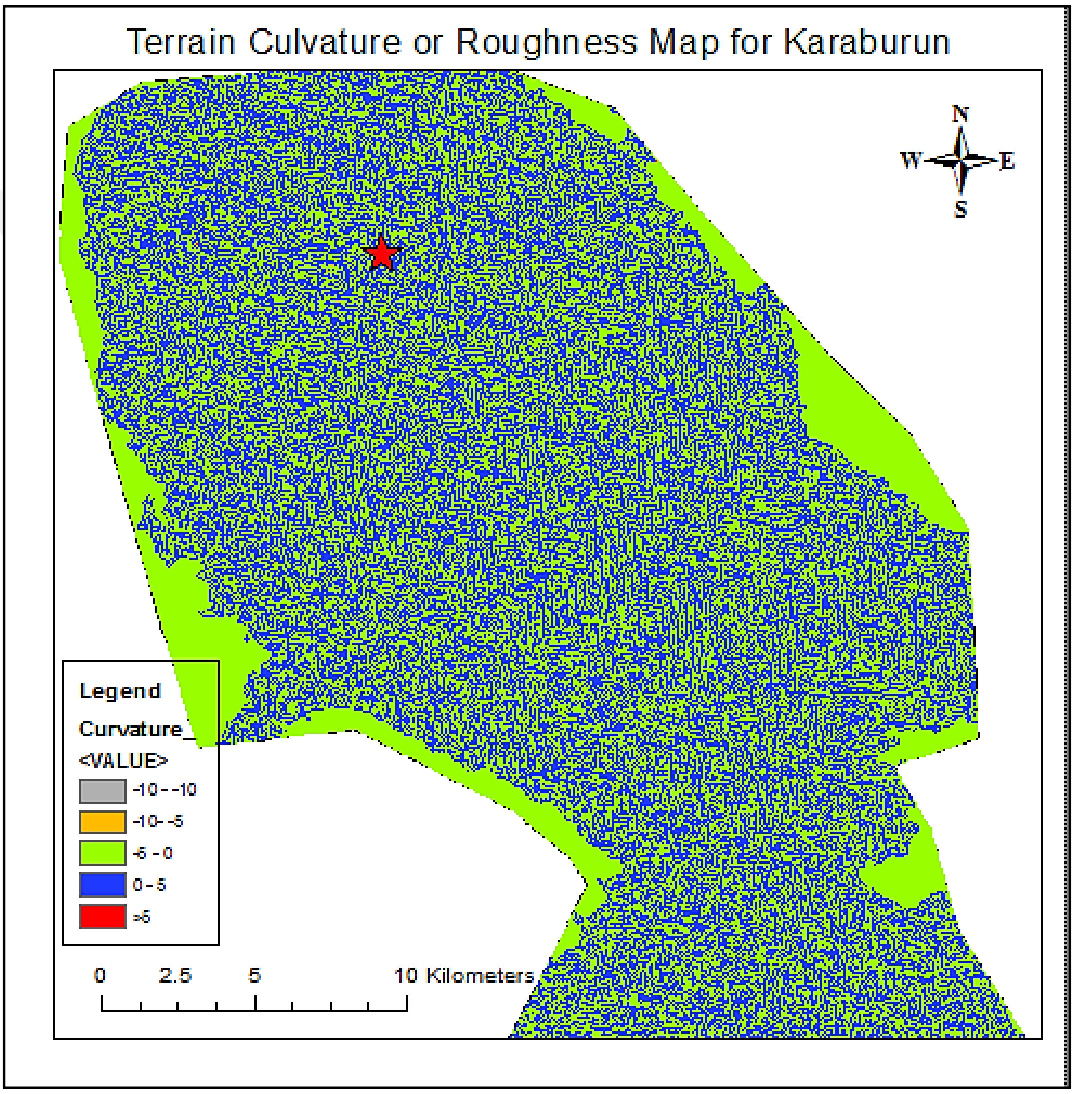

Figure 5.21 Terrain curvature or roughness Map for Karaburun

The study attempted to establish the effect of terrain roughness on the likelihood of occurrence of EI landslides. So, after calculating the terrain roughness, a fuzzy membership was derived from terrain roughness layer which was calculated in ArcGIS. The terrain roughness layer was calculated from the slope angle extracted from the Karonga DEM using Spatial Analyst Tools. A presentation of terrain roughness using fuzzy membership is given in Figure 5.22. The membership values indicate a probability of 0.3 – 0.7 (Figure 5.22).

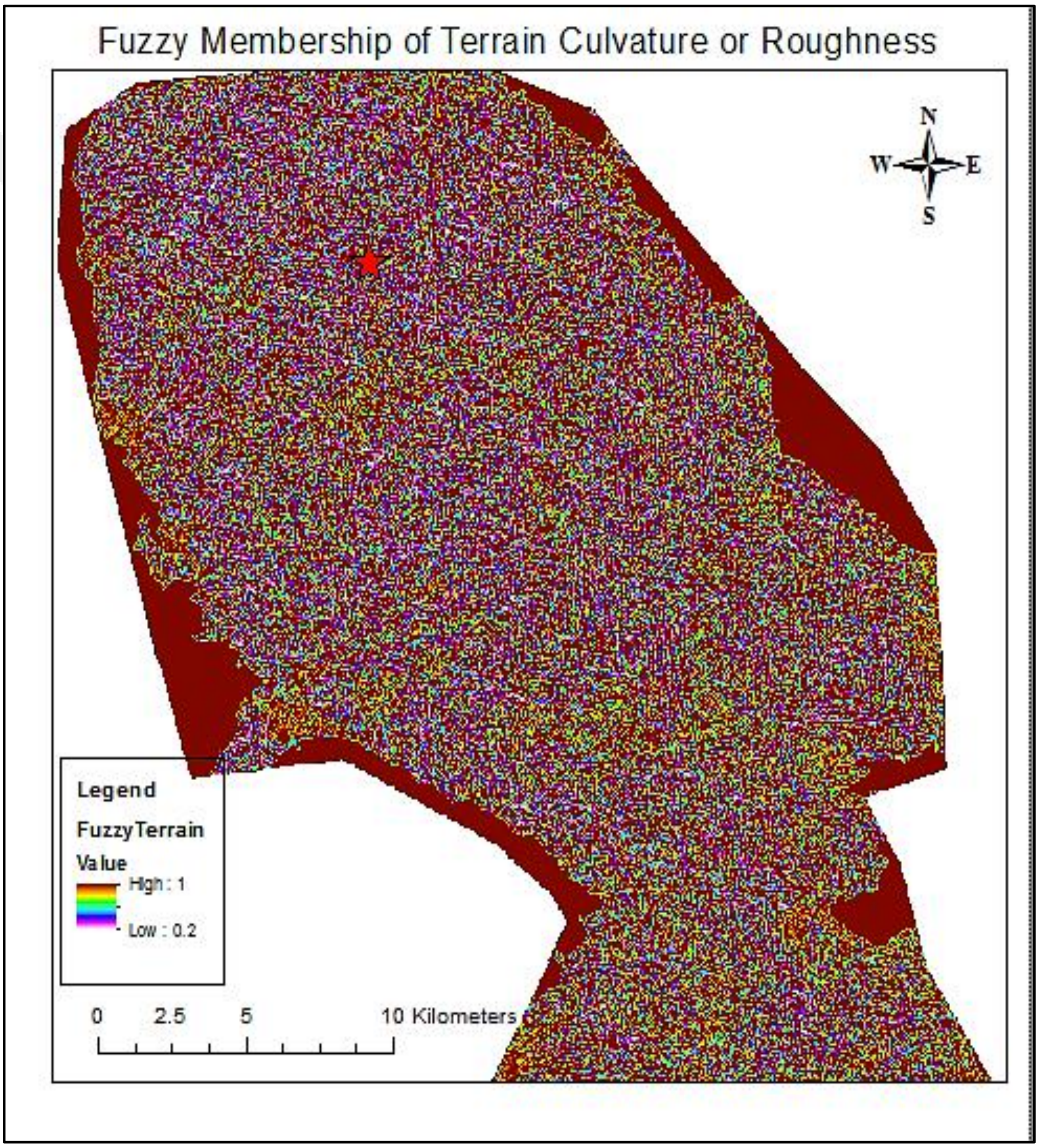

Figure 5.22 Fuzzy memberships Map of terrain roughness or curvature

5.8.6 Material Type

CAMEL utilises qualitative interpretations of geologic materials when determining the locations and susceptibility of EI landslides. Unlike the aforementioned layers, which were derived using ArcGIS from a base DEM, the material type layer is created using knowledge and interpretation of the formations, assemblages and general distribution of lithologies. The material type value is selected from the predetermined scale between 1 and 5 developed by Miles and Keefer (Figure 5.23). One (1) indicates the strongest material and five (5) the weakest. For instance, the "strongest" material would be intact, cohesive, unweathered granite with no distinct cleavage planes and the weakest would consist of Quaternary landslide material. In CAMEL, material strength correlates with the susceptibility of a material to move during a seismic event.

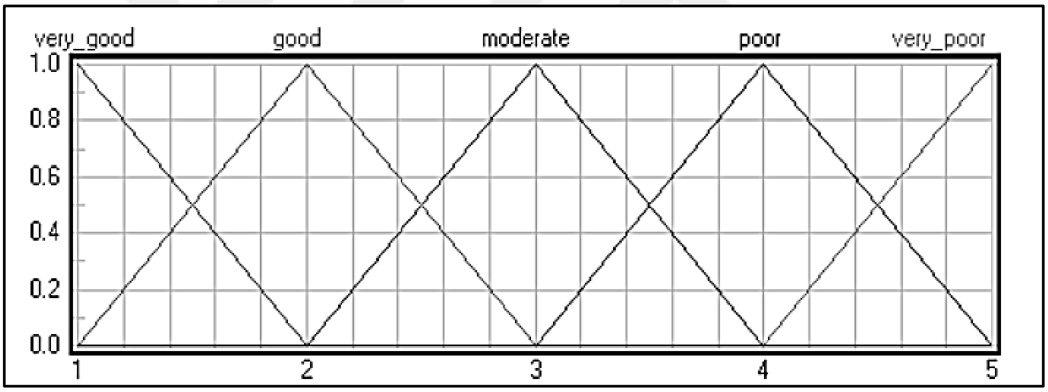

Figure 5.23 Membership function of the material type/geology (Miles and Keefer 2007)

In this regard, since the epicentre of the 1949 Karaburun earthquake is situated in the clastic unit, which is sedimentary lithologic unit, a value of 3 from the scale could be assigned. This decision is supported by the comprehensive review study on geology versus occurrence of landslides in which it was noted that EI landslides tend to be concentrated in the tertiary sedimentary rocks (Figure 4.39 – Figure 4.45) with a percentage of ≥ 40%. Thus the membership value for the Karaburun geology is 0.6 [(3/5)*100]

5.8.7 Soil Depth

The soil depth, as seen in the variable input by Miles and Keefer (2009), represents the mantle of unconsolidated material on top of the bedrock geology. Because of unavailability of data on soil depth default threshold was used. In the event that data is unavailable for soil depth, Miles and Keefer (2007) recommended the use of 3 meters as a threshold since it is the depth at which the CAMEL excludes deep seated landslide from the possibility module. Thus, during this study 4 meters was adopted for soil depth which has an equivalent fuzzy value of 0.5.

5.8.8 Moisture

As discussed in the design of the CAMEL approach, the *hMoisture* variable, describes the degree to which the analysis ground layer is saturated. The Karaburun earthquake took place in July which is a summer season in Turkey. With reference to the standard moisture values (Figure 5:11) developed by Miles and Keefer (2007), values between 25%-50% was adopted which gives an average value of 37.5%. The membership value at 37.5% is approximately 0.56.

5.8.9 Shake Intensity

As mentioned earlier on, shake intensity variable is based on the USGS ShakeMap intensity scale which is similar to the Modified Mercalli Intensity (MMI) scale, but is a ratio scale (Miles & Keefer, 2007). A ShakeMap offers a representation of ground shaking generated by an earthquake. The information on ShakeMap gives distinctive information from the earthquake and epicentre that are released after an earthquake because it focuses on the ground shaking generated by earthquake, rather than the parameters describing the earthquake source (USGS, 2011).

ShakeMap is automatically generated by combining instrumental measurements of shaking with information on the local geology and earthquake location and magnitude to estimate shaking variations throughout a geological area (Wald, Worden, Quitoriano, & Pankow, 2006). However, due to lack of data on ShakeMap for the 1949 Karaburun earthquake, an effort was made to derive an estimated value of PGA through a well-studied relationship between earthquake magnitude and earthquake intensity measure by Modified Mercali Intensity (MMI) scale (Table 5.11).

Table 5.11 Typical relationship between earthquake magnitude and typical Modified (USGS,

Magnitude (Mw)	**MMI**	**Description**
1.0 - 3.0	I	Not felt
3.0 - 3.9	II - III	Felt quite noticeably, vibrations similar to the passing of a truck.
4.0 - 4.9	IV - V	Felt by nearly everyone, Some dishes, and windows broken. Unstable objects overturned
5.0 - 5.9	VI - VII	slight to moderate in well-built ordinary structures; considerable damage in poorly built
6.0 - 6.9	VII - IX	Moderate to considerable damage
7.0 and higher	VIII or higher	Considerable to total damage in ordinary substantial buildings

In the case of the 1949 Karaburun earthquake the Ms 7.0 (Mw 6.7) the equivalent intensity of the earthquake falls in the range of VII – IX. The intensity information is significant as it is applied to estimate the PGA of an earthquake in the case where data is unavailable.

A study by Keefer on the 40 earthquakes revealed that a minimum intensity for occurrence of landslides is MMI VII (Keefer, 1984). Keefer's study also demonstrated that the minimum MMI for coherent and lateral spreads is higher than that of disrupted landslides. A comprehensive study of landsliding caused by 22 New Zealand earthquakes by Hancox (2010) gave a minimum intensity for landsliding MM VI, and the most common intensities MM VII–VIII. The threshold for liquefaction was observed to be MM VI and MM VII for sand boils, and MM VIII for lateral spreading.

Another study by Qi et al. (2010b) after the Wenchuan 2008 earthquake yielded similar results as Keefer's (Figure 5.24). Statistics indicated that all landslides occurred in the area with seismic intensity above VI and kept increasing through VIII until reaching its summit in region ≥ X.
From these findings, it can be inductively concluded that there is a tangible possibility that landslides could have occurred during the 1949 Karaburun earthquake.

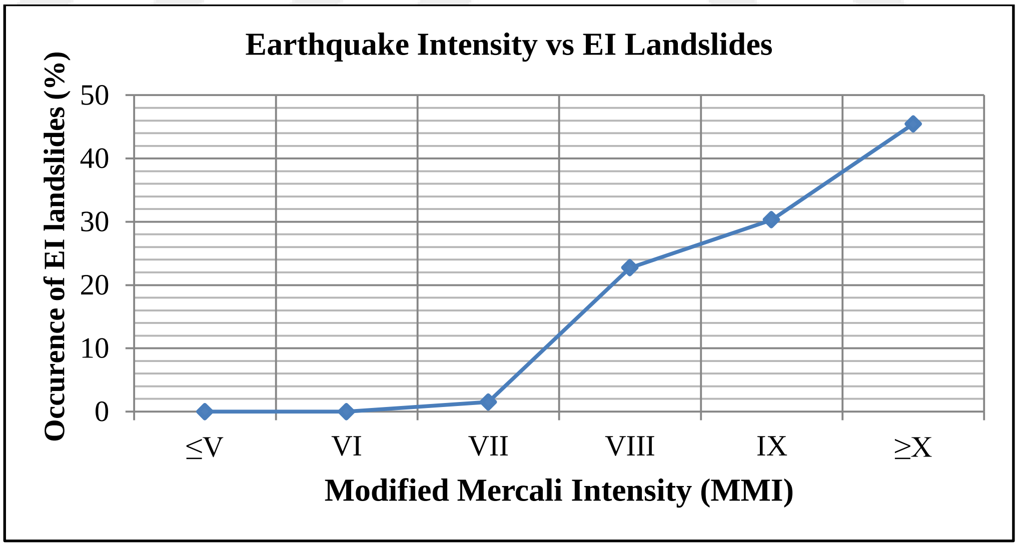

Figure 5.24 Relationship between landslides and the seismic intensity (Data from Qi et al., 2010b)

Wald et al. (2006), who originally conceived the idea of ShakeMap in 1996, provided the world with the means of generating PGA, velocity maps and instrumentally derived, estimated MMI map for earthquakes.

By cataloguing and studying the geotechnical properties of earthquake Wald et al. (2006) devised a standard presentation of PGA (Table 5.12). Thus, the estimated intensity map is derived from ground-motions recorded by accelerographs and represents intensities that are likely to have been associated with the ground motions.

Table 5.12 Representative ShakeMap as developed (Wald et al., 2006)

PERCEIVED SHAKING	Not felt	Weak	Light	Moderate	Strong	Very strong	Severe	Violent	Extreme
POTENTIAL DAMAGE	none	none	none	Very light	Light	Moderate	Moderate/Heavy	Heavy	Very Heavy
PEAK ACC.(%g)	<.17	.17-14	1.4-39	3.9-92	9.2-18	18-34	34-65	65-124	>124
PEAK VEL.(cm/s)	<0.1	0.1-1.1	1.1-3.4	3.4-8.1	8.1-16	16-31	31-60	60-116	>116
INSTRUMENTAL INTENSITY	I	II-III	IV	V	VI	VII	VIII	IX	X+

A reference to the representative ShakeMap table by Wald (2006) indicate the Karaburun 1949 earthquake, with MMI of VII – IX, has an estimated PGA values between 0.18 to 1.00 which gives an estimated average PGA of 0.59.

5.9 Evaluation of Membership Function

In order establish the possibility of occurrence of landslides during the 1949 Karaburun earthquake in the absence of landslides data, the information from landslide inventories between 1998-2015 was integral in the determination of the weights of parameters. Weights of parameters we established by using the fuzzy logic component in CAMEL which is integrated in GIS. Table 5.13 provides a summary of the weights that were determined through critical observation and inferences.

The weights were obtained for topographic parameters (Slope height, slope angle, terrain roughness, and slope aspect), material type, soil depth, and moisture and shake intensity. The weights were then summed up to derive a weighted sum which enabled to inductively draw a conclusion.

The weighted sum of 0.54 was obtained from the analysis. The weighted sum, which is above 0.50, imply that earthquake induced landslides might have occur during and/or after the 1949 Karaburun earthquake. The finding appears to vindicate Gazioglu (2005) who was convinced that the 1949 Karaburun earthquake might have induced some landslides but lamented that the lack of information on the occurrence of landslides was a big hindrance to work on EI landslides in the area.

Table 5.13 Summary of the fuzzy membership to assess DoS in relation to susceptibility to EI landslide

Variable	Fuzzy DoS values	Mean fuzzy DoS	Comment (on possibility of occurrence of EI landslides)
Slope Height	0.40 – 0.60	0.50	Average DoS
Slope Angle	0.20 – 0.80	0.50	Average DoS
Terrain Roughness	0.30 – 0.70	0.50	Average DoS
Slope Aspect	0.20 – 1.0	0.60	Relatively high DoS
Material Type	3/5	0.60	Relatively high DoS
Soil Depth	0.5	0.50	Average DoS
Moisture	37%	0.56	Fair DoS
Shake Intensity	0.18-0.65	0.59	Relatively high DoS
Total weighted sum		**0.54**	**Possibility of occurrence of landslides**

CHAPTER SIX
CASE STUDY OF KARONGA; MALAWI

6.1 Location of Study Area

Karonga is situated in the Northern part of Malawi with geographical coordinates; 11° 22' 0" South, 34° 10' 0" East (Figure 6.1). The area is within the Malawi Rift System, (MRS) which forms part of the East African Rift System (EARS) (Figure 6.1 insert). EARS has attracted the interest of the geoscientists around the globe who are craving to fully comprehend the rifting process and the likely consequences. The geologicak setting of Karonga exposes it to natural hazards such as earthquakes and landslides along the faulted margins in response to ground shaking. Msilimba & Holmes (2005) and Msilimba (2006) have documented a number of landslides in the Northern part of Malawi, partculary in Mzimba area contiguous to Karonga. The focus of their studies has been on rainfall and anthropogenic activities as landslides triggering factors. But the location of Karonga within the EARS, as shown in Figure 6.1, vividly suggests that the area is potentially exposed to seismic activities that may induce landslides.

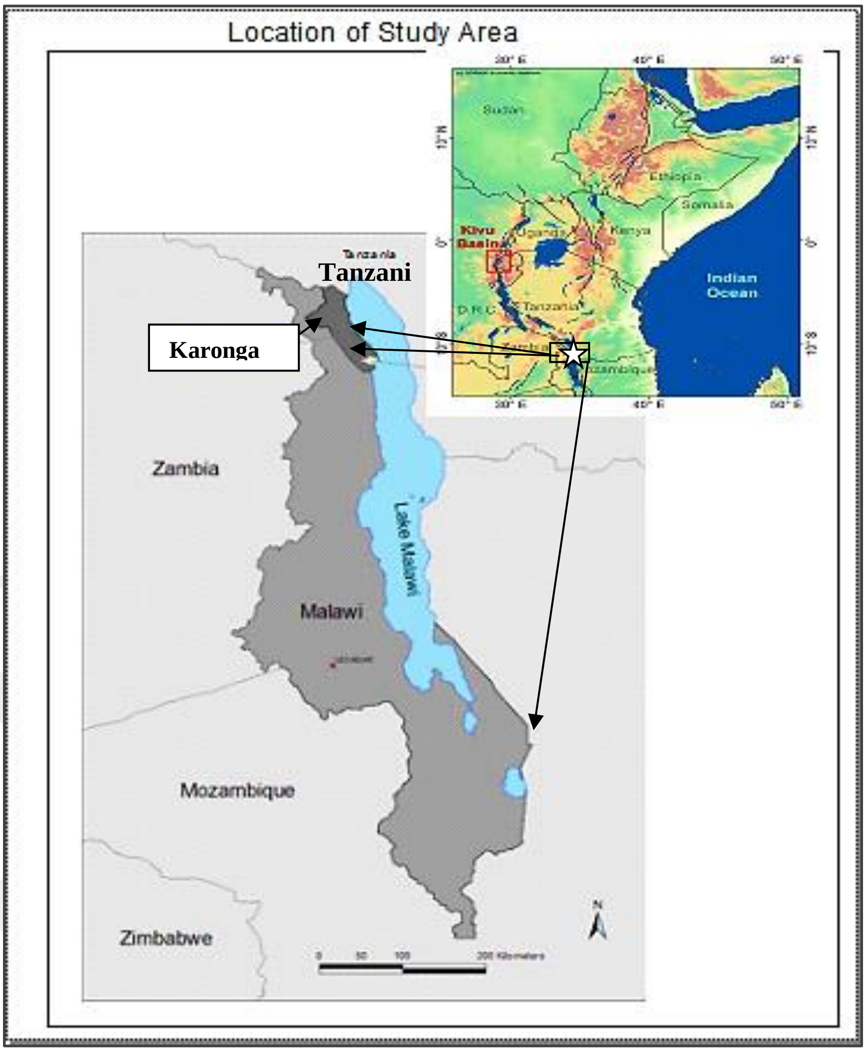

Figure 6.1 Location of study area (Extracted from Google Maps and replotted in ArcGIS). The insert shows the EARS

6.2 Geology of the Study Area

Karonga is predominant underlain by Precambrian to Lower Palaeozoic metamorphic and igneous rocks that make up the basement complex of Malawi. Unconformably overlying the basement complex are several patches of the Karoo sediments and Cretaceous to Recent sediments such as lacustrine and fluvial sediments (Macheyeki et al., 2015). The basement complex is dominated by gneisses (biotite and amphibolite gneisses, Figure 6.2) and granitic intrusions of Umbendian tectonic domain that extends from Southern Tanzania to Malawi.

The Karoo sandstone and shales with coal seams, which are assigned relative dates of the Upper Carboniferous to Triassic period, were deposited in basin greatly controlled by faults characterised by N–S and NW–SE trends (Ray, 1975). Cretaceous to Pleistocene Lacustrine sediments lay unconformable to the basement complex gneisses. The lacustrine sediments include: Dinosaur, Chiwondo, Chitimwe, Mwesia and Sungwa beds (Figure 6.2). The lakeshore plain is predominantly covered by beach sands, alluvium and marsh deposits of Upper Pleistocene to recent age.

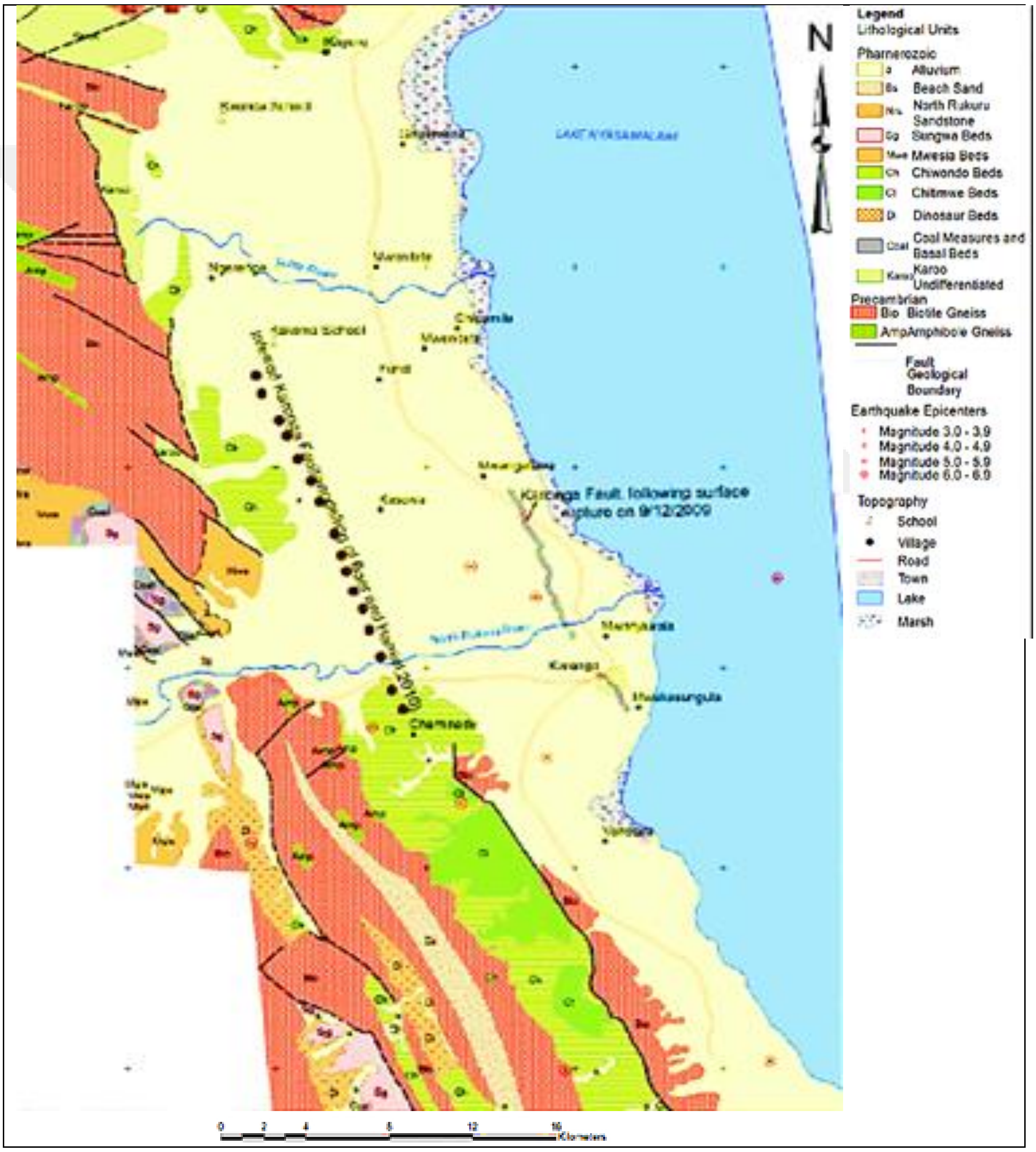

Figure 6.2 Geological Map of the study area (Karonga area) showing lithological units and associated faults in the area. The Karonga fault that caused the December 2009 earthquake is also shown in red as a thick line on the eastern side (Macheyeki et al., 2015)

6.3 Seismotectonic Setting

Karonga lies within the MRS which forms the southern part of EARS. The EARS extends from the Red Sea/Gulf of Aden to Malawi and it is seismically active beyond. Biggs, Nissen, Craig, Jackson, & Robinson (2010), who applied the GPS-derived model, found that EARS has extension rates are 3.7–3.8 mm/yr. Further, Biggs et al. (2010), established that the southern East African Rift (SEAR) has an has a remarkably large seismogenic thickness of 35-40 km, which is apparently responsible for tilted basins and very long faults with potential for 7 – 8 magnitude normal-faulting earthquakes (Figure 6.4). It was not surprising that from 6th – 8th December 2009, swallow earthquake sequence (Mw > 5.5) hit the Karonga area of Nothern Lake Malawi (Table 6.4). The main shock (Mw 6.0) was preceded by foreshocks with magnitudes 5.8, 5.9 and 5.4. The epicentre situated 50 km West of the rift-bounding Livingstone Fault, within the hanging-wall (Figure 6.4).

Aside the four large earthquakes, Hamiel, Baer, Kalindekafe, Dombola & Chindandali (2012) discovered that a swarm of 29 small earthquakes (Mw ≥ 4), nine of which were larger than body-wave magnitude (*M*b = 5), occurred. Biggs et al. (2010) made efforts to model the seismic behaviour for the largest 4 earthquakes (the 6th, 8th, 12th and 19th December). The modelling also revealed a normal-faulting mechanism with a depth of 20 km whose orientation and location were consistent with rupture of small patch of the Livingstone Fault. A study by Macheyeki et al. (2015) concur with the findings of Biggs et al. (2010) on fault type. According to Macheyeki et al. (2015), the Karonga fault, is a normal fault which trends N290 – N350 and close to the surface it dips at higher angles due West.

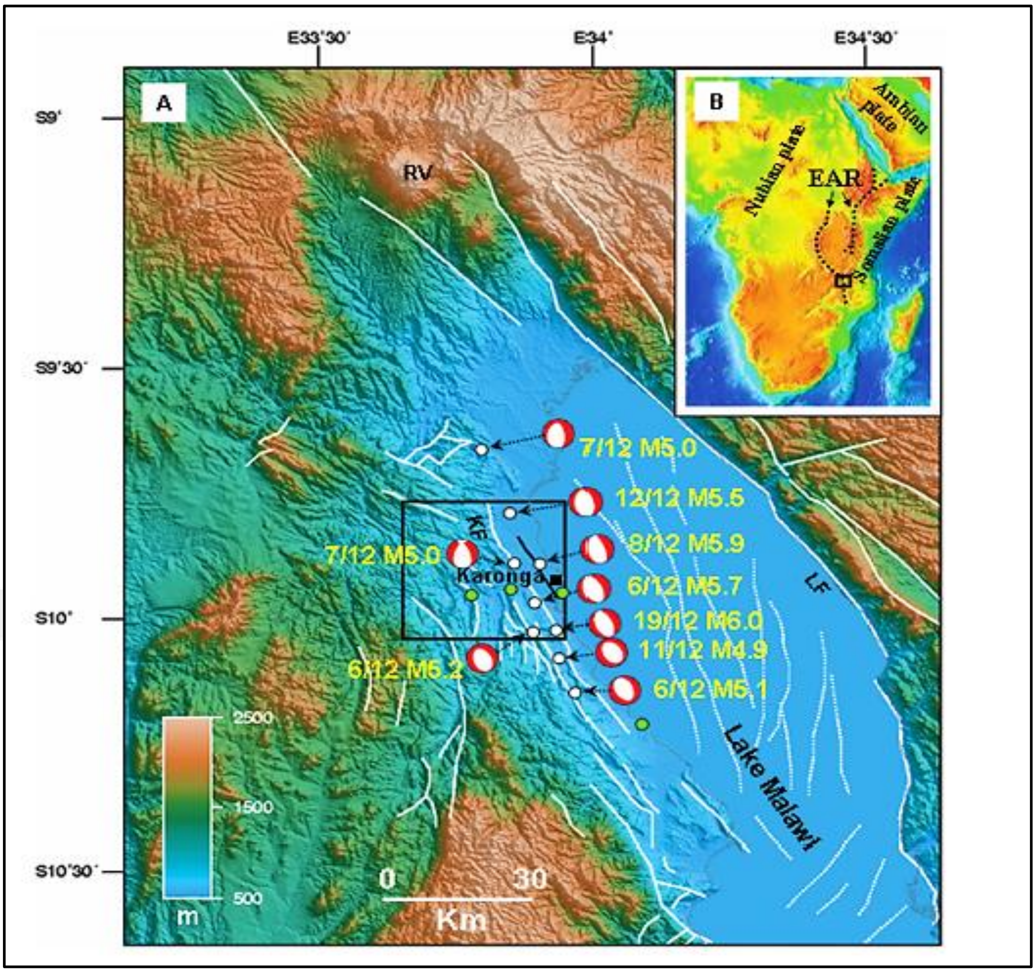

Figure 6.4 The tectonic setting of the study area (Karonga). The insert shows the EARS. And the landsat image of northern Lake Malawi with focal mechanisms of the 2009 Karonga earthquakes (Hamiel et al., 2012). KF represent Karonga Fault and LF stands for Livingstone fault.

Table 6.1 List of the earthquakes that occurred in Karonga 2009 (Biggs et al., 2010)

Date	Magnitude(M_w)	Latitude	Longitude	Depth	Casualties
6/12/09	5.8	10.16°S	33.82°E	10 km	
8/12/09	5.9	9.948°S	33.878°E	8 km	1
12/12/09	5.4	9.96°S	33.88°E	10 km	
19/12/09	6.0	10.108°S	33.84°E	6 km	3

6.4 Earthquake Damage

The Malawi Government declared the Karonga earthquake a National Disaster on 21st December and the area was described as a seismically dangeous area. Macheyeki et al. (2015) and Hamiel et al. (2012) reported that over 1000 houses collapsed, a further 2900 were damaged, 300 people were wounded, and 4 were killed. The earthquake was also characterised by rift structures and ground fractures in this region (Figure 6.3).

Figure 6.3 The damage experienced during the 2009 Karonga earthquakes (Hamiel et al., 2012). (a & b) Show Surface rupture after the 2009 earthquake. (c) Road parting due to the impact of rupturing and (d) collapsing building due to series of earthquakes in 2009.

6.5 Assessment of Possible Landslides Occurrence

The EARS is characterised by natural hazards such as earthquakes, volcanic eruptions and landslides along the fault margins in response to ground shaking (Macheyeki et al., 2015). The most recent devastating earthquake in the Eastern and Southern Africa regions is the Karonga earthquake in Malawi which took place on 19th December, 2009 with a magnitude of Mw 6.0. After the 2009 Karonga earthquake only the geotechnical aspect and damage of the earthquake were analysed by seismological and geological experts in the area. There was no attempt undertaken to investigate if the earthquake had induced landslides. This implies that no information or documentation on landslides is available. From this background, the study also made an attempt to assess the possibility of the occurrence of landslides after the 2009 Karonga earthquake. To accomplish this objective through the application of ArcGIS and CAMEL, the following parameters were taken into account: Slope Height, slope angle, terrain roughness, material type, soil depth, moisture and shake intensity. The four topographical parameters; elevation, slope angle, slope aspect and slope curvature were used for correlation with susceptibility of landslide occurrence.

The topographic parameters: Slope height, slope angle, slope aspect, and slope curvature were extracted from the Karonga DEM at 30 m×30 m resolution which was obtained from ASTER GDEM V2 and downloaded from http://gdex.cr.usgs.gov/gdex/. To extract the weights for topographic parameters, the Karonga DEM was run in CAMEL which is embeded in Arc GIS (Figure 6.5).

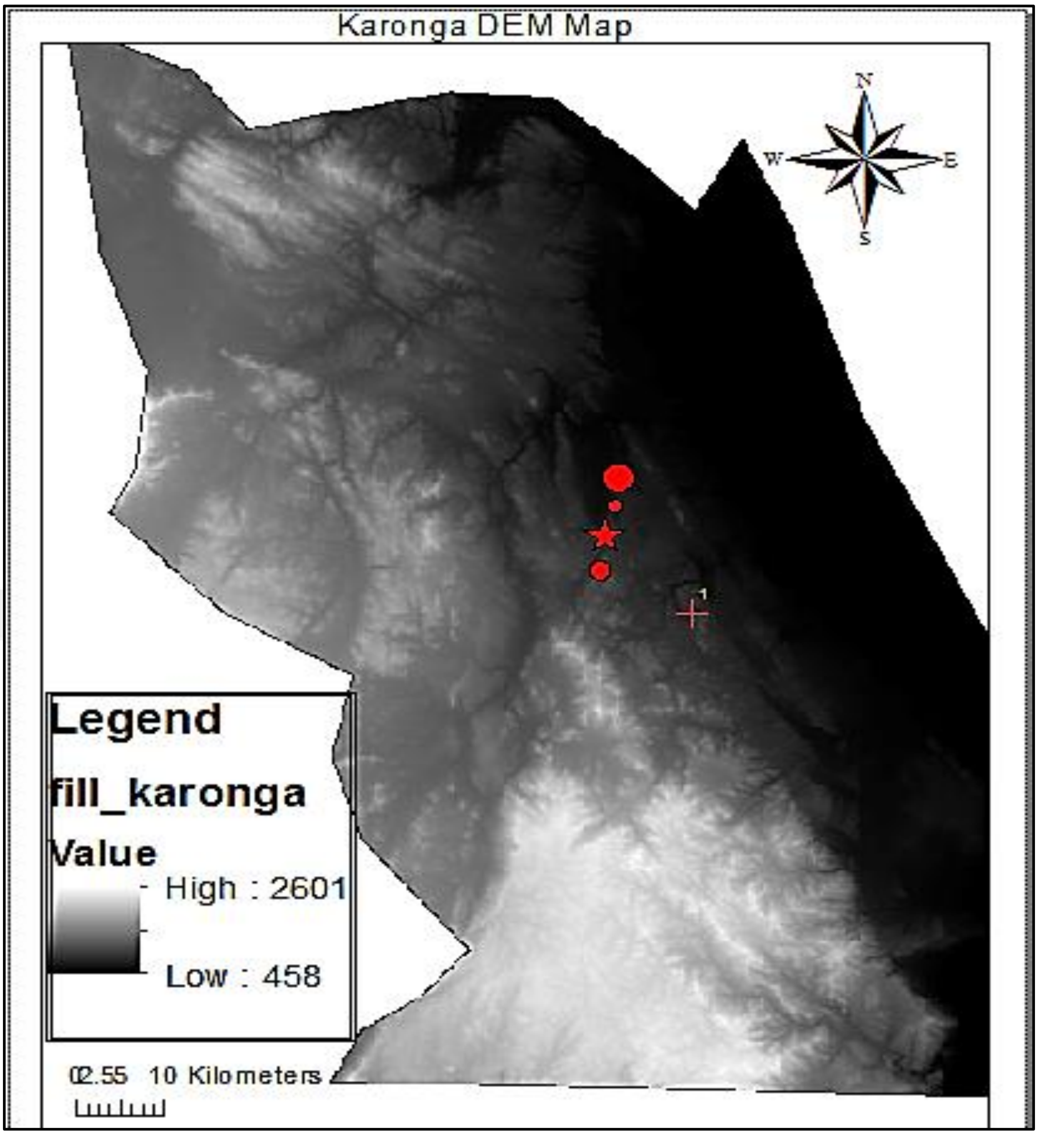

Figure 6.5 Digital elevation model for Karonga (The star is the epicenter of the Karonga main shock and the dots represent foreshock and the size is with respect to magnitude)

6.5.1 Slope Height

Slope height was directly calculated from the Karonga DEM in ArcGIS through the Spatial Analyst Tools “surface analysis. Before running the slope height layer, a fill command in Spatial Analyst Tools “hydrology” was run to correct surface irregularities. After calculating the slope height, I reclassified the slope height at intervals of 500m (Figure 6.6).

As noted in the review, slope heights between 750m and 1500m have high susceptibility of landslide occurrence in an event of a strong ground shaking. From Figure 6.6, it shows that the epicentre of the earthquakes lie in the 500-1000 m category.

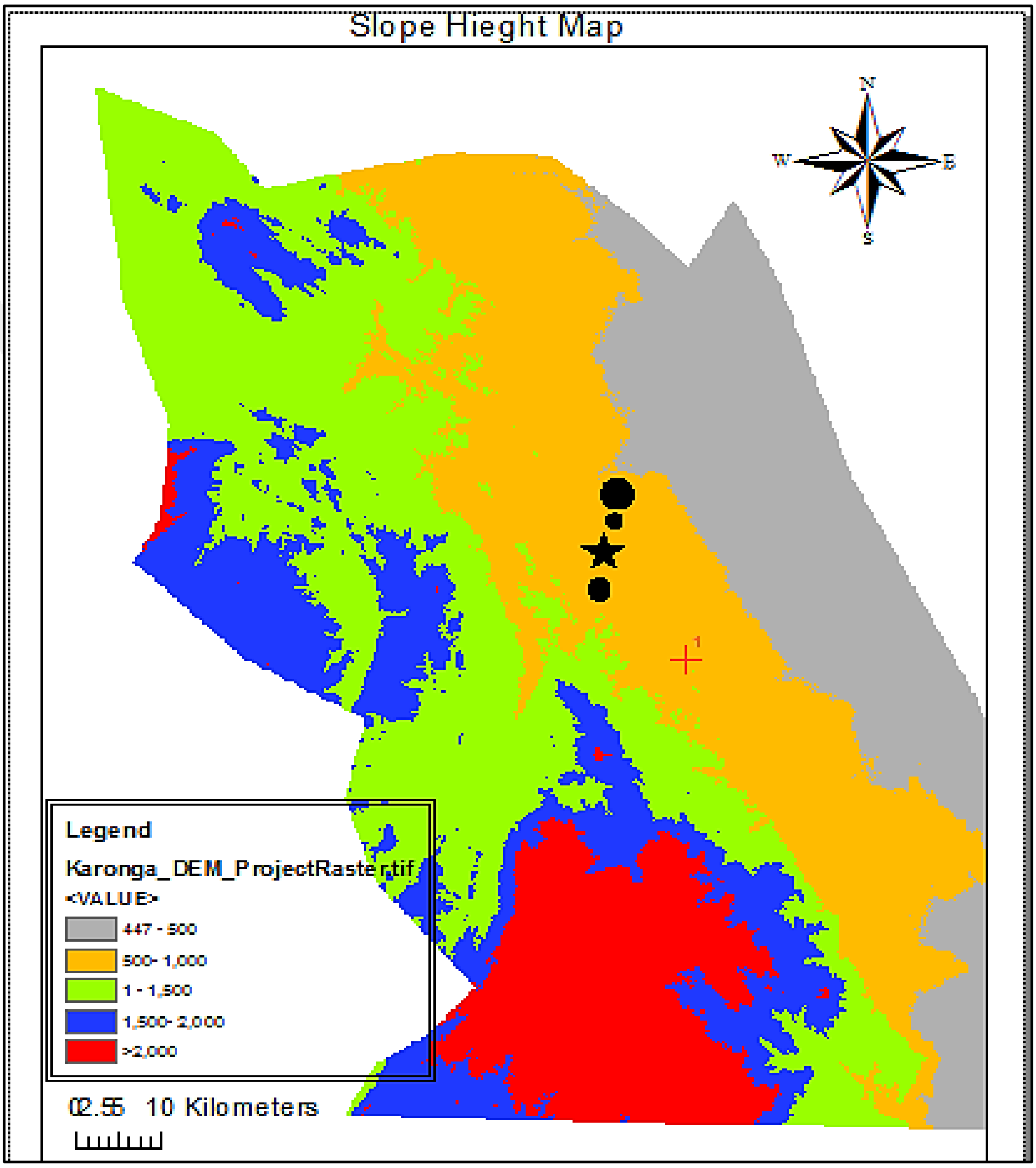

Figure 6.6 Slope height map derived from the Karonga DEM (The star represents the epicenter of the main earthquake and the dots represent the foreshocks – the bigger the dot the higher the magnitude)

To assess the influence of the slope height variable, the layer of slope height was then run in CAMEL integrated in ArcGIS to test for the variable's fuzzy membership. The fuzzy membership was attained by running the slope height layer calculated from the Karonga DEM in ArcGIS through the Spatial Analyst Tools using 'surface analysis' (Figure 6.7). It can be observed that the epicentre of the Karonga earthquake lies in the slope membership value of around 0.4. This implies a low probability of the variable to cause landslides.

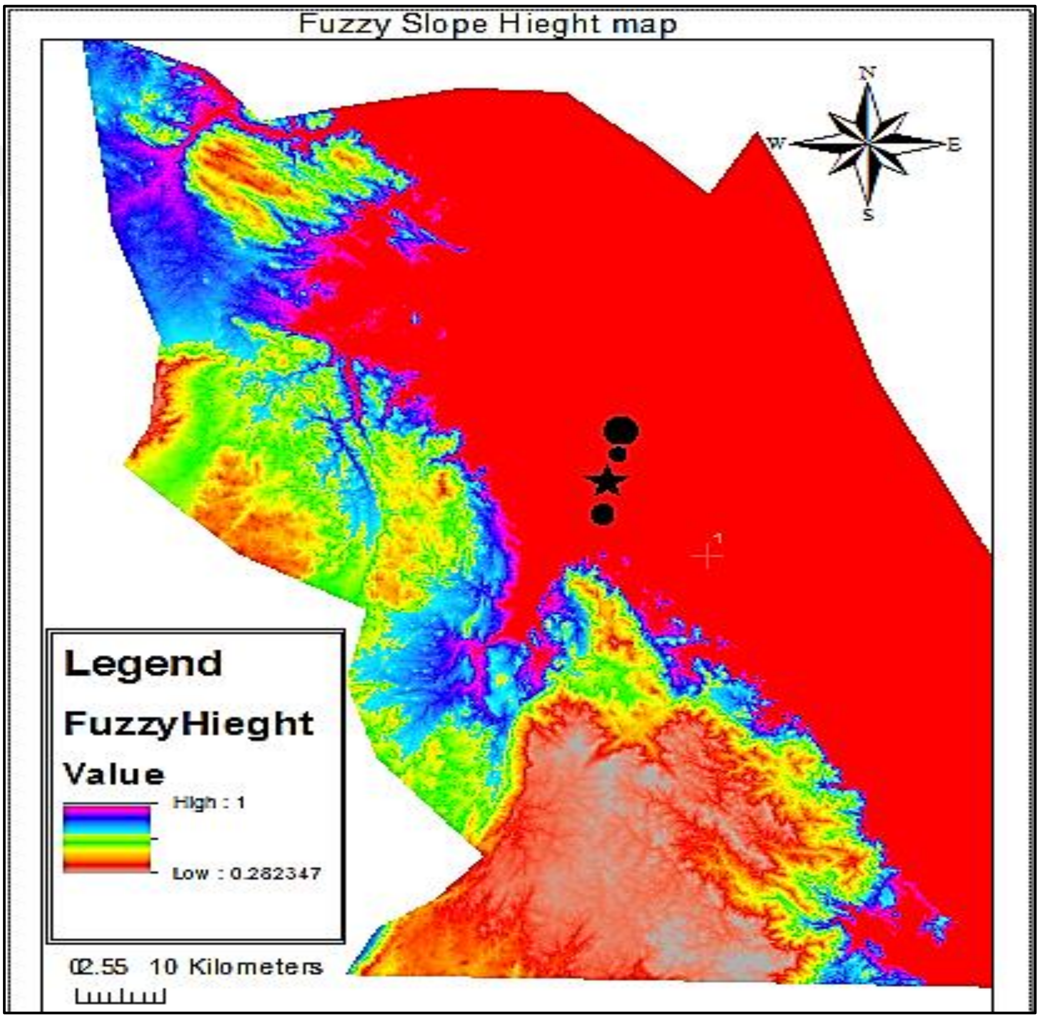

Figure 6.7 Slope height Map derived from the Karonga DEM (The star represents the epicenter of the main earthquake and the dots represent the foreshocks – the bigger the dot the higher the magnitude)

6.5.2 Slope Angle

The slope angle was directly calculated from the Karonga DEM in ArcGIS through the Spatial Analyst Tools “surface analysis. Then reclassification was done for slope angle at intervals of 10°. From the possibility module rule block expressing knowledge about *pSlopeAngle* developed by Miles and Keefer (2007) shown in Figure 6.8, the susceptibility values generally increase with the slope angle, but slopes exceeding 35° (classes 8– 13) are more susceptible to landsliding. It can be noted from the slope angle Map that categories 10-20^o, 20-30^o, 30-40^o and 40-50^o are common.

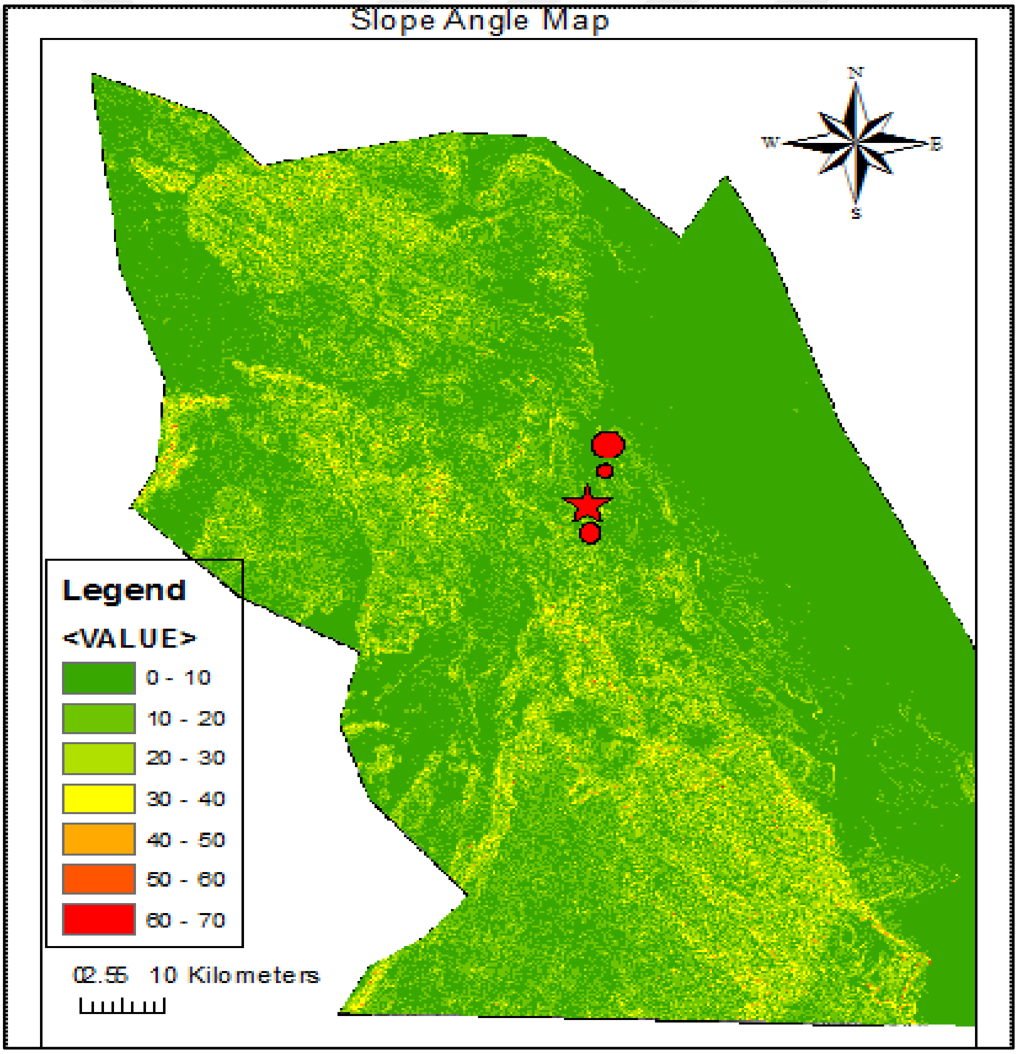

Figure 6.8 Slope angle Map derived from the Karonga DEM (The star is the epicenter of the Karonga main shock and the dots represent foreshock and the size is with respect to magnitude).

After computing slope angle from the Karonga DEM in ArcGIS through the Spatial Analyst Tools using 'surface analysis', the layer of slope angle was then run in CAMEL incorporated in ArcGIS to test for its fuzzy membership. It can be observed that the epicentre of the Karaburun earthquake lies in the slope membership value 0.2 – 0.6 (Figure 6.9).

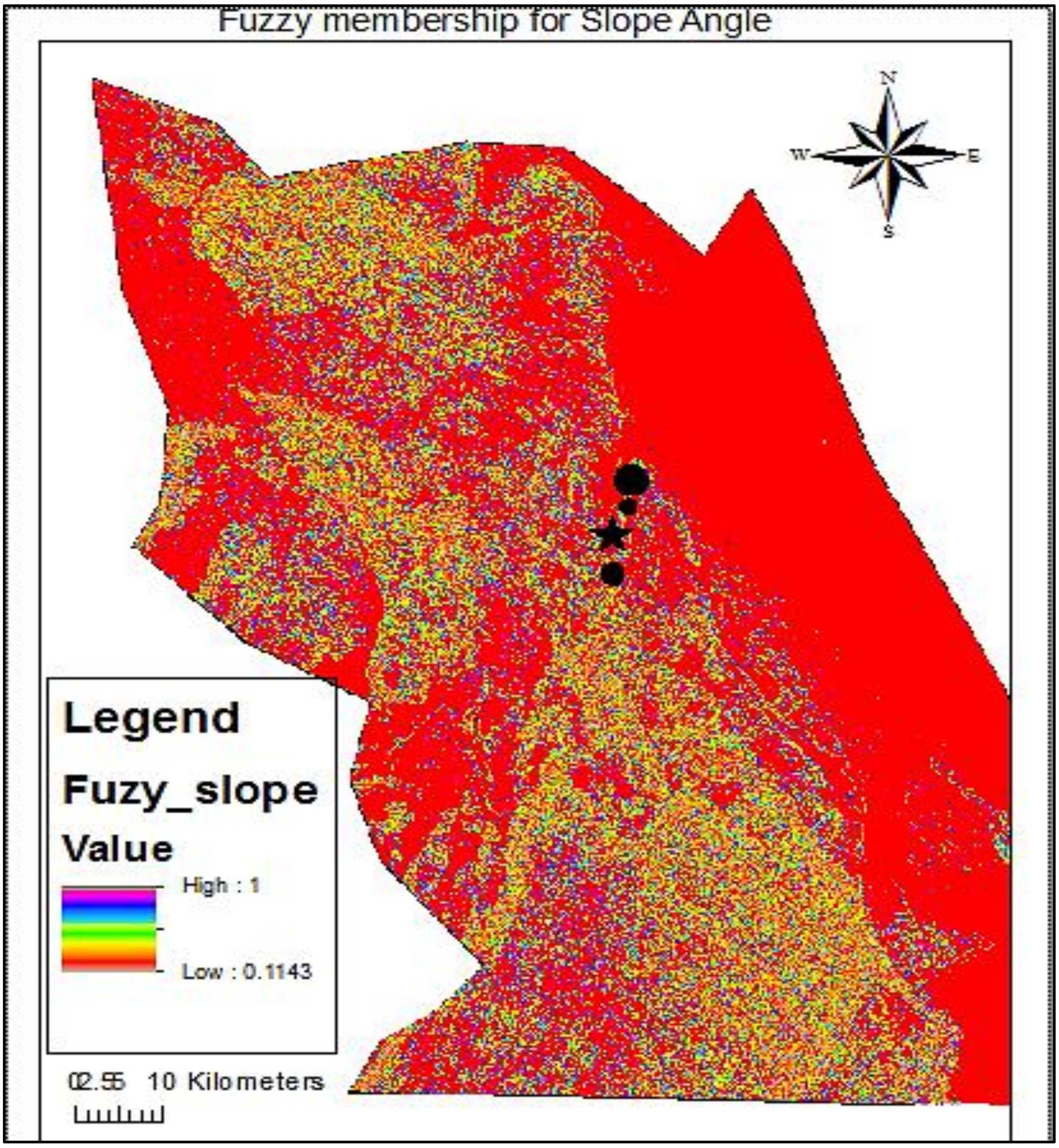

Figure 6.9 Fuzzy slope angle Map derived from the Karonga DEM (The star is the epicenter of the Karonga main shock and the dots represent foreshock and the size is with respect to magnitude).

6.5.3 Slope Aspect

Slope aspect values were also calculated from the Karonga DEM in ArcGIS through the Spatial Analyst Tools "surface analysis. The slope aspect was separated into nine classes for the study, including flat, N, NE, E, SE, S, SW, W, and NW as presented in Figure 6.10.

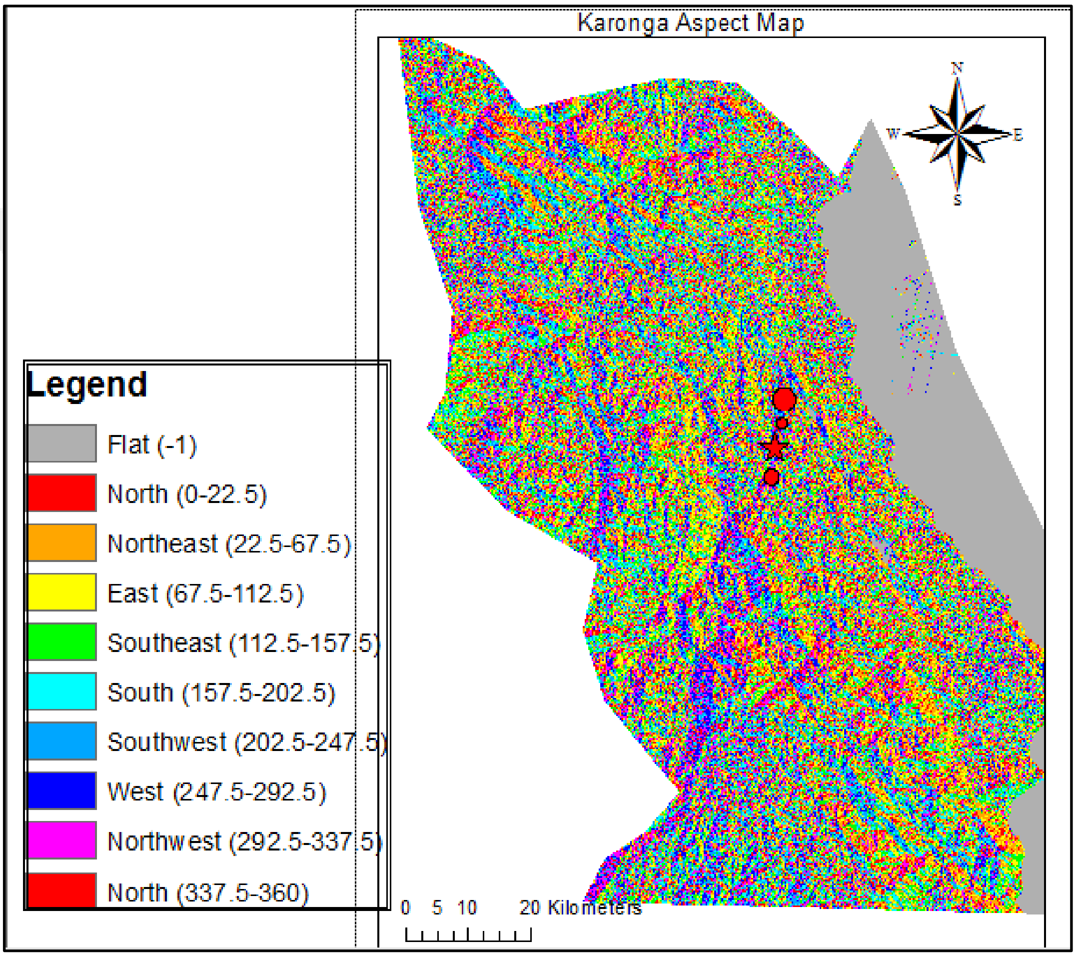

Figure 6.10 Aspect Map of Karonga (The star is the epicenter of the Karonga main shock and the dots represent foreshock and the size is with respect to magnitude)

From slope aspect layer, a fuzzy membership of slope aspect was extract in order to relate probability of occurrence of EI landslides with respect to slope orientation. The fuzzy slope aspect values were obtained after running the calculated slope aspect values which were calculated from the Karonga DEM in ArcGIS through the Spatial Analyst Tools “surface analysis. Figure 6.11 presents a Map of the fuzzy membership of aspect.

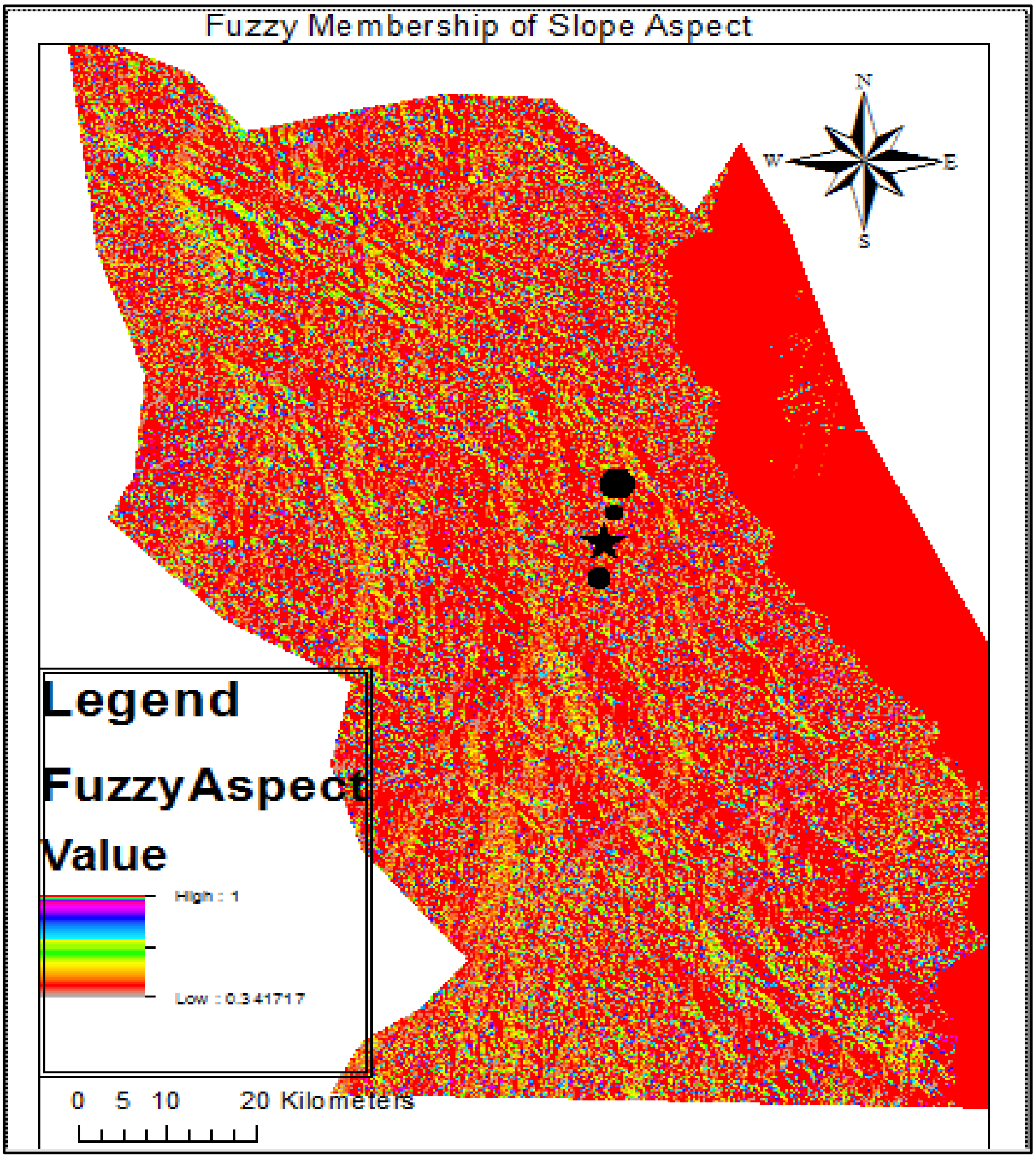

Figure 6.11 Fuzzy slope aspect map of Karonga (The star is the epicenter of the Karonga main shock and the dots represent foreshock and the size is with respect to magnitude)

6.5.4 Terrain Roughness

The terrain roughness is the second derivative of elevation in the down-slope-direction, with calculations done in degrees. The terrain roughness layer is attained by merely rerunning the surface analyst under the spatial analyst tool on the slope angle. It can be observed from Figure 6.12 that the terrain roughness values are confined in the range of -2– 0 and 0 - 2. The Terrain roughness Map indicates dominance of positive curvatures representing more convex surfaces than concave surfaces which are represented by negative values.

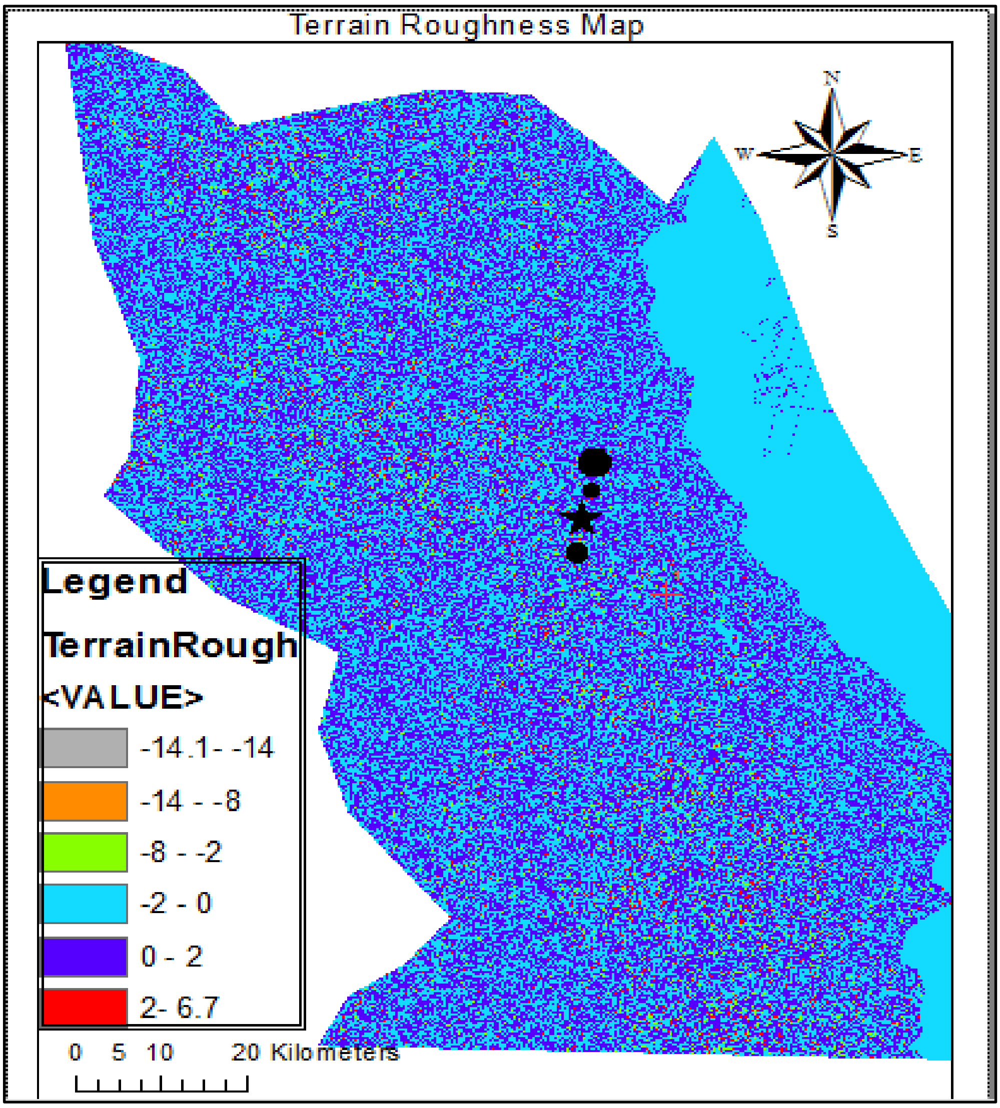

Figure 6.12 Terrain roughness calculated from the Karonga DEM (The star is the epicenter of the Karonga main shock and the dots represent foreshocks and the size is with respect to magnitude).

After calculating the terrain roughness, a fuzzy membership was derived from terrain roughness layer which was calculated in ArcGIS. The terrain roughness layer was calculated from the slope angle extracted from the Karonga DEM using Spatial Analyst Tools. A presentation of terrain roughness using fuzzy membership is given in Figure 6.13. The membership values indicate a probability of 0.2 – 0.6

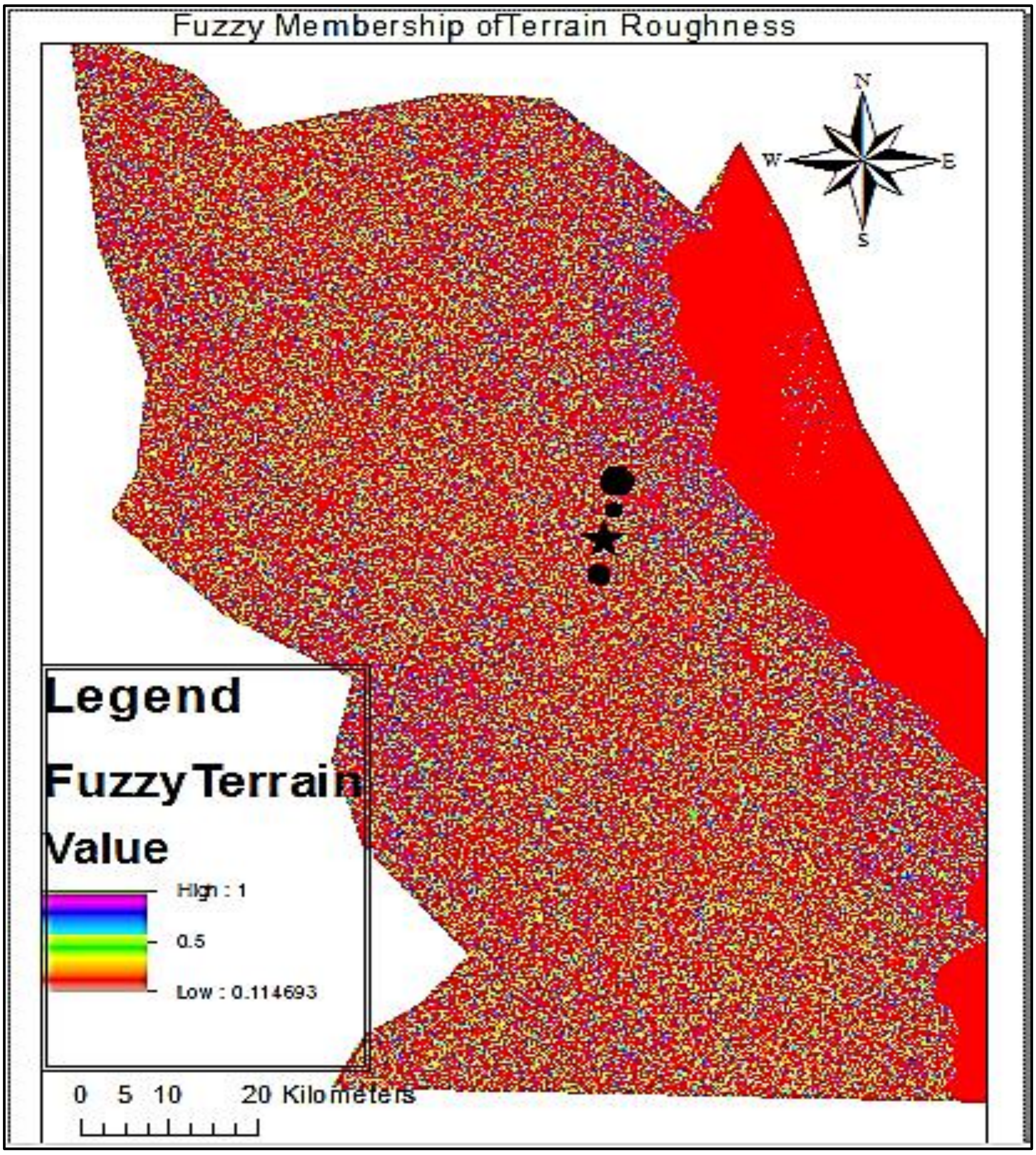

Figure 6.13 Fuzzy membership of Terrain roughness calculated from the Karonga DEM (The star is the epicenter of the Karonga main shock and the dots represent foreshocks and the size is with respect to magnitude)

6.5.5 Material Type

As indicated earlier in this study, CAMEL utilises qualitative interpretations of geologic materials when determining the locations and susceptibility of EI landslides. Unlike the aforementioned layers, which were derived using ArcGIS from a base DEM, the material type layer is created using knowledge and interpretation of the formations, assemblages and general distribution of lithologies. The material type value is selected from the predetermined a scale between 1 and 5 developed by Miles and Keefer. One (1) indicates the strongest material and five (5) the weakest. For instance, the "strongest" material would be intact, cohesive, unweathered granite with no distinct cleavage planes and the weakest would consist of Quaternary landslide material. In CAMEL, material strength correlates with the susceptibility of a material to move during a seismic event.

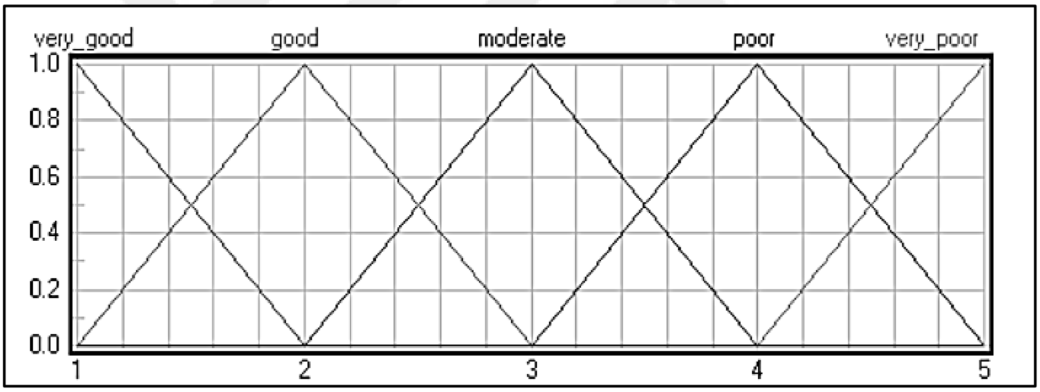

Figure 6.14 Reference membership function of the material type/geology (Miles and Keefer 2007)

The Karonga geology, as discussed in the geology section of the study area, is dominated by the sedimentary Karroo System which overlays the basement complex (igneous and metamorphic rocks). The Karroo system extends from the Permian period to the Triassic period. Since the epicentre of the 2009 Karonga earthquake is located in the sedimentary Karroo system adjacent to the alluvium, the membership function value of material type is derived from the scale value of 3-4 which gives an average value of 3.5. A scale value of 3.5 gives a membership function of 0.7 [(3.5/5)*100], indicating a 70% chance of landslides occurrence.

6.5.6 Soil Depth

The data on depth for Karonga, just as with the Kara Buru 1949 case study, was unavailable and the recommended 3 meters threshold was applied. The threshold is applied since it is the depth at which the CAMEL excludes deep seated landslide from the possibility module (Miles and Keefer 2007). Thus, during this study 3 meters was adopted for soil depth which has an equivalent fuzzy value of 0.5.

6.5.7 Moisture

As it has been demonstrated in the design of the CAMEL approach, the *hMoisture* variable, describes the degree to which the analysis ground layer is saturated. The 2009 Karonga earthquake took place in December which is a dry-wet period in Malawi. Based on this the values between 25%-50% (average 37.5%) was applied to derive the membership function. With reference to the standard moisture values (Figure 5:11) developed by Miles and Keefer (2007), the average value of 37.5% has a membership function of approximately 0.56.

6.5.8 Shake Intensity

As discussed by Miles & Keefer (2007), a ShakeMap offers a representation of ground shaking generated by an earthquake. But, just as the Karaburun 1949 case study, the information ShakeMap was not available for use. Consequently, an estimate of the intensity and PGA were derived in the same manner as the 1949 Karaburun earthquake by making reference to the MMI table and Representative ShakeMap table. The ground shaking levels at sites throughout the region varies depending on the distance from the earthquake, propagation of seismic waves and the lithologic and soil conditions at sites. In the case of the 2009 Karonga earthquake Mw 6.0 the equivalent intensity of the earthquake falls in the range of VI – VII of the MMI. As demonstrated by Hancox (2010), Qi et al. (2010b) and Keefer (1984), the threshold MMI for occurrence of landslides is VII. This implies that the possibility of landslides occurrence is very low or negligible.

Regarding PGA value, MMI of VI – VII, has an estimated PGA values between 0.18 and 0.34 which gives an estimated average PGA value of 0.26 g (Table 6.3).

Table 6.2 Representative ShakeMap as developed (Wald et al., 2006).

PERCEIVED SHAKING	Not felt	Weak	Light	Moderate	Strong	Very strong	Severe	Violent	Extreme
POTENTIAL DAMAGE	none	none	none	Very light	Light	Moderate	Moderate/Heavy	Heavy	Very Heavy
PEAK ACC.(%g)	<.17	.17-14	1.4-39	3.9-92	9.2-18	18-34	34-65	65-124	>124
PEAK VEL.(cm/s)	<0.1	0.1-1.1	1.1-3.4	3.4-8.1	8.1-16	16-31	31-60	60-116	>116
INSTRUMENTAL INTENSITY	I	II-III	IV	V	VI	VII	VIII	IX	X+

6.6 Evaluation of Membership Function

In order establish the possibility of occurrence of landslides during the 2009 Karonga earthquake the information from landslide inventories between 1998-2015 was integral in the determination of the weights of parameters. Weights of parameters were established by using the fuzzy logic component in CAMEL which is integrated in GIS. Table 6.3 provides a summary of the weights that were determined through critical observation and inferences. The ranking and weighting were performed for topographic parameters (Slope height, slope angle, terrain roughness, and slope aspect), material type, soil depth, and moisture and shake intensity. The weights were then summed up to derive a weighted sum which enabled to inductively draw a conclusion. The weighted sum of 0.44 obtained from the analysis is below par for a possibility of occurrence of landslides. This implies that EI landslides would not occur under these conditions.

Table 6.3 Summary of the fuzzy membership to assess DoS in relation to susceptibility to EI landslides

Variable	Fuzzy DoS values	Average fuzzy DoS	Comment (on possibility of occurrence of EI landslides)
Slope Height	0.30 – 0.50	0.40	Low DoS
Slope Angle	0.20 – 0.60	0.40	Low DoS
Terrain Roughness	0.35 – 0.70	0.35	Low DoS
Slope Aspect	0.10 – 0.60	0.35	Low DoS
Material Type	3.5/5	0.70	High DoS
Soil Depth	0.5	0.50	Average DoS
Moisture	37.5%	0.56	Relatively high DoS
Shake Intensity	0.18-0.34	0.26	Low DoS
Total weighted sum		**0.44**	**Unlikelihood of landslides occurrence**

Another aspect worthy noting is that the karonga fault has been identified and established as a normal fault (Biggs et al., 2010 and Macheyeki et al., 2015). The comprehensive review done on 30 earthquakes has shown that normal fault type has a very low probability of EI landslides occurrence as compared to thrust fault. One of the reasons is attributable to non-violent nature of the tensile forces operating at normal faulting system. Basically, extensional forces acting on normal faults pull the fault blocks apart in which case the hanging wall moves down along the divergent boundaries relative to the footwall unlike at the thrust fault where the hanging wall rides over the footwall with a violent collision due to compressive forces along convergent boundaries. Thus, by inductive inference the 2009 Mw 6.0 earthquake in Karonga area could not have caused landslides in as far as fault type is concerned. However, surface ruptures are extensively recorded and reported by Hamiel et al. (2012) and Biggs et al. (2010)

CHAPTER SEVEN
DISCUSSION AND CONCLUSION

The second objective of this study was to assess the feasibility of occurence of landslides after the 1949 (Mw 7.0) İzmir-Karaburun and the 2009 Karonga, Malawi (Mw 6.0) earthquakes using the possibility module of CAMEL and GIS. In this regard, a quasi-quantitative approach was used to draw inference on the possibity of occurence of landslides by applying the knowledged gained from the documented worldwide landslides inducing earthquakes. Weights of parameters I established by using the fuzzy logic component in CAMEL which is integrated in GIS have been tabulated in Table 5.13 and Table 6.3. The weighted sum of DoS for Karaburun was found to be 0.54 which implies that there was a fair probability that EI landslides would have occurred during and/or after the 1949 Karaburun earthquake.

For the 2009 Karonga earthquake, the weighted sum of DoS of 0.44 was obtained from the analysis. An evaluation of the weighted sum indicates that the value is below par for a possibility of occurrence of landslides. Thus, EI landslides would not have been expected to have occurred. In addition, the Karonga fault along which the earthquake occurred has been identified and established as a normal fault. In this regard, the comprehensive review done on 30 earthquakes has shown that normal fault earthquake type has a very low likelihood of instigating EI landslides occurrence due to attributably non-violent nature of the tensile forces operating at normal faulting system. However, widespread ground fractures were observed after the Karonga earthquake.

In conclusion, earthquakes are surely among the main trigger of catastrophic landslide which result in severe human casualties, property losses and environmental degradation. EI Landslides are caused by the interplay of controlling factors: the earthquake parameters (magnitude, PGA, earthquake duration, fault rapture dynamics), and site properties (geology, tectonic settings and topography). Therefore, no single factor could be picked out as the dominant causative agent of the EI landslides over the other because the effectiveness of one factor in inducing landslides is dependent on the other factors. Most authors on EI landslides hint that long-term landslides susceptibility assessment has typically put emphasis on rainfall-induced landslides events to model susceptibility as they occur more frequent than EI landslides leading to under-representation of earthquake triggered landslides risk. Under-representation of earthquake-triggered landslides also comes from the evident complexity of analysing EI landslides since it incorporates various disciplines such as geology, geophysics, seismology and geotechnics

It has also been found that CAMEL and GIS can be applied to assess a possibility of landslides occurrence in the absence of landslides data. However, the effectiveness of the predicting the possibility occurrence of landslides relies on the availability of DEM, material type, ShakeMap and moisture content which are input variables. A great care must also be exercised during the observation and interpretation of the DoS to draw a conclusion.

7.1 Limitations

1) The major limitation of the study is the lack of field investigation component due to financial constraints. This would have greatly strengthened and validated the findings.
2) Unavailability of data on ShakeMap, soil depth and moisture compelled the researcher to infer the weights of these parameters by making reference to conventional standards.

REFERENCES

Abramson, L. W., Lee, T. S., Sharma, S., & Boyce, G. M. (2002). *Slope stability and stabilisation geomorphology.* New York: John Wiley and Sons Ltd.

Aktuğ, Bahadır., Kılıçoğlu, A. (2006). Recent crustal deformation of İzmir, Western Anatolia and sorrounding regions as deduced from repeated GPS measurements and strain field. *Journal of Geodynamics, 41,* 471– 484.

Alfaro, P., Delgado, J., García-tortosa, F. J., Lenti, L., López, J. A., López-casado, C., et al. (2012). Widespread landslides induced by the Mw 5 . 1 earthquake of 11 May 2011 in Lorca , SE Spain. *Engineering Geology, 138* (4), 40–52.

American Geophysical Union (2017). Retrieved on 02, May, 2016 from http://blogs.agu.org/landslideblog/2009/10/07/more-images-of-the-earthquake-triggered-landslides-in-sumatra/.

American Geophysical Union (2017). Retrieved on 13, March 2016 from http://blogs.agu.org/landslideblog/2013/05/12/the-wenchuan-earthquake-five-years-on/.

American Geophysical Union (2017). Retrieved on 22, March 2016 from http://blogs.agu.org/landslideblog/2016/02/04/muzaffarabad-1/)

Anderson, M. G., & Richards, K. S. (1989). *Slope stability; geotechnical engneering and geomorphology.* New York: John Wiley and Sons Ltd.

Arias, A. (1970). *A measure of earthquake intensity. Seismic Design for Nuclear Power Plant,* ed. R.J. Hansen. MIT Press: Cambridge.

Avşar, A. (1997). *General assessment of landslides in İzmir metropitan area*. MSc Thesis. Dokuz Eylül University, İzmir.

Ayalew, L., & Yamagishi, H. (2005). The application of GIS-based logistic regression for landslide susceptibility mapping in the Kakuda-Yahiko Mountains,Central Japan. *Geomorphology*, *65* (05), 15–31.

Aydan, O., & Ulusay, R. (2015). A quick report on the 2015 Gorkhan (Nepal) Earthquake and its geo-engineering aspects. *International Association for Engineering Geology and the Environment, 10*, 25-35.

Barnard, P. L., Owen, L. A., Sharma, M. C., & Finkel, R. C. (2001). Natural and human-induced landsliding in the Garhwal Himalaya of northern India. *Geomorphology, 40* (01), 21-35

Biggs, J., Nissen, E., Craig, T., Jackson, J., & Robinson, D. P. (2010). Breaking up the hanging wall of a rift - border fault : The 2009 Karonga earthquakes , Malawi. *Geophysical Research Letters, 37,* 1–5.

Bommer, J. J., & Rodri´guez, C. E. (2001). Earthquake induced landslides in central America. *Engineering Geology 63*, 189–220.

Bouhadad, Y. (2010). Earthquakes- induced landslides in Algeria : The Laalam , March 20 th (M w = 5 . 2), 2006 earthquake. *Earthquake Engineering Center, 12*, 5–9.

Bourdeau, C., Lenti, L., Martino, S., Ozel, O., & Yalcinkaya, E. (2015). Local Seismic Response Analysis in the Large Büyükçekmece (Turkey) Landslide Area by Detailed Engineering-Geological and Numerical Modelling. *6th International Conference on Earthquake Geotechnical Engineering (10-2015).*

Budimir, M. E. A., Atikson, P. M., & Lewis, H. G. (2015). Seismically-induced landslides hazards and exposure modelling in southern California based on the 1994 Northridge, California earthquake event. *Landslides*, *12*, 895-910. Springer Verlag Berlin Heidelberg

Byrne, T. B. (2002). *Geology and geophysics of an arc-continent collision, Taiwan.* USA: Department of Geology and Geophysics, U-2045.

Cetin, K. O., Isik, N., & Unutmaz, B. (2004). Seismically induced landslides at Degirmendere Nose , Izmit Bay during Kocaeli (Izmit) -Turkey earthquake. *Soil Dynamics and Eartquake Engineering*, *24*, 189–197.

Chakraborty, I., Ghosh, S., Bhattacharya, D., & Bora, A. (2011). Earthquake induced landslides in the Sikkim-Darjeeling Himalayas - An aftermath of the 18 th September 2011 Sikkim earthquake. *Soil Dynamics and Eartquake Engineering*, *07*, 1–8.

Chalkias, C., Ferentinou, M., & Polykretis, C. (2014). GIS-Based Landslide Susceptibility Mapping on the Peloponnese Peninsula, Greece. *Geosciences*, *4*, 176–190.

Chigira, M., & Yagi, H. (2006). Geological and geomorphological characteristics of landslides triggered by the 2004 Mid Niigta prefecture earthquake in Japan. *Engineering Geology*, *82*, 202–221.

Chousianitis, K., Del Gaudio, V., Kalogeras, I., & Ganas, A. (2014). Predictive model of Arias intensity and Newmark displacement for regional scale evaluation of earthquake-induced landslide hazard in Greece. *Soil Dynamics and Earthquake Engineering*, *65*, 11–29.

Clague, J. J., & Stead, D. (2012). *Landslides; types, mechanisms and modeling.* New York, USA: Cambridge University Press.

Collins, B. D., Kayen, R., & Tanaka, Y. (2012). Spatial distribution of landslides triggered from the 2007 Niigata Chuetsu – Oki Japan Earthquake. *Engineering Geology*, *127*, 14–26.

Dai, F. C., Xu, C., Yao, X., Xu , L., Tu , X. B. et al. (2010). Spatial distribution of landslides triggered by the 2008 Ms 8.0 Wenchuan earthquake, China. *Asian Earth Sciences*, *65*, 205-221.

Dan, G., Sultan, N., Cattaneo, A., Jacques, D., Dan, G et al. (2010). *Mass-transport deposits on the Algerian margin (Algiers area) : morphology , lithology and sedimentary processes*. HAL Archives-Ouvertes-Insu 00467046, 05, 3-10

Delgado, J., García-tortosa, F. J., Garrido, J., Loffredo, A., & López-casado, C. (2015). Seismically-induced landslides by a low-magnitude earthquake : The M w 4 . 7 Ossa De Montiel event (central Spain). *Engineering Geology*, *196*, 280–285.

Delgado, J., Garrido, J., López-casado, C., Martino, S., & Peláez, J. A. (2011). On far fi eld occurrence of seismically induced landslides. *Engineering Geology*, *123*, 204–213.

Dangol, V., Yagi , H., & Higaki, D. (2013). *Bhedetar landslide, eastern Nepal: Aftermath of the Sikkim earthquake* (18th September 2011). K. Ugai et al (Eds). *Earthquake Induced Landslides.*

Dellow, G., Yetton, M., Massey, C., Archibald, G., Barrell, D. J. A et al. (2011). Landslides caused by the 22 february 2011 Christchurch Earthquake and management of landslide risk in the immediate aftermath. *Bulleting of the New Zealand Society for Earthquake Engineering*, *44* (4), 227–238.

Erdoğan, B., Altinler, D., Güngör, T., Özer, S. (1990). Stratigraphy of Karaburun. *Bulletin of the Mineral Resources of Exploration Institute Turkey, 111,* 0–23.

Esposito, E., Porfido, S., Simonelli, A. L., Mastrolorenzo, G., & Iaccarino, G. (2000). Landslides and other surface e ff ects induced by the 1997 Umbria – Marche seismic sequence. *Engineering Geology*, *58*, 353–376.

Flentje, P. N & Chowdhury, R. (2010). *Geotechnical analysis of slopes and landslides - achievements and challenges*. Retrievied March 15, 2016 from http//ro.uow.edu.au/eispapers/1736

Fortunato, C., Martino, S., Prestininzi, A., & Romeo, R. W. (2012). Nuova versione del Catalogo italiano degli Effetti Deformativi Indotti da forti Terremoti (CEDIT) new release of the italian catalogue of earthquake-induced ground failures. *Engineering Geology and Environment*, *2*, 63–75.

Garc-Rodriguez, M. J. (2010). Assessment of earthquake-triggered landslide susceptibility in El Salvador based on an Artificial Neural Network model. *Natural Hazards and Earth System Science, 10*, 1307–1315.

Gazioglu, C. (2005). 1881 and 1949 earthquakes at the Chios-Cesme Strait (Aegean Sea) and their relation to tsunamis. *Natural Hazards and Earth System Science, 5*, 717–725.

Gorum, T., van Westen, C. J., Korup, O., van der Meijde, M., Fan, X. et al. (2013). Complex rupture mechanism and topography control symmetry of mass-wasting pattern, 2010 Haiti earthquake. *Geomorphology, 184*, 127–138.

Hamiel, Y., Baer, G., Kalindekafe, L., Dombola, K., & Chindandali, P. (2012). Seismic and aseismic slip evolution and deformation associated with the 2009 – 2010 northern Malawi earthquake swarm , *East African Rift. Geophysical Journal International*, *191*, 898–908.

Hancox, G. T., Perrin, N. D., & Dellow, G. D. (2002). Recent studies of historical Earthquake Induced Landslides, ground damage and MM intensity in New Zealand. *Bulletin of the New Zealand and Society for Earthquake Engineering, 35 (2) 10-15*.

Harp, B. E. L., & Crone, A. J. (2006). Landslides triggered by the October 8 , 2005 , Pakistan. Earthquake and associated landslide-dammed reservoirs. *Geomorphology, 94*, 1-9

Hashmoto, M., Fukushima, Y. & Takada, Y. (2012). Coseismic deformations of the 2011 Tohoku , Japan , earthquake and triggered events derived from Alos / Palsar. *Disaster Prevention Research Institute, 661*, 5-9.

Jibson, R. W. (1993). Predicting earthquake induced landslides displacement using newmark's sliding block analysis. *Transportation Research Records, 1411*,85-98.

Jibson, R. W., Harp , E. L., Schulz, W., & Keefer, D. K. (2004). Landslides triggered by the 2002 Denali fault, Alaska, earthquake and the inferred nature of the strong shaking. *Earthquake Spectra, 20 (3)*, 669–691.

Jibson, R. W., Harp, Edwin, L., Schulz, W. & Keefer, D. K. (2006). Large rock avalanches triggered by the M 7 . 9 Denali Fault , Alaska , earthquake of 3 November 2002. *Engineering Geology, 83,* 144-160.

Jibson, R. W. (2007). Regression models for estimating coseismic landslide displacement. *Engineering Geology, 91*, 209–218.

Jibson, R. W. (2011). Methods for assessing the stability of slopes during earthquakes. A retrospective: *Engineering Geology, 122,* 43-50.

Jibson , R. W. (2013). *Treatise on geomorphology*. *Mountain and hillslope geomorphology*. San Diego: Academic Press.

Johnson, C. W.C, Bürgmann W. R and Pollitz, F. F. (2015). Rare dynamic triggering of remote M≥5.5 earthquakes from global catalog analysis. *Journal of Geophysical Research Solid Earth*, 120, 1748-1761.

Ju-Jiang, H. (2000). Chi-Chi earthquake induced landslides in Taiwan. *Earthquake Engineering and Engineering Seismology 1* (1).

Kaiser, A., Holden, C., Beavan, J., Beetham, D., Benites, R. et al. (2012). The M w 6 . 2 Christchurch earthquake of February 2011 : preliminary report, 8306(April 2016). *Geology and Geophysics, 55* (1), 67-90.

Kamp, U., & Owen, L. A. (2016). GIS-based landslide susceptibility mapping for the 2005 Kashmir earthquake region, (November 2008). *Geomorphology, 101*, 631-642.

Kamp, U., Growley a, B. J., Khattak , G. A., & Owen, L. A. (2008). GIS-based landslide susceptibility mapping for the 2005 Kashmir earthquake region. *Geomorphology, 101,* 631–642.

Keefer, D. K. (1984). Landslides caused by earthquakes. *Geological Society of America Bull, 95,* 406-421. United States Geological.

Keefer, D. K. (1989). Statistical analysis of an earthquake induced landslides. *Engineering Geology, 58,* 231-249.

Keefer, D. K. (1993). The susceptibility of rock slope to earthquake induced failure. *Geological Engineering, 30* (3), 353-361.

Keefer, D. K. (2000). Statistical analysis of an earthquake induced landslides distribution — the 1989 Loma Prieta , California event. *Geology Enginnering, 58,* 231-249.

Keefer, D. K., Wartman, J., Navarro, C., Rodriguez-marek, A., & Wieczorek, G. F. (2006). Landslides caused by the M 7 . 6 Tecomán , Mexico Earthquake. *Engineering Geology, 86,* 183–197.

Keefer, D. K. (2013). *Landslides generated by earthquakes: Immediate and Long-terrm effects*. In J. F. Shroder, (ed.), L.A. Owen, (ed.); Treastise on Geomorphplpgy (5thed), Tectonic Tectonic Geomporphology. San Diego: Academic Press.

Kıncal, C., Akgün, K. A. M & Koca, Y. (2009). Landslide susceptibility assessment in the Izmir (West Anatolia , Turkey) city center and its near vicinity by the logistic regression method. *Environmental Earth Science, 59,* 745-756.

Korup, O. (2010). *Earthquake-triggered landsldes Spartial pattern and impacts*. Swiss Federal Research İnstitutes WSL/SLF, CH-7260 Davos.

Kramer, S. L. (1996). *Geotechnical earthquake engineering.* Upper Saddle River, New Jersey: Prentice-Hall Inc.

Khazai, B., & Sitar, N. (2003). Evaluation of factors controlling earthquake-induced landslides caused by Chi-Chi earthquake and comparison with the Northridge and Loma Prieta events. *Engineering Geology, 71,* 79–95.

Khazai, B., & Sitar, N. (2004). Evaluation of factors controlling earthquake-induced landslides caused by Chi-Chi earthquake and comparison with the Northridge and Loma Prieta events. *Engineering Geology, 71* (2), 79–95.

Kieffer, D. S., Eeri, M., Jibson, R., Eeri, M., Rathje, E. M. et al. (2006). Landslides Triggered by the 2004 Niigata Ken Chuetsu , Japan , Earthquake. *Earthquake Spectra, 22* (03), 47–73.

Kutluca, A. K., & Ozdemir, S. (2008). Landslide , Earthquake & Flood Hazard Risks of İzmir Metropolitan City , A Case : Altindag Landslide Areas. *International Journal of Environmental, Chemical, Ecological, Geological and Geophysical Engineering, 2* (12), 159–164.

Lee, C., Huang, C., Lee, J., Pan, K., Lin, M. et al. (2008). Statistical approach to earthquake induced landslide susceptibility. *Engineering Geology, 100,* 43–58.

Lei, C. I. (2012). Earthquake-Triggered Landslides. *1st Civil and Environmental Engineering Student Conference*, (06), 1–6.

Lin, M., & Tung, C. (2003). A GIS-based potential analysis of the landslides induced by the Chi-Chi Earthquake. *Engineering Geology, 71*, 63–77.

Macheyeki, A. S., Mdala, H., Chapola, L. S., Manhiça, V. J., Chisambi, J., et al,. (2015). Active fault mapping in Karonga-Malawi after the December 19 , 2009 Ms 6 . 2 seismic event, *Journal of African Earth Sciences, 102,* 233–246.

Mahdavifar, M. R., Solaymani, S., & Jafari, M. K. (2006). Landslides triggered by the Avaj , Iran earthquake of June 22 , 2002. *Engineering Geology, 86,* 166–182.

Mahmood, I., Qureshi, S. N., Tariq, S., Atique, L., & Iqbal, M. F. (2015). *Analysis of landslides triggered by October 2005, Kashmir Earthquake* – PLOS Currents Disasters

Meunier, P., Hovius, N., & Haines, A. J. (2007). Regional patterns of earthquake-triggered landslides and their relation to ground motion. *Earth and Planetary Science Letters, 34*, 1–5.

Meunier, P., Hovius, N., & Haines, J. A. (2008a). Topographic site effects and the location of earthquake induced landslides. *Earth and Planetary Science Letters, 275* (3-4), 221–232.

Meunier, P., Hovius, N., & Haines, J. A. (2008b). Topographic site effects and the location of earthquake induced landslides. *Earth and Planetary Science Letters, 275* (3-4), 221–232.

Messaoudi, A., Laouami, N., & Mezouer, N. (2012). Topographic effects on the seismic responses of slopes. *15WCEE LISBOA.*

Miles, S. B., & Keefer, D. K. (2007). *Comprehensive areal model of earthquake-induced landslides : Technical Specification and User Guide*. Retrieved May 12, 1016 from http://pubs.ugs.gov/of/2007/1072/of2007-1072_2

Miles, S. B., & Keefer, D. K. (2009). Evaluation of CAMEL — comprehensive areal model of earthquake-induced landslides. *Engineering Geology, 104*, 1–15.

Msilimba, G. G., & Holmes, P. J. (2005). A Landslide hazard assessment and aulnerability appraisal arocedure : Vunguvungu / Banga Catchment. *Natural Hazards, 34*, 199–216.

Mousavi, M. S., Omidvar, B., Ghazban, F., & Feyzi, R. (2011). Quantitative risk analysis for earthquake induced landslides —Emamzadeh Ali, Iran. *Engineering Geology 122*, 191–203.

Nandi, A., & Shakoor, A. (2009). A GIS-based landslide susceptibility evaluation using bivariate and multivariate statistical analyses. *Engineering Geology, 110,* 11–20.

Natural hazards (2007). Retrieved on 07, April 2016 from http://mceer.buffalo.edu/research/Reconnaissance/Peru8-15-07/01-lg.jpg.

Oberhänsli, R., & Chen, F. (2011). Geodynamic Significance of the Early Triassic Karaburun Granitoid (Western Turkey) for the Opening History of Neo-Tethys. *Turkish Journal of Earth Science*, *20*, 255–271.

Parker, R.N, Hancox, G.T, Petley, D.N, Massey, C.L, Densmore, A.L., and Rosser, N.J. (2015). Spartial Distribution of Earthquake induced landslides and hilslope preconditioning in the Northwest island New Zeland. *Earth Science Dynamics, 3*, 501-525.

Parise, M., & Jibson, R. W. (2000). A seismic landslide susceptibility rating of geologic units based on analysis of characteristics of landslides triggered by the 17 January , 1994 Northridge , California earthquake. *Engineering Geology, 58*, 251–270.

Qi, S., Xu, Q., Lan, H., Zhang, B., & Liu, J. (2010a). Spatial distribution analysis of landslides triggered by 2008 . 5 . 12 Wenchuan. *Engineering Geology, 116* (1-2), 95–108.

Rathje, E. M., Wang, Y., Stafford, P. J., Antonakos, G., & Saygili, G. (2014). Probabilistic assessment of the seismic performance of earth slopes. *Bull Earthquake Engineering*, *12*, 1071–1090.

Ray, P. K. C., Parvaiz, I. R., Thakur, V. C., Dadhwal, V. K & Bhat, F. A (2009). Analysis of seismicity-induced landslides due to the 8th October 2005 earthquake in Kashmir Himalaya. *Current Science*, *97* (12), 1742-1750

Rodrigues, C. E, Bommer, J. J., & Chandler, R. J (1999). Earthquake induced landslides: 1980 – 1997. *Soil Dynamics and Earthquake Engineering, 18,* 325-346.

Sepúlveda, S. A., Serey , A., Lara, M., Pavez , A., & Rebolledo, S. (2010). Landslides induced by the April 2007 Aysén Fjord earthquake, Chilean Patagonia. *Landslides*, *7*,483–492.

Saygili, G., Rathje, E. M., & Asce, M. (2008). Empirical Predictive Models for Earthquake-induced sliding displacements of slopes. *Journal of Geotechnical and Geoenvironmental Engineering*, *134*, 790–803.

Schernthanner, H. (2004). Fuzzy Logic Method for Landslide Susceptibility Mapping , “ Rio Blanco ”, Nicaragua 2 . Study Area 3 . *Landslides 4*, 200-206

Shahabi, H., & Hashim, M. (2015). Landslide susceptibility mapping using GIS-based statistical models and Remote sensing data in tropical environment. *Scientific Research Eassay*, 1–15.

Swank, M.W. (2007). *Computer modeling of landslides generated by the 1906 San Francisco earthquake*. MSc Thesis. San Jose State University

Tang, C., Ma, G., Chang, M., Li, W., Zhang, D. Jia, T.et al. (2015a). Landslides triggered by the 20 April 2013 Lushan earthquake , Sichuan. *Engineering Geology*, *187*, 45–55.

Tang, C., Ma, G., Chang, M., Li, W., Zhang, D. et al. (2015b). Landslides triggered by the 20 April 2013 Lushan earthquake , Sichuan, *Engineering Geology*, *187*, 45–55.

Tasnimnews, retrieved (2016). Retrieved on 02, may 2016 from https://www.tasnimnews.com/en/news/2015/08/28/842409/landslides-kill-five-in-nepal-quake-zone

Trandafir, A. C., Tjok, K., & Long, X. (2012). Numerical Insights into Mechanisms of earthquake induced catastrophic landslides on gentle slopes. *Natural Hazards,* 379, 38-51.

Travasarou, T., Bray, J.B. & Abrahamson, A. (2003). Empirical attenuation relationship for Arias Intensity. *Earthquake Engineering and Structural Dynamics, 32*, 1133-1155.

Umar, Z., Pradhan, B., Ahmad, A., Neamah, M., & Shafapour, M. (2014). Earthquake induced landslide susceptibility mapping using an integrated ensemble frequency ratio and logistic regression models in West Sumatera Province , Indonesia. *Catena, 118*, 124–135.

United States Geological Survey (USGS) (2010). Shake map, Retrrieved on May 15, 2016 from https://earthquake.usgs.gov/learn/topics/mag_vs_int.php

United States Geological Survey (USGS) (2011). Shake map, Retrrieved on May 15, 2016 from http://earthquake.usgs.gov/earthquakes/shakemap/background.php

Uzel, B., & Sözbilir, H. (2013). İzmir – Balıkesir transfer Structural evidence for strike-slip deformation in the I zone and consequences for late Cenozoic evolution of western Anatolia (Turkey). *Geodynamics, 65*, 94–116.

Wald, D. J., Worden, B. C., Quitoriano, V., & Pankow, K. L. (n.d.). *ShakeMap ® Manual*. United States Geological Survey.

Walker, B.F. & Fell, R. (1987). *Geotechnical Engineering of Dams*. London UK: CRS Press.

Wang, X.G & Wang, D. (2010). Relationships between ground motion parameters. *earthquake Science*, *23* (3), 233-242

Wartman, J., Cox, B., Meneses, J., Moreno, V., & Olcese, M. (2008). Landslides triggered by the 15 August 2007 M8 . 0 Pisco , Peru earthquake. *European Geoscience Union, 10.*

Wartman, J., Dunham, L., Tiwari, B. & Pradel, D. (2013). Landslides in eastern Honshu the May 12, induced by the 2011 off the Pacific coast of Tohoku earthquake. *Seismological Society of America*, *103* (2B), 1503-1521.

Wilson, R.C & Keefer, D.K . (1985). Prediction areal limits of earthquake induced landslides Sin Zrong; earthquake hazard in the Los Angeles region-An earthquake perspective. *Unıted States Geological Survey Professional Paper*, *1360*, 317-345

Wilson, R. C. (1993). *Relation of arias intensity to magnitude and distance in california*. Retrieved March, 24, 2016 from http://pubs.ugs.gov/of/1993/0556/report.

Xu, C., Shyu, J. B. H. & Xu, X. (2014). Landslides triggered by the 12 January 2010 Port-au-Prince, Haiti, Mw = 7.0 earthquake: visual interpretation, inventory compiling, and spatial distribution statistical analysis. *Natural Hazards Earth System Science*, 14, 1789–1818

Xu, C., Xu, X., Yao, X. & Dai, F. (2014). Three (nearly) complete inventories of landslides triggered by the May 12, 2008 Wenchuan Mw 7.9 earthquake of China and their spatial distribution statistical analysis. *Landslides 11*, 441–461

Xu, C., & Xu, X. (2014a). Statistical analysis of landslides caused by the Mw 6.9 Yushu, China, earthquake of April 14, 2010. *Natural Hazards*, *72*, 871–893.

Xu, C., & Xu, X. (2014b). The spatial distribution pattern of landslides triggered by the 20 April 2013 Lushan earthquake of China and its implication to identification of the seismogenic fault. *China Science Bull*, *59*, 1416–1424.

Xu, C., Xu, X., Yao, Q., & Wang, Y. (2013). GIS-based bivariate statistical modelling for earthquake- triggered landslides susceptibility mapping related to the 2008 Wenchuan earthquake , China. *Quartenary Journal of Engineering Geology and Hydrogeology*, *46*, 221–236.

Yagi , H., Sato , G., Higaki, D., & Yam, M. (2009). Distribution and characteristics of landslides induced by the Iwate–Miyagi Nairiku Earthquake in 2008 in Tohoku District, Northeast Japan. Landslides (2009). *Landslides*, *6*, 335–344.

Yalcin, A. (2008). GIS-based landslide susceptibility mapping using analytical hierarchy process and bivariate statistics in Ardesen (Turkey): Comparisons of results and confirmations. *Catena*, *72*, 1–12.

Zaruba, Q., & Mencl, V. (1982). *Landslides and their control.* Elsevier Scientific Publishing Co.

APPENDICES

Appendix A: Hazard module of CAMEL

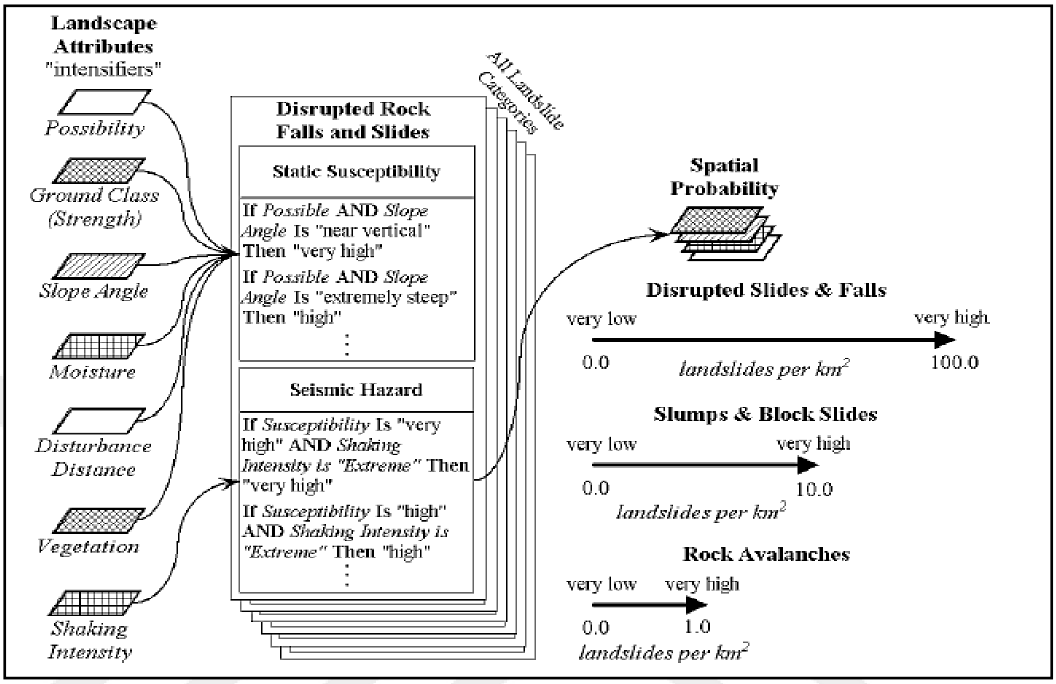

Design of the hazard module of CAMEL (Miles & Keefer, 2007; 2009)

Appendix B: CAMEL input variables – variables and modifiers for hazard module

Variable Name	Units	Min	Max	Fuzzy Variable Labels
hDisturbanceDist	Meters	0	200	close far
hGroundClass	Relative (ratio) Units	1	5	very_good good moderate poor very_poor
hMoisture	Percent	0	100	very_low low medium high very_high not_very_low
hShakeIntensity	ShakeMap (MMI)	4	10	light moderate strong very_strong severe violent extreme
hSlopeAngle	Degrees from the horizontal	5	65	very_gradual gradual medium_gradual medium medium_steep steep very_steep extremely_steep near_vertical
hVegetation	Percent	0	100	sparse dense

Appendix C: Membership functions of disturbance distance for CAMEL hazard module

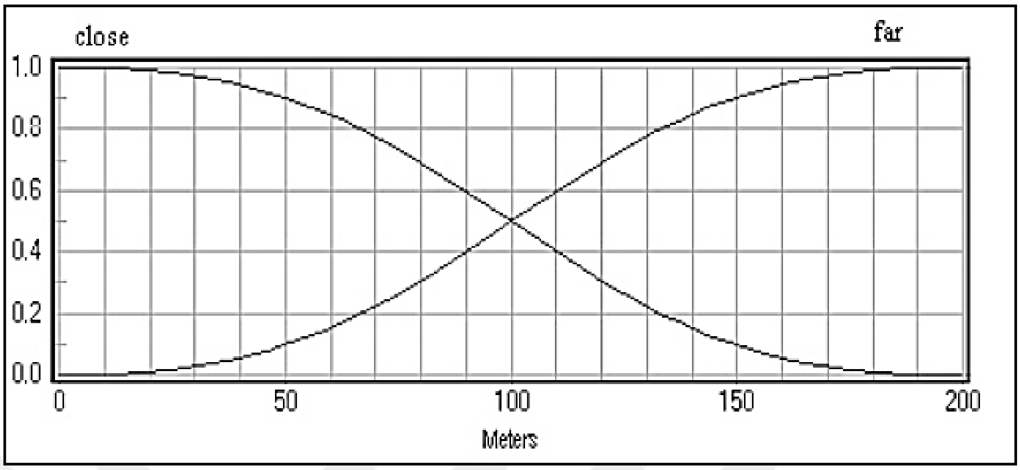

Membership functions of Disturbance Distance for hazard module (Miles & Keefer, 2007)

Appendix D: Membership functions of ground class for CAMEL hazard module

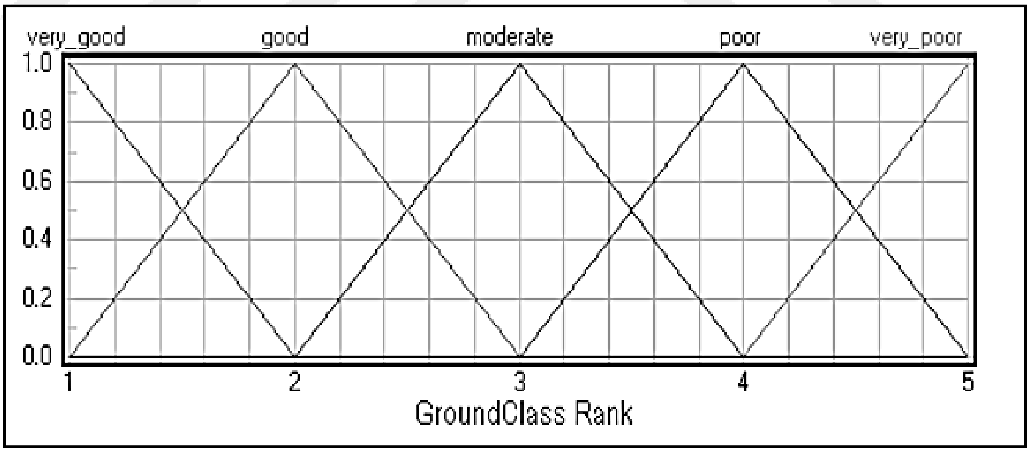

Membership functions of ground class for CAMEL hazard module (Miles & keefer, 2007)

Appendix E: Knowledge describing increasing likelihood of landslides with respect to quality of rock cementation or induration

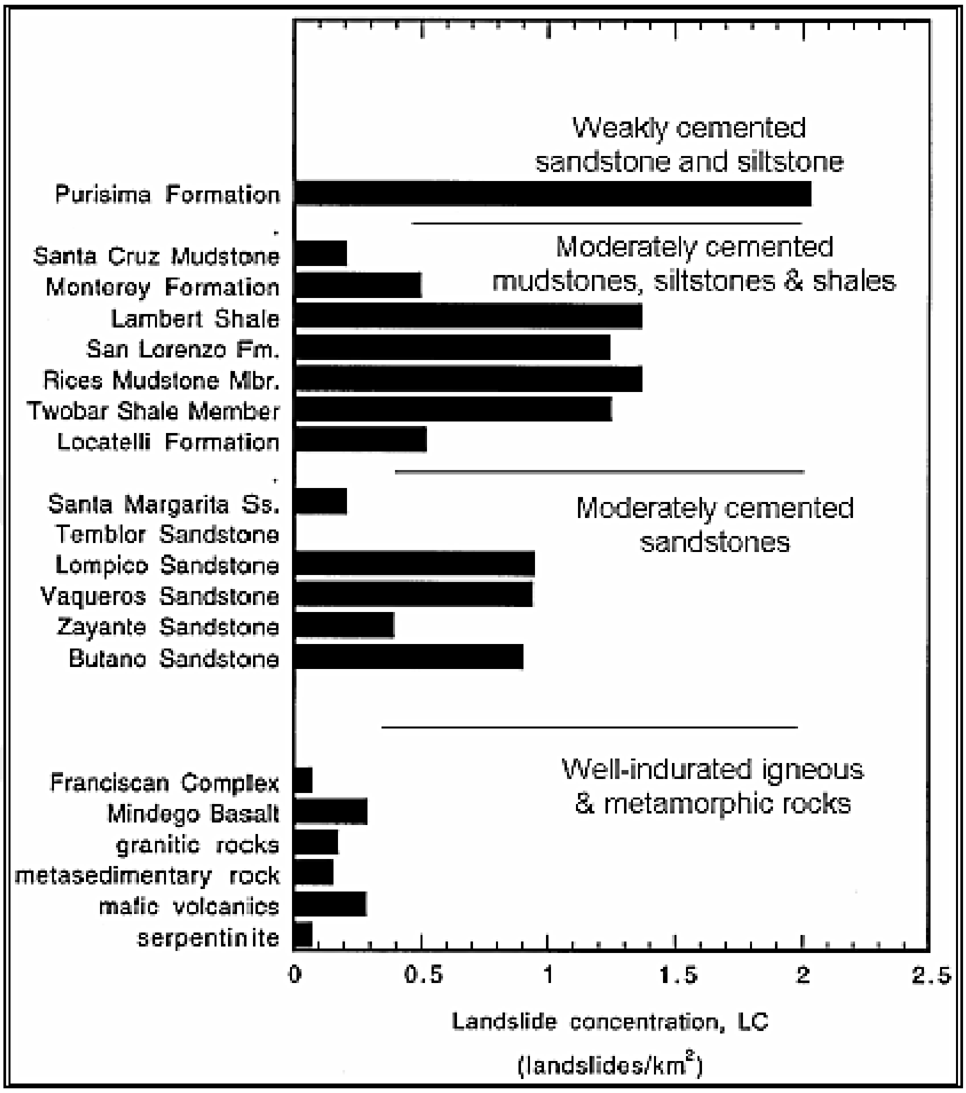

Description of the increasing likelihood of landslides with respect to quality of rock cementation or induration (Miles & Keefer, 2009)

Appendix F: Membership functions of moisture variable for CAMEL hazard module

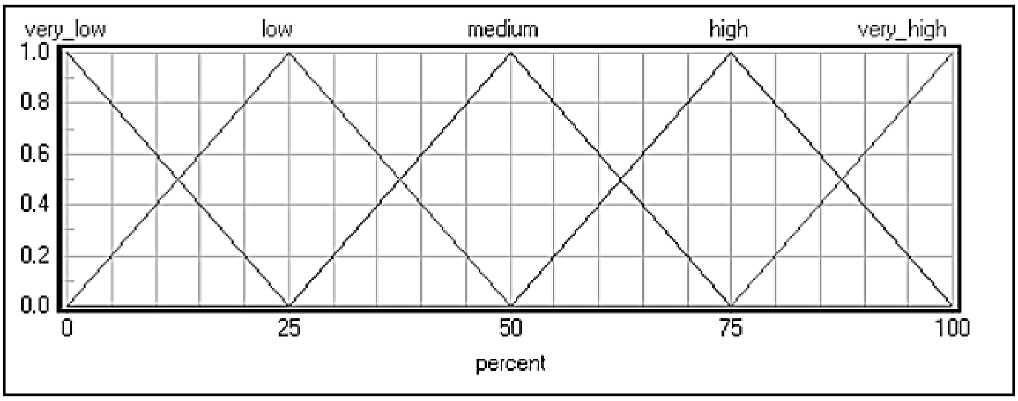

Membership functions of moisture for CAMEL hazard module (Miles & Keefer, 2007)

Appendix G: Membership functions of shake intensity for CAMEL hazard module

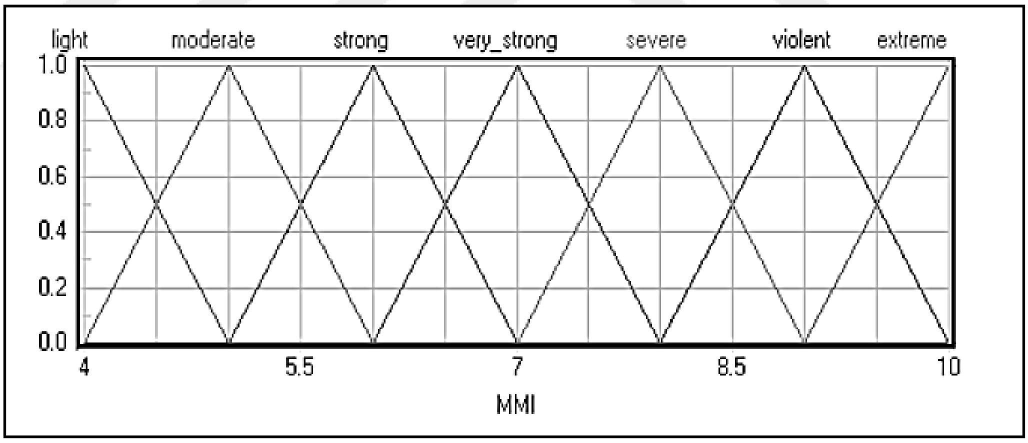

Membership functions of shake up intensity for CAMEL hazard (Miles & Keefer, 2007)

Appendix H: Seismic variables rule block for disrupted rock slides and falls

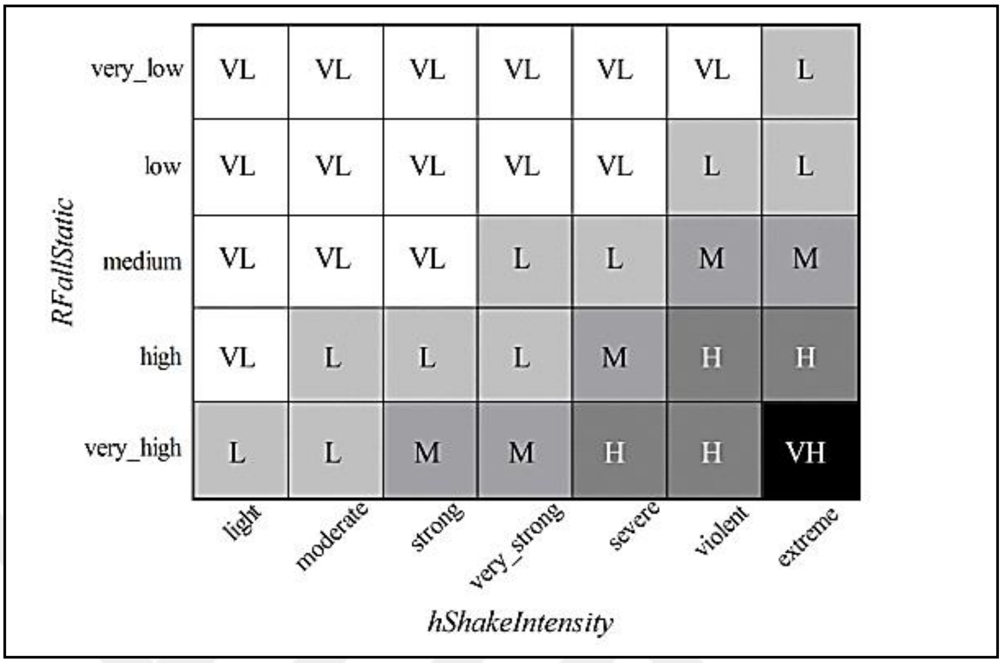

Shake intensity for probable occurrence EI landslides (Keefer, 1984)

Appendix I: Membership functions of slope angle for CAMEL hazard module

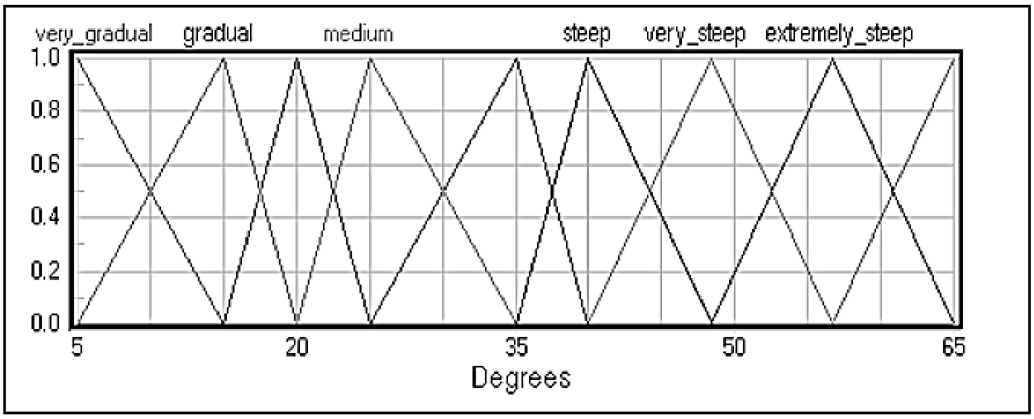

Membership functions of slope angle for hazard module (Miles & Keefer, 2007)

Appendix J: Membership functions of Vegetation variable for CAMEL hazard module

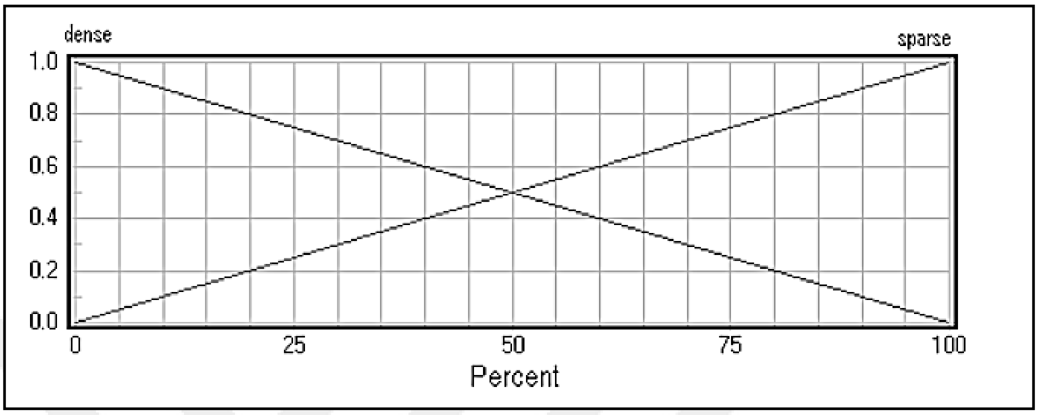

Membership functions of vegetation variable for CAMEL hazard module (Miles & Keefer, 2007)

Appendix K: Abbreviations and Acronyms

AGU	American Geophysical Union
ASTER	Advanced Space borne Thermal Emission and Reflection Radiometer
CAMEL	Comprehensive Areal Model of Earthquake induced Landslides
CEDIT	Catalogue of Earthquake –Induced Ground Failures (Italian)
CEA	Chinese Earthquake Administration
CW	Computing with Words
DEM	Digital Elevation Model
DLR	Department of Land and Resources
DoS	Degree of Support
EARS	East African Rift System
FS	Factor of Safety
GSD	Geological Survey Department of Malawi
HEA	Horizontal Equivalent Acceleration
MHEA	Maximum Horizontal Equivalent Acceleration
MRS	Malawi Rift System
KOERI	Kandilli Observatory and Earthquake Research Institute
LAA	landslides affected area
LC	Landslides Concentration
LANDSAT	Land Remote-Sensing Satellite (System)